ESTIMATING SPATIOTEMPORAL VARIABILITY OF MAIZE CROP EVAPOTRANSPIRATION IN THE MOOI RIVER CATCHMENT, SOUTH AFRICA: A CROP COEFFICIENT APPROACH USING SATELLITE REMOTE SENSING-BASED VEGETATION INDICES

Gerhard Olivier
42000300

DFGGR91
Supervisor: Prof David William Hedding

DEPARTMENT OF GEOGRAPHY
UNIVERSITY OF SOUTH AFRICA

Submitted in partial fulfilment of the requirements for the degree
MASTER OF SCIENCE (GEOGRAPHY)

January 2024

Student: Gerhard Olivier

Supervisor: Prof. David William Hedding

Department: Geography, University of South Africa

Degree: Master of Science (Geography)

Abstract

In an area experiencing semi-arid conditions, such as the Mooi River catchment, it is crucial to ascertain the evapotranspiration rate accurately. Evaluating evapotranspiration is beneficial in areas where the water demand surpasses its availability. This is particularly true in semi-arid and arid areas where the lack of water is increasingly impacting economic well-being and obstructing sustainable development. Developed by the Food and Agriculture Organization of the United Nations (FAO) in 1998, the crop coefficient approach estimates actual evapotranspiration (ET_c) of crops using the equation $ET_c = ET_o * K_c$, where ET_o is reference evapotranspiration, and K_c is the crop coefficient. However, this approach, assuming uniform crop conditions, does not account for spatial variations in crop growth conditions, leading to limitations in reflecting the actual water use of crops. Using satellite remote sensing and vegetation indices, such as the Normalised Difference Vegetation Index (NDVI) and the Soil Adjusted Vegetation Index (SAVI), can overcome these limitations by accounting for the spatial and temporal variability in crop conditions and growth. NDVI was found to have a superior correlation with the FAO tabulated crop coefficients compared to SAVI. It was therefore chosen to compute the new K_c values to be used in the ET_c crop coefficient equation as it accurately reflects real-time crop growth conditions and environmental impacts. The findings of this study underscore significant discrepancies in the spatial variation of ET_c across the Mooi River catchment, revealing notable variation in evapotranspiration, particularly the lower rates in the southwest during the growing season. The study evidenced temporal variations between ET_c values calculated from FAO tabulated K_c and those derived from NDVI-adjusted K_c throughout different maize cultivation phases of the year, emphasising, in particular, the need for precise assessment methods during the initial maize growth stages. Time-series analysis revealed that the average ET_c in the Mooi River catchment begins at a low level, marking its minimum at 1.614 mm during the maize's initial growth stage. It then undergoes a steady ascent, reaching a peak of 8.83 mm at 85 days after planting before gradually decreasing to 2.89 mm as it approaches harvest. The significant ET_c variations revealed in the maize growth cycle emphasise the need to consider several factors in agricultural assessments, such as climate, soil, and human activities. The developed maps and models offer critical tools for stakeholders, promoting efficient water use and sustainability in

semi-arid areas, thereby increasing food security. The research also highlights the potential of this approach for different crops and regions, underscoring its significance for water allocation management and yield evaluations, particularly in arid zones. The insights gained, necessary for understanding drought impacts and water-related crop stresses, pave the path for sustainable water management and increased food security across similar agricultural settings.

Abstract (in Afrikaans)

In 'n area met semi-droë toestande soos die Mooirivier-opvanggebied, is die akkurate bepaling van die tempo van evapotranspirasie van kardinale belang. Evaluering van evapotranspirasie is voordelig in gebiede waar die wateraanvraag die beskikbaarheid oorskry. Dit is veral belangrik in semi-droë en droë areas waar waterskaarste die ekonomie beïnvloed en volhoubare ontwikkeling belemmer. Die Voedsel- en Landbou-organisasie van die Verenigde Nasies (FAO) het die gewaskoëffisiëntbenadering in 1998 ontwikkel om werklike evapotranspirasie (ET_c) van gewasse te skat met die vergelyking $ET_c = ET_o * K_c$, waar ET_o verwysings evapotranspirasie is, en K_c die gewaskoëffisiënt. Hierdie benadering neem egter nie ruimtelike variasies in gewasgroeitoestande in ag nie, wat die vermoë daarvan beperk om werklike watergebruik te weerspieël. Om hierdie beperkings te oorkom, kan satelliet-afstandwaarneming en plantegroei-indekse soos die Genormaliseerde verskil plantegroei-indeks (NDVI) en die Grondaangepaste plantegroei-indeks (SAVI) gebruik word om ruimtelike en tydelike variasies in gewastoestande en groei in ag te neem. NDVI is bevind om 'n beter korrelasie te hê met die FAO se getabuleerde gewaskoëffisiënte in vergelyking met SAVI. Dit is dus gekies om die nuwe K_c-waardes te bereken wat gebruik sou word in die ET_c gewaskoëffisiëntvergelyking, aangesien dit werklike tyd gewasgroeiomstandighede en omgewingsimpakte akkuraat weerspieël. Die bevindings van hierdie studie beklemtoon beduidende teenstrydighede in die ruimtelike variasie van ET_c oor die Mooirivier-opvanggebied, en toon opmerklike variasie in evapotranspirasie aan, veral laer tellings in die suidweste gedurende die groeiseisoen. Die studie het tydelike variasies tussen ET_c waardes wat bereken is vanaf FAO getabuleerde K_c en dié wat afgelei is van NDVI-aangepaste K_c deurheen verskillende tye van die jaar, getoon, en beklemtoon veral die behoefte aan presiese assesseringsmetodes gedurende die aanvanklike groei stadiums. Tydreeksanalise het aan die lig gebring dat die gemiddelde ET_c in die Mooirivier-opvanggebied begin by 'n lae vlak, met sy minimum op 1.614 mm gedurende die aanvanklike groeifase van mielies. Dit ondergaan dan 'n gestadige styging, en bereik 'n piek by 8.83 mm 85 dae na plant tyd, voor dit geleidelik afneem tot 2.89 mm soos dit nader aan oes tyd kom. Die studie se beduidende ETc-variasies wat in die mieliegroeisiklus aan die lig gebring is, beklemtoon die

noodsaaklikheid om verskeie faktore, soos klimaat, grond en menslike aktiwiteite, in landbou-evaluasies in ag te neem. Die ontwikkelde kaarte en modelle bied kritieke hulpmiddels vir belanghebbendes, wat doeltreffende watergebruik en volhoubaarheid in semi-droë gebiede bevorder, en sodoende voedselsekerheid verhoog. Die navorsing beklemtoon ook die potensiaal van hierdie benadering vir verskillende gewasse en streke, en beklemtoon die belangrikheid daarvan vir watertoewysingsbestuur en opbrengs-evaluasies, veral in droë sones. Die insigte wat verkry is, wat nodig is om droogte-impakte en waterverwante gewasstremmings te verstaan, baan die pad vir volhoubare waterbestuur en verhoogde voedselsekuriteit oor soortgelyke landbou-omgewings.

Abstract (in Zulu)

Endaweni enezimo ezinogwadule, njengendawo egcina amanzi e-Mooi River, kubalulekile ukuqinisekisa izinga lokuphefumula kokuhwamuka kwamanzi ngokunembile. Ukuhlola ukuhwamuka kokuphefumula kunenzuzo ezindaweni lapho isidingo samanzi sidlula ukutholakala kwawo. Lokhu kuyiqiniso ikakhulukazi ezindaweni ezingelona ugwadule ngokugcwele nalezo eziwugwadule lapho ukuntuleka kwamanzi kuba nomthelela omkhulu empilweni yezomnotho futhi kuvimbe intuthuko esimeme. Ukwakhiwa kwayo yiNhlangano Yezokudla Nezolimo yeNhlangano Yezizwe Ezihlangene (i-FAO) ngo-1998, indlela yokusebenza kahle yezitshalo ilinganisela kuyizinga lokuphefumula kokuhwamuka (LK) kwezitshalo kusetshenziswa ngokulinganayo LK = NKo $*$ Kc, lapho NKo kuyireferensi yokuphefumula kokuhwamuka, futhi i-Kc iesebenza kahle yezitshalo . Kodwa-ke, le ndlela, kucatshangelwa izimo ezifanayo zezitshalo, ayibali ukwehluka kwezindawo ezimweni zokukhula kwezitshalo, okuholela emikhawulweni ekuboniseni ukusetshenziswa kwamanzi kwangempela kwezitshalo. Ukusebenzisa inzwa eyinkomba neyirimothi yesathelayithi nezimila, njenge i-Normalized Difference Vegetation Index (NDVI) kanye ne-Soil Adjusted Vegetation Index (SAVI), kunganqoba le mikhawulo ngokubala ukuhlukahluka kwendawo kanye nesikhashana ezimeni zezitshalo nokukhula. I-NDVI itholwe inokuhlobana okuphakeme okuphathelene nokusebenza kahle kusivuno esifakwe kuthebula ye-FAO uma kuqhathaniswa ne-SAVI. Ngakho-ke kwakhethwa ukubala amanani amasha e-Kc azosetshenziswa ku-ETc crop coefficient equation njengoba ibonisa ngokunembile izimo zokukhula kwezitshalo zesikhathi sangempela nomthelela wemvelo. Okutholwe kulolu cwaningo kugcizelela umehluko omkhulu ekuhlukeni kwendawo NKc ngaphesheya kwendawo egcina amanzi e-Mooi River, okuveza ukuhluka okuphawulekayo kokuphefumulela kokuhwamuka, ikakhulukazi amazinga aphansi eningizimu-ntshonalanga ngesikhathi sokukhula. Ucwaningo lwafakazela ukwehluka kwesikhashana phakathi kwamanani NKc abalwe ku-FAO yethebula i-Kc

kanye nalawo atholakala ku-NDVI elungiswe i-Kc kuzo zonke izigaba zokutshala ummbila ezihlukene zonyaka, okugcizelela ikakhulukazi isidingo sezindlela zokuhlola ezinembayo phakathi nezigaba zokuqala zokukhula kommbila. Ukuhlaziywa kochungechunge lwesikhathi kwaveza ukuthi isilinganiso so -NKc endaweni egcina amanzi e-Mooi River siqala ezingeni eliphansi, siphawula ubuncane baso ku-1.614 mm ngesikhathi sokukhula kommbila. Ibe seyikhuphuka kancane, ifike ku-8.83 mm ezinsukwini ezingama-85 ngemuva kokutshala ngaphambi kokwehla kancane kancane ibe ngama-2.89 mm njengoba sekusondele ukuvuna. Ukwehluka okubalulekile ko-NKc okuvezwe emjikelezweni wokukhula kommbila kugcizelela isidingo sokucabangela izici ezimbalwa, njengesimo sezulu, inhlabathi, kanye nemisebenzi yabantu, ekuhloleni kwezolimo. Amabalazwe athuthukisiwe namamodeli ahlinzeka ngamathuluzi abalulekile kubabambiqhaza, ekhuthaza ukusetshenziswa kwamanzi ngendlela efanele kanye nokusimama ezindaweni ezisagwadule, ngaleyo ndlela kwandise ukuvikeleka kokudla. Ucwaningo luphinde luveze amandla ale ndlela ezitshalweni nasezifundeni ezahlukene, lugcizelela ukubaluleka kwayo ekulawuleni ukwabiwa kwamanzi kanye nokuhlolwa kwesivuno, ikakhulukazi ezindaweni ezomile. Ukuqonda okuzuziwe, okudingekayo ukuze kuqondwe imithelela yesomiso kanye nengcindezi yezitshalo ehlobene namanzi, kuhlahla indlela yokulawulwa kwamanzi okusimeme kanye nokwanda kokuvikeleka kokudla kuzo zonke izimo zezolimo ezifanayo.

Declaration

I, Gerhard Olivier, declare that the dissertation, which I hereby submit for the degree Master of Science (Geography) at the University of South Africa, is my own work and has not previously been submitted by me for a degree at this or any other tertiary institution.

Signature:

Date:

15-Jan-2024

Acknowledgements

First and foremost, my deepest gratitude goes to my wife, Esti. Her enduring patience and unwavering support, particularly during the countless hours spent at my desk, have been my steadfast anchor throughout this journey. Additionally, I owe immense thanks to my family and friends, whose continuous encouragement and belief in me over the years have been invaluable sources of strength and motivation.

I wish to express sincere appreciation to Professor David William Hedding at UNISA. His guidance, mentorship, and academic expertise have been pivotal in the shaping and completion of my Master's degree. Special thanks are also due to Jaun van Loggerenberg, whose invaluable insights during the early stages of project conceptualization laid the foundation for this research endeavour.

Table of Contents

Acronyms and Abbreviations

BREB:	Bowen Ratio-Energy Balance
BREBS:	Bowen Ratio-Energy Balance System
DAE:	Days After Emergence
DAP:	Days After Planting
EVI:	Enhanced Vegetation Index
ET:	Evapotranspiration
ET_c:	Actual Evapotranspiration
ET_o:	Reference Evapotranspiration
FAO:	The Food and Agriculture Organization
K_c:	Crop Coefficient
K_{cb}:	Dual Crop Coefficient
LAI:	Leaf Area Index
NDVI:	Normalized Difference Vegetation Index
METOIC:	Mapping Evapotranspiration at high Resolution with Internalized Calibration
MAXENT:	Maximum Entropy
QGIS:	Quantum GIS
RS:	Remote Sensing
SEBAL:	Surface Energy Balance over Land
SEBS:	Surface Energy Balance System
SDM:	Species Distribution Model
SAVI:	Soil Adjusted Vegetation Index
VI:	Vegetation Index
UN:	United Nations
WUE:	Water Use Efficiency

List of Figures

List of Tables

List of Equations

Chapter 1: Introduction

1.1. Background

Evapotranspiration (ET) is a critical component of the water cycle, representing the amount of water lost to the atmosphere as a result of evaporation from soil and plant surfaces as well as transpiration from plant stomata (Jarmain & Klaasse, 2012; Ramoelo *et al*., 2014; Jovanovic *et al*., 2015; Zhang *et al*., 2016). Two-thirds of the world's rainfall is returned to the atmosphere as evapotranspiration (Jato-Espino *et al*., 2017). Thereby, after precipitation, evapotranspiration is the parameter of the terrestrial hydrological cycle that is most significant (Shoko *et al*., 2015). Because it directly impacts crop productivity and water usage efficiency, correct prediction of ET is crucial for effective water management in agricultural systems. Correct ET estimation can also help assess the regional water supply and guide policy decisions regarding water management and allocation (Suyker & Verma, 2009; Wu *et al*., 2021; Liu *et al*., 2022). Rainfed agriculture is an essential part of food production in many world regions. It supports millions of people's livelihoods and contributes to global food security (Wani *et al.*, 2009). However, rainfed agriculture depends heavily on precipitation which can vary considerably across space and time, affecting crop yields and food production (Rockstrom *et al*., 2010). Understanding crop water requirements in rainfed and irrigated systems is critical for managing and allocating water. ET estimation is particularly challenging because of the complicated connections between environmental elements and plant physiology, unpredictability in water supply, and soil moisture conditions (Allen *et al.*, 1998; Cha *et al.,* 2020). Most of South Africa's territory is classified as semi-arid, with an average annual rainfall of 495 millimetres compared to yearly global rainfall averages of 814mm per year and an average annual evaporation rate of 1800mm. South Africa is therefore considered a water-scarce country (WWF-SA, 2016). The Mooi River catchment falls within the semi-arid region of South Africa, receiving an average of 600 mm per year, 200 mm below the global rainfall average (Lynch *et al*., 2001; Schulze, 1997). Therefore, understanding crop water requirements in this region can play a pivotal role.

Ground-based techniques and instruments for measuring ET, like weighing lysimeters, evaporation pans, soil moisture balances, atmometers, the Bowen Ratio Energy Balance System (BREBS), and Eddy Covariance devices, have historically been used. Still, they can be costly, time-consuming, and spatially constrained as they are considered point-based measurements preventing ET from being estimated over large spatial extents and, as a result, from measuring the spatial variability of ET, for example, on a regional scale (Unlu, 2010; Gibson *et al*., 2013). Because of its extensive coverage, regular revisits, and affordability, satellite remote sensing has

become a popular method for ET estimation, making it an attractive option for ET estimation in remote and economically disadvantaged regions. As they represent the physiological status of vegetation and its reaction to environmental elements, vegetation indices (VIs) produced from satellite remote sensing data have demonstrated particular promise in assisting with the calculation of ET (Gibson *et al*., 2013).

The Food and Agriculture Organization (FAO) developed the crop coefficient method for ET_c estimation in 1998. This method only requires meteorological information from the user without needing any equipment or complex computation (Allen *et al*. 1998). This is a widely used approach for estimating crop ET_c, likely because of its simplicity. The method works by multiplying reference evapotranspiration (ET_o) (calculated from meteorological data) by a crop coefficient (K_c) (retrieved from a manual developed by the FAO). Still, it has limitations, particularly in its reliance on crop coefficients that do not always reflect the actual water use of crops in varying environmental conditions, for example, assuming that crop conditions in a field are spatially uniform. Satellite remote sensing and associated vegetation indices (for example, NDVI and SAVI) offer a solution for this limitation by accounting for variability in crop coefficients resulting from the natural variability of crop conditions and growth, spatially and temporally.

This study aims to estimate maize crop evapotranspiration variability across space and time in the Mooi River catchment by integrating the FAO's crop coefficient approach with satellite imagery. Either the Normalized Difference Vegetation Index (NDVI) or the Soil-Adjusted Vegetation Index (SAVI) will be used, based on which demonstrates the strongest linear relationship with the FAO's tabulated crop coefficients. The chosen vegetation index will be used to adjust the crop coefficient values found in the FAO manual using its corresponding regression model. This regression model will then generate new (adjusted) crop coefficient values that mirror the natural variability of the crop conditions in the study area. By doing so, it will be possible to estimate the actual evapotranspiration (ET_c) values more accurately compared to using the generic crop coefficient values from the FAO manual.

The study area comprises 2808 fields growing various crops, including maize, soybeans, sunflowers, and lucerne, each planted at different points during the 2021-2022 growing season. During a site visit to the study area, 193 maize fields were identified and marked by recording the GPS coordinates of each field's centre. An objective of this study is to detect all remaining maize fields among the total of 2808 in the Mooi River catchment that were not spotted during the site visit—a species distribution model (SDM) known as MAXENT was used to accomplish this.

Of the 193 identified fields, 28 shared similar planting dates (between November 10 to November 15, 2021), while the planting dates of the remaining 165 fields are unknown. Given that plant growth stages significantly impact evapotranspiration rates, plants sown at different times will display different evapotranspiration rates at a given moment. As a result, only the fields with planting dates aligned with those of the 28 confirmed fields from the site visit, were selected for estimating actual evapotranspiration in this study. The Leaf Area Index (LAI) was used as a proxy for the planting dates, helping to pinpoint fields that were likely planted at the same time as the known group of 28 fields.

1.2. Aim of the study

This study aims to determine how maize crops' actual evapotranspiration (ETc) varies over space and time within the Mooi River catchment using satellite multispectral vegetation indices and the crop coefficient approach.

1.3. Objectives of the study

1. To identify all maize fields in the study area using satellite imagery and a species distribution model (SDM) based on a ground-truthed sample of maize fields identified during a site visit.
2. To identify and categorise maize fields in the study area based on their planting dates during the 2021/2022 growing season, facilitating a comparative analysis of ET across different fields.
3. To determine and analyse the duration of each growth stage in maize during the growing season, ensuring that satellite imagery and associated index data are assigned to the appropriate crop coefficient values.
4. To determine the reference evapotranspiration (ET_o) for each maize field within the study area, providing a baseline for evaluating actual ET and water needs.
5. To calculate the mean NDVI and SAVI values for each field in the study area.
6. To adjust the tabulated crop coefficient (K_c) values using a simple linear regression model based on the satellite vegetation index values and the existing tabulated crop coefficient (K_c) to derive new (K_c) values for each of the fields in the study area.
7. To calculate the actual ET (ET_c) for each maize field within the study area, aiming to provide precise water use data for effective agricultural water management.
8. To generate spatial and temporal maps of ET_c, offering a visual representation of ET variations across the study area, aiding in decision-making for crop and water management.

1.4. Problem statement

The problem this dissertation addresses is the limitation of the FAO56 crop coefficient method in accounting for the spatial and temporal variability of evapotranspiration (ET) estimation. The FAO56 method simplifies ET estimation but assumes uniform crop conditions, often not reflecting actual water use in varied environmental settings. This dissertation proposes the integration of satellite remote sensing, particularly using vegetation indices like NDVI and SAVI, to enhance the FAO56 method. Satellite imagery can capture spatial and temporal variations in plant growth and vigour, significantly affecting ET. This approach aims to refine ET estimation for maize crops in the Mooi River catchment, yielding more accurate ET_c values by adjusting the FAO's crop coefficients to reflect natural variability in crop conditions.

1.5 Dissertation structure

Chapter 1 sets the foundation for the research, introducing the importance of evapotranspiration (ET) in agriculture and water management. It explores traditional ground-based ET measurement methods, their limitations, and the emerging potential of satellite remote sensing for ET estimation, specifically focusing on maize crops in South Africa's Mooi River catchment. Chapter 2 comprehensively reviews local and international literature to define evapotranspiration and its influencing factors. This chapter also delves into the concepts of reference evapotranspiration (ET_o) and crop coefficient (K_c), and how they relate to actual evapotranspiration (ET_c). It then discusses satellite-based remote sensing models used for ET estimation and provides an overview of related studies both within South Africa and internationally. Chapter 3 provides a detailed geographical description of the study area, along with essential background information, and outlines the structure and various phases of the research methodology. Chapter 4 details the results obtained after implementing the methodology, encompassing phases from maxent modelling to calculating actual ET and creating spatiotemporal maps. Chapter 5 delves into a thorough discussion of the research findings, highlighting significant insights. Finally, Chapter 6 concludes the dissertation, emphasising the importance of the research findings and offering recommendations for future studies in this field.

Chapter 2: Literature Review

This chapter sets out to define the term 'evapotranspiration' (ET), as well as those factors that regulate ET. It is followed by an explanation of reference evapotranspiration (Et_o) and crop coefficient (K_c) and how these concepts relate to actual evapotranspiration (ET_c). The chapter continues with a discourse on satellite-based remote sensing models for estimating evapotranspiration. Lastly, an overview of international and South African remote sensing studies on evapotranspiration is provided.

2.1. Evapotranspiration

Evapotranspiration (ET), also known as actual ET or consumptive use, is a process whereby water is lost through a combination of transpiration from plant leaves and evaporation from soil surfaces (Fig. 2.1) (Jarmain & Klaasse, 2012; Ramoelo *et al*., 2014; Jovanovic *et al*., 2015). On crop fields, transpiration often plays the most significant role in evapotranspiration (Sello, 2019). Still, according to the FAO (1998), during the planting season, nearly 100% of ET comes from evaporation, while at full crop cover, more than 90% of ET comes from transpiration. Evaporation from the soil is mainly influenced by the amount of solar radiation reaching the soil surface. This amount decreases as the crop canopy develops over the growing season, creating more shade over the soil, and once the crops are fully developed covering the ground, transpiration becomes the main component of ET (Allen *et al*., 1998; Sello, 2019). The evapotranspiration rate is expressed in millimetres (mm) per unit time. The rate represents the amount of water lost from a cropped surface in units of water depth. The time unit can be an hour, day, decade, month, entire growing period, or calendar year (Allen *et al.*, 1998).

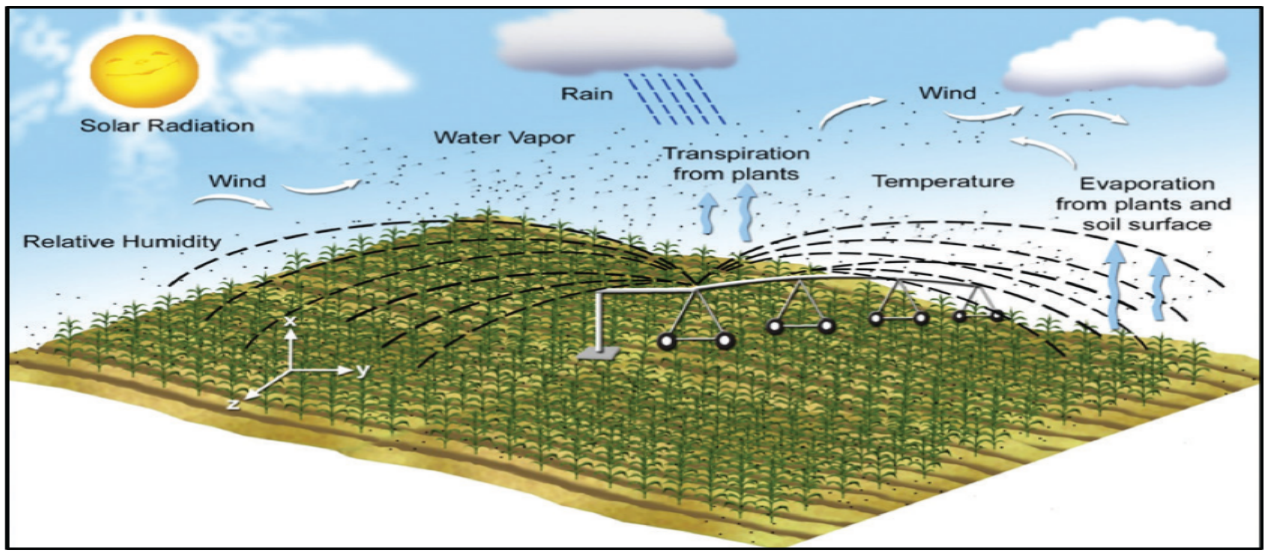

Figure 2.1: Depiction of the evapotranspiration process (Irmak, 2017).

2.2. Factors regulating evapotranspiration

ET varies depending on the heterogeneity of the landscape and topography, meteorological parameters, crop characteristics, soil characteristics and environmental factors (Fig. 2.2) (Jovanovic *et al*., 2015). Therefore, ET can vary significantly over time and space. The main meteorological factors that influence the rate of ET are solar radiation, humidity, air temperature and wind speed (Allen *et al*., 1998; Jovanovic *et al*., 2015). In addition, the physical characteristics of crops play an essential role in evapotranspiration processes, as pointed out by Allen *et al.* (1998). Therefore, when assessing ET in crop fields, characteristics including crop type, leaf shape, crop height, leaf albedo and growth stage should be considered (Allen *et al.*, 1998; Brown, 2000).

A plant's stage of development, density and size influence ET to some extent (Allen *et al*., 1998; Dye, 2013). Large plants and regions with thick plant canopies tend to increase the ET rate as opposed to smaller crop types in areas with limited plant canopies that typically decrease evapotranspiration (Brown, 2000; Sello, 2019). Differences in crop height, transpiration, reflection, crop roughness, crop rooting characteristics and ground cover result in variations in evapotranspiration levels for different crops under the same environmental conditions (Brown, 2000; Courault *et al*., 2003; Sello, 2019). In addition, environmental factors such as low soil fertility, inappropriate soil salinity, lack of soil nutrients, compact soil surfaces, substandard soil management, and the presence of pests and diseases may affect evapotranspiration (Allen *et al*., 1998).

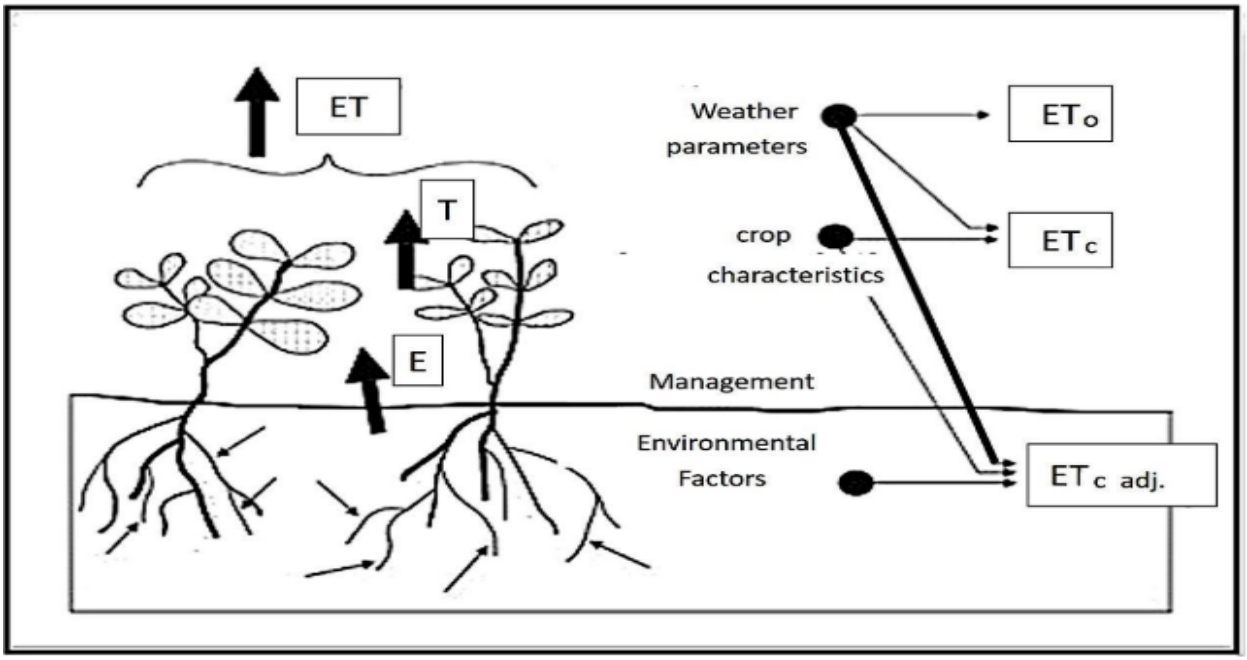

Figure 2.2: Factors regulating the rate of evapotranspiration (Allen et al., 1998).

2.3. Meteorological factors

2.3.1. Solar radiation and air temperature

Evapotranspiration is an energy-dependent process, and the energy related to meteorological and environmental factors regulates the rate at which it occurs (Huang & Fry, 2000). According to Liou & Kar (2014), ambient air temperature is determined by the amount of heat that reaches the Earth's surface and by the amount of solar radiation absorbed by the atmosphere. The ET rate of crops is influenced by sensible heat, where the air moves over crops and controls evapotranspiration (Allen *et al*., 1998; Liou & Kar, 2014). Conversely, where air temperature is lower and solar radiation less, for example, in cloudy, cool weather, moisture reduction by evapotranspiration is less compared to warm sunny weather (Allen *et al*., 1998). Solar radiation regulates ET by influencing the temperature of plants through the amount of radiation absorbed. The more the plant temperature increases, the higher the rate of ET will be (Kim & Beard, 1988; Beard *et al*., 1992; Huang & Fry, 2000).

2.3.2. Relative humidity

Decreases in ambient relative humidity result in increased ET rates as the transpiration rate depends on the vapour pressure gradient between the plant's stomatal cavity and the atmosphere (Huang & Fry, 2000). In contrast to humid regions, arid and semi-arid areas can experience relative humidity of 10% or less during summer months coupled with high temperatures, which results in water use rates far more significant than those observed in humid regions (Beard *et al.,* 1992).

2.3.3. Wind speed

Wind speed influences the convective heat fluxes between the atmosphere and the soil surface and the airflow over the soil surface (Cascone *et al.*, 2019). When vaporising water, the air above the evaporating surface becomes saturated with water vapour. If this air is not continuously replaced with drier air, the driving force for water vapour removal and the evapotranspiration rate decreases (Allen *et al., 1998)*. Wind can also increase the rate of ET by disturbing the leaf boundary layer through several mechanisms, including leaf collisions, which at higher wind speeds cause abrasions that induce higher rates of water loss through the plant cuticle. It has been found that plants constantly exposed to higher wind speeds tend to develop smaller stomata and have much lower osmotic potentials than those not frequently exposed to wind (Grace & Russel, 1977; Huang & Fry, 2000).

2.3.4. Soil characteristics

The soil factors that affect ET include soil temperature, saturated and unsaturated flow characteristics, and moisture content (Carow, 1985; Wang *et al*., 2012; Cascone *et al*., 2019). All species experience greater ET rates with increasing soil temperatures, and some studies (for example, Barbieri *et al*., 2012; Hussain *et al*., 2019) have demonstrated that ET is directly correlated with the amount of available soil water. Additionally, because cooler temperatures are typically associated with higher moisture content soils, soil moisture content can also alter ET. This is generally seen in the early phases of the growing season in locations with summer rainfall, especially in spring (Carow, 1985; Wang *et al*., 2012).

2.4. Importance of measuring evapotranspiration

The spatiotemporal distribution of water availability is controlled by terrestrial evapotranspiration. It is the centre of the Earth system's water, carbon, and energy cycles (Liu *et al*., 2020). According to most estimates, evapotranspiration absorbs over 50% of the sun's energy and transmits over 60% (up to 70% in arid locations) of the rainfall into the atmosphere (Yao *et al*., 2013). ET_c rates also control groundwater recharge and feedback to continental precipitation patterns (Liu *et al*., 2022). Therefore, understanding hydrological fluctuations requires precise and ongoing estimations of the spatiotemporal distribution of ET. Estimating evapotranspiration can provide insight into regional water management in a changing climate, including drought monitoring and agricultural water consumption efficiency (Wu *et al*., 2021; Liu *et al*., 2022).

In agriculture, evapotranspiration is an essential aspect of measuring crop water use and an important factor affecting crop productivity (Suyker & Verma, 2009). An accurate estimation of evapotranspiration from crops is crucial in irrigation management and crop yield assessments, particularly in arid regions**.** For example, in maize-soybean systems, much research has been conducted on the impact of water-related stress on crop development and yield (Denmead & Shaw, 1960; Musick & Dusek, 1980; Suyker & Verma, 2009). In addition, when rainfed agriculture occurs in semiarid regions where annual precipitation is often below potential evapotranspiration demands, continuously measuring ET throughout the growing season can assist in forecasting the potential impact of droughts on crop yields during the growing season (Stewart & Peterson, 2014). Low rainfall during the growing season can cause deficits in the amount of soil moisture available for ET from rainfall, thereby causing actual evapotranspiration (ET_c) to be less than potential ET during some years, which can result in lower-than-expected yields at harvest time (Stewart & Peterson, 2014). In some areas, fallow periods (when no crops are grown on fields) accumulate soil moisture to offset the difference between growing season precipitation and

potential ET. Conservation tillage or no-till can significantly increase the amount of soil moisture available before the start of the growing season and hence offset a deficit in the amount of soil moisture available for ET during the growing season (Stewart *et al*., 2010; Peterson *et al*., 2012). Hassan-Esfahani *et al*. (2014) point out that evapotranspiration measurements are essential in determining agriculture's current and future water needs. This is particularly relevant for South Africa, as a water-scarce country, since it requires better estimations of crop water use to assess and improve water conservation strategies and to optimise decision-making in the allocation of water resources in the context of agriculture. Since ET reflects crop water requirements under different environmental and meteorological conditions, measuring ET in the Mooi River catchment of South Africa can provide valuable insights regarding regional water demand and that of varying maize cultivars under various conditions.

2.4.1. Water-use efficiency

Water Use Efficiency (WUE) is a critical component of water conservation initiatives and is typically measured as the ratio of harvested biomass to accumulated ET. The effectiveness of various crops and cultivars under various environmental conditions in dryland and irrigated settings, as well as the impact of specific crop management strategies on WUE and ET, are all evaluated along with irrigation management practices (Djaman *et al*., 2018; Hussain *et al*., 2019). For example, Zeri *et al*. (2013) note that WUE is an essential indicator of bioenergy crop performance as it depends on how effectively crops utilise available soil moisture to produce biomass. Consequently, estimating ET is crucial for sustainable agriculture, especially with remote sensing techniques that enable doing so across large spatial extents and at a low cost. It was discovered by Barbieri *et al*. (2012) that narrow rows consistently increased crop ET during the early stages of crop growth but that the initial increases in ET were diluted during the season and ultimately negligible in terms of WUE. This is another example of how ET estimation can be used to assess WUE.

2.4.2. Irrigation management

Improving irrigation water management for crop production is becoming important in many areas of the world as water supplies shrink and the competition with ever-expanding urban areas continue to increase (Ko & Piccinni, 2008). Most consumptive use of irrigation water is transported to the atmosphere as evapotranspiration. Consequently, measuring ET is vital in irrigation management, particularly in locations where total freshwater supplies are low. A study by Ko & Piccinni (2008) on maize yield responses under different crop evapotranspiration-based irrigation management strategies found that over three years, the maize yield was highest at 100% ET-

based irrigation compared to 75% and 50%, respectively and concluded that ET-based irrigation is one of the most efficient water delivery schemes, resulting in greater WUE and grain yield with less water input.

2.5. Estimation of evapotranspiration

2.5.1. Conventional methods for ET estimation

Traditional methods for estimating ET, such as weighing lysimeters, evaporation pans, soil moisture balances, atmometers, the Bowen Ratio Energy Balance System (BREBS), and Eddy Covariance, have been extensively used to study ET (Gibson *et al*., 2013). The industry standard for measuring ET has for many years been the lysimeter because of its high degree of accuracy and for being the most direct method. Different types of lysimeters exist and generally work by extracting a soil core (monolith) from the ground and placing it into a container which contains a scale. The crop is cultivated inside the monolith in the container, and any weight loss of the monolith is attributed to soil evaporation, transpiration, as well as drainage loss by recording water that seeps out the bottom of the container, thereby computing the total ET (Evett *et al*., 2009; Unlu, 2010). However, these units are rare and not frequently used outside of research since they are expensive and immobile (Jensen *et al*., 1990). According to Unlu (2010), the Bowen ratio-energy balance (BREB) micrometeorological approach has frequently been employed to calculate ET as an alternative to the lysimeter due to its simplicity, robustness, and low cost. This method estimates latent heat flux from a surface using measurements of air temperature and humidity gradients, net radiation, and soil heat flux (Todd *et al*., 2000). Eddy covariance is similar to the BREB method in that it is also a micrometeorological approach. However, Eddy covariance is a more direct method as it directly measures turbulent fluxes, and heat or gas exchange between the underlying surface and the atmosphere *in situ,* thereby calculating evapotranspiration from these parameters (Launiainen *et al*., 2005).

All of these conventional techniques are point-based measurements, meaning they prevent ET from being estimated over large spatial extents and, as a result, from measuring ET's spatial variability, for example, on a regional scale (Unlu, 2010). Additionally, most of them are too expensive and impractical for many farmers to use, which prevents ET measurements from being done in most farming practices despite their crucial role in water conservation and understanding crop water requirements under various environmental conditions (Unlu, 2010). However, with advances in satellite technology and data acquisition, satellite-based remote sensing methods of measuring ET are growing in popularity. They can, therefore, overcome the

shortcomings of these conventional, point-based methods, particularly their lack of accounting for spatiotemporal variability (Gibson *et al*., 2013).

2.5.2. Satellite-based Remote Sensing methods for estimation of evapotranspiration

Using satellite-based remote sensing (RS) to calculate ET has become popular in recent decades. This can be attributed to its high cost-effectiveness, comprehensive and high-frequency coverage, and sufficient accuracy (Zhang *et al.*, 2016). Gibson *et al.* (2013) point out that remote sensing technology holds great promise by allowing specific water resource situations to be monitored long-term. Estimation of ET using RS started in the 1970s and has evolved into many approaches (Fig. 2.3), each with its advantages and limitations. Therefore, no consensus exists on the most accurate model (Zhang *et al.*, 2016).

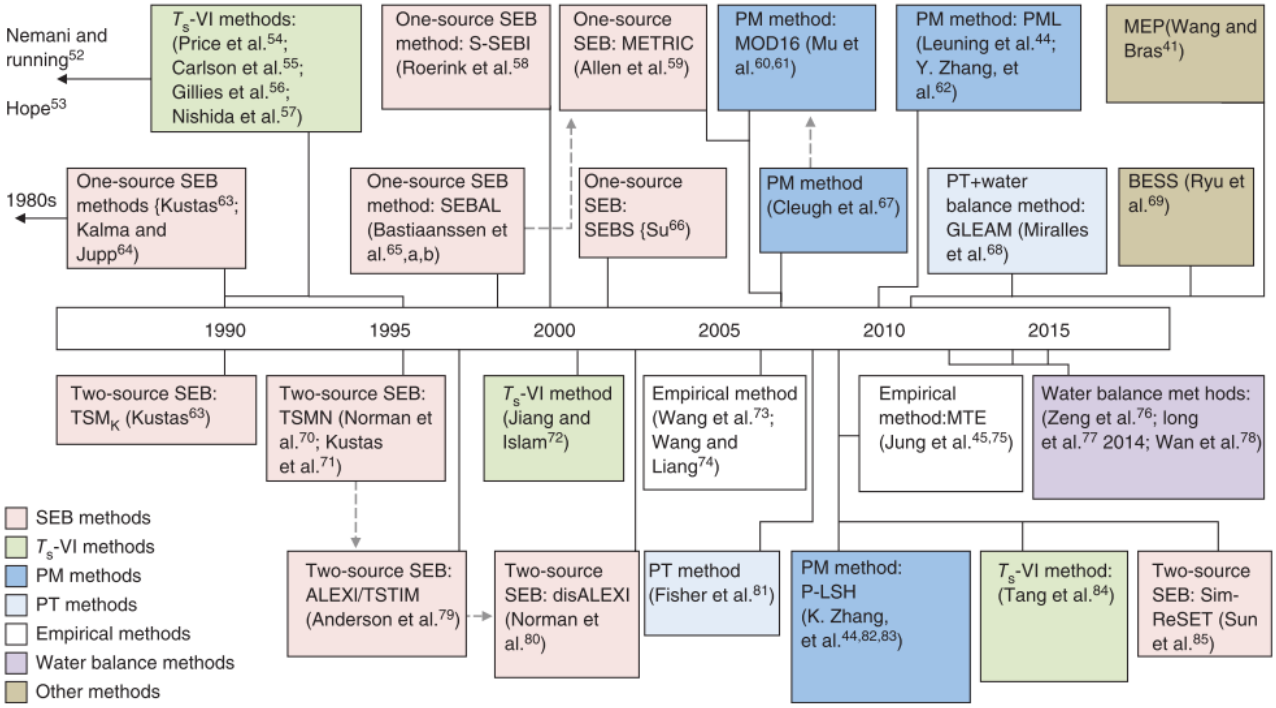

Figure 2.3: Important publications that have influenced the course of remote sensing-based ET estimation (adopted from Zhang et al., 2016).

The major RS approaches (see Table 2.1) include Surface Energy Balance Methods (single- and dual-source models) such as the Surface Energy Balance over Land (SEBAL), Surface Energy Balance System (SEBS), and Mapping Evapotranspiration at high Resolution with Internalized Calibration (METOIC) as well as empirical methods that involve the use of statistically-derived relationships between ET and vegetation indices such as normalised difference vegetation index (NDVI) or the enhanced vegetation index (EVI) (also called VI-ET_o

method), physically-based methods including the Penman-Monteith and Priestly-Taylor methods, Ts-VI Space methods, and the Water Balance method (Courault *et al.*, 2005; Nagler *et al.*, 2005; Liou & Kar, 2014; Zhang *et al.*, 2016; Majozi *et al.*, 2017).

The FAO56 crop coefficient method, is a practical and widely accepted method for estimating ET_c (where Et_c is obtained as a product between reference evapotranspiration (ET_o) and a crop coefficient (K_c). Although considered a conventional method in its basic form, there have been advances in remote sensing technologies in an attempt to increase its accuracy by accounting for spatial and temporal variability in crop and field conditions; thus, making this method suitable to use over large spatial extents. Since its integration with remote sensing technology and specifically vegetation indices, this method has also been referred to as the VI-ET_o method (Mateos *et al.,* 2013). The VI-ET_o approach is simpler compared to energy balance methods since it needs fewer measurements, and although it ignores ET reduction due to stomata closure caused by soil moisture vapour deficit (detected by energy-balance methods), it assumes that stomata closure has a relatively small effect on ET reduction compared to the effect that the size of the crop has. It also considers the reduction of growth - an indirect but important effect of crop water stress according to Mateos *et al.* (2013). Gonzalez-Dugo *et al*. (2009) evaluated several models based on the energy balance and the VI-ET_o method using a limited dataset of eddy covariance measurements of ET made over maize and soybean crops in Iowa (United States of America). That study showed that estimates of the two selected energy-balance models were satisfactory and that the estimates from the VI-ET_o method were as good as those obtained with the energy-balance models.

2.6. Crop Coefficient (K_c)

The crop coefficient (K_c) incorporates those factors that distinguish the crop that is being studied from a standard reference surface i.e., the Et_o surface. These coefficient values are often obtained from the Food and Agricultural Organization (FAO) of the United Nations (UN) Irrigation and Drainage Paper No. 56, where they are tabulated for the practical purpose of crop water management by farmers and engineers (Kamble *et al*., 2013). K_c is the quantitative form of the growth of a crop over time, and it is also called a crop growth curve (Mokhtari *et al*., 2018).

2.6.1. Factors Affecting Crop Coefficient

The factors that influence the crop coefficient include the crop type, soil, climate, and stage of crop growth (Allen *et al*., 1998). Therefore, different types of crops at different growth stages and in different environmental conditions have different crop coefficients (Fig. 2.4). Differences in

albedo, crop heights, aerodynamic properties, and leaf and stomata properties are factors that vary between different types of crops and therefore affect K_c between different types of crops. In terms of climate, the same factors that reference evapotranspiration are determined by affecting the crop coefficient, including humidity and wind speed. For example, as Allen *et al*. (1998) explain, the aerodynamic properties of maize are greatly different from that of Alfalfa reference grass and, therefore, the crop coefficient for maize increases as wind speed increases and as relative humidity decreases in a given area. Finally, the crop growth stage influences the crop coefficient since the ground cover, crop height, and leaf area all change throughout the different growth stages. The stages can be distinguished between initial, crop development, mid-season, and late season (Fig. 2.4) (Irmak, 2017).

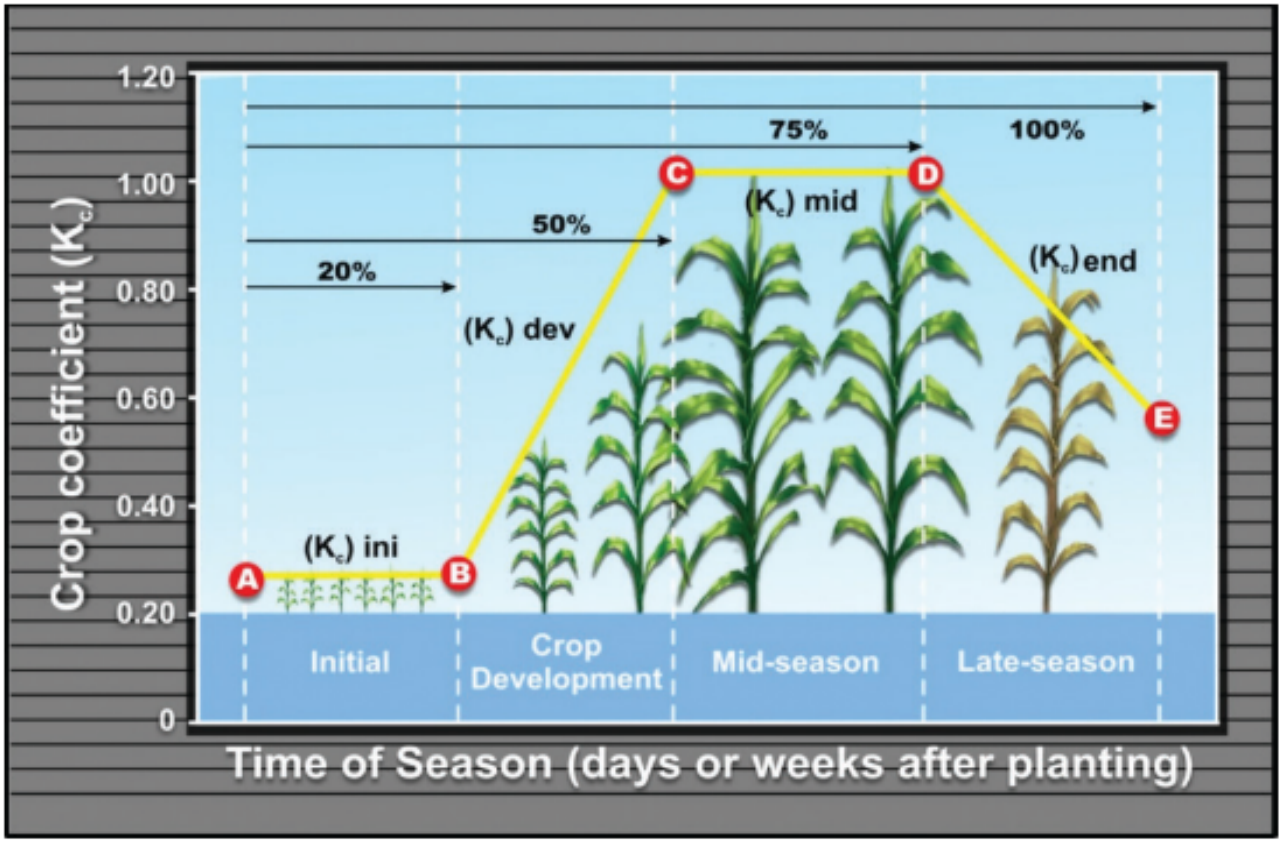

Figure 2.4: The four different growth stages of maize crops (Irmak, 2017).

Table 2.1: Summary of main RS methods, including their advantages and limitations (adopted from Zhang et al., 2016).

Model	Advantages	Assumptions/Limitations	E Partition	Minimum Forcing Data Reqs.
Open-source SEB	Simple, low requirement for metrological data	Only available for clear-sky; requires parameterization of excessive resistance and local calibration; susceptible to T_s and T_a errors; requires scaling of instantaneous to daily values	No partition	R_n, T_s, T_a
One-source spatial variability SEB	Simple, low requirement for metrological data	Only available for clear-sky; requires parameterization of excessive resistance and local calibration; susceptible to T_s and T_a errors; requires scaling of instantaneous to daily values	No partition	R_n, T_s, T_a
Two-source SEB	Simple, low requirement for metrological data	Only available for clear-sky; high sensitivity to surface temperature errors; requires scaling of instantaneous to daily values	Soil and vegetation components	R_n, T_s, T_a
Two-source time differencing SEB	Low requirement for meteorological forcing; reduced sensitivity to absolute $T_s - T_a$ differences; does not need local calibration	Only available for clear-sky; high sensitivity to surface temperature errors; requires scaling of instantaneous to daily values	Soil and vegetation components	R_n, T_s
T_s-VI methods	Low sensitivity to T_s errors; low metrological data requirement	Only available for clear-sky; relationships derived from T_s-VI space is oversimplified; requires scaling of instantaneous to daily values	Soil and vegetation components	R_n, T_s, *VI*
PM models	Process-based, physically sound, temporally continuous coverage, flexible time step, no or low requirements for surface temperature	High meteorological forcing requirements; simplified or semi-empirical estimate of canopy conductance	Soil, vegetation, and/or open water components	R_n/radiations, T_a, *VPD* or air vapor pressure, and LAI/VI
PT models	Simple; moderate requirement for meteorological forcing	Many simplifications of physical processes; requires ground heat flux as an input or assumes that it is negligible; applied on a monthly time scale	Soil and vegetation components	R_n, T_a, albedo, water vapor pressure; P, θ, and snow water equivalent needed for GLEAM
MEP model	Low requirement for meteorological forcing	Requires continuous land surface temperature to produce continuous E record	Soil and vegetation components	R_n, T_s, q_s
Water balance methods	Simple and easy to be applied	Cannot directly derive gridded E values; has coarse spatiotemporal resolution; sensitive to precipitation data error	No partition	P, Runoff, and ΔS_W
Other water-carbon linkage methods	Considering the linkage between carbon and water fluxes	Can have high requirements for forcing data and be impacted by data gaps and errors but differ in different models; empirical carbon–water relationships may be used	Usually partition into soil and vegetation components	Varies among different models.
Empirical models	Simple, easy to apply	Requires calibration; degraded capability outside of calibration area; over-simplification of physical processes; subject to weather condition if land surface temperature is required	Usually do not partition E	Varies for different models

2.6.2. Plant physiology factors

Evapotranspiration can vary greatly among crop cultivars within a species as water absorption, translocation, and transpiration are affected by many plant-morphological and physiological factors (Shearman, 1986). Shoot and root characteristics of plants are among the characteristics that affect the variability in ET between species and cultivars, along with differences in canopy configuration and growth habit, stomatal density and regulation, and leaf rolling or folding characteristics (Huang & Fry, 2000). According to Beard (1973), rooting characteristics are a significant factor in water absorption and hence have a significant impact on ET as well as water use efficiency. For example, root length density at deep soil depths has been highly correlated with water uptake (Huang & Fry, 2000). Deep plant rooting enhances water uptake from deeper soil profiles where soil moisture is available, and plants with greater root length density in deep soil layers are more capable of maintaining water uptake and stomatal conductance when soil moisture decreases compared to those with lower root length density (Carrow, 1996; Qian *et al*. 1997). Furthermore, the height of different plant species and cultivars also has an effect on ET. For example, taller than average cultivars of maize are exposed more to turbulent airflow compared to shorter cultivars and may, therefore, have higher ET rates (Huang & Fry, 2000.). Plant density (number of individuals per unit of ground area) is another factor that influences ET. Evapotranspiration can increase at lower plant densities when a relatively open canopy allows for more movement of air around plants, thereby increasing water loss from advective forces (Milani, 2019). Air that is directly above bare ground in lower plant density situations tends to be warmer than that above dense canopies. Therefore, the warmer air flowing around the plants also contributes to higher ET (Milani, 2019).

2.7. Single and dual crop coefficients

The K_c can follow either a single or dual approach. The single approach integrates the relationship between ET_c and ET_o into a single K_c which represents averaged evaporation and transpiration values from a typical cropped surface for typical frequencies of wetting (Eq. 2.1):

$$Kc = \frac{ETc}{ETo}$$

Equation 2.1: The single crop coefficient approach.

whereas, in the dual approach, crop transpiration and soil evaporation are considered separately in two individual factors (Eq. 2.2), namely the basal crop coefficient (K_{cb}) and the soil evaporation coefficient (K_e) (Allen *et al.*, 1998; Ding *et al.*, 2015; Pocas *et al.,* 2020).

$$(Kcb + Ke) = \frac{ETc}{ETo}$$

Equation 2.2: The dual crop coefficient approach.

The single K_c approach was introduced in FAO-24 (1977) long before the dual approach, where standard K_c values are listed (including in FAO-56,1998), is used to construct a standard K_c curve for standard and optimal agronomic conditions. The dual crop coefficient approach was introduced in 1998 in the FAO-56 document in order to account for variations in K_c caused by wetting events. Compared to the single K_c approach, the dual K_c approach can offer more precise estimates of daily ET_c since the soil evaporation component is calculated separately. This is especially true for days following rainfall or irrigation events since wetting events can cause increased soil evaporation, thereby causing the actual K_c values to deviate from the single, averaged K_c curve (Hunsaker *et al.*, 2005). However, as pointed out by Mateos *et al.* (2013), the application of the dual coefficient approach is limited by the lack of knowledge of the dates of irrigation and/or rainfall events. When dealing with large areas this is particularly problematic, making the dual approach not viable in such cases. The single crop coefficient approach is therefore more practical in these cases as it assumes typical wetting conditions. Furthermore, even if dates of wetting events are available from weather stations for example, when dealing with large areas, the high spatial variability of rainfall in some areas such as the South African Highveld can introduce unnecessary errors in the estimation of K_{cb} values and curves for areas and fields that are located far from weather stations (Landman *et al*., 2001; Cook *et al*., 2004; Reason *et al*., 2005; Rouault, 2014). Therefore, the lack of data in terms of wetting events and the location of the study area being on the Highveld of South Africa, contributed to the decision of using the single crop coefficient approach for this study.

For both the single and dual approach, K_c and Kc_b values are tabularized in FAO-56 as well as FAO-24 for a large diversity of crops (Allen *et al*., 1998; Doorenbos & Pruit, 1977). The single crop coefficient values which will be used in this study are listed for three main stages of crop growth namely initial (Kc_{ini}), mid (Kc_{mid}), and end (Kc_{end}) (Allen *et al*., 1998). The tabulated values for Kc_{mid} and Kc_{end} represent those for a sub-humid climate with an average daytime minimum relative humidity (RH_{min}) of approx. 45% and with calm to moderate wind speeds

averaging 2m/s. For more humid or arid conditions, or for more or less windy conditions, the K_c coefficients for the mid-season and end of season stage should be adjusted (Allen *et al*., 1998).

2.8. Crop coefficient curve and satellite vegetation indices

Using only the generalized crop coefficient values from the FAO Drainage Paper No.56 to calculate ET can contribute to estimates that deviate considerably from actual crop evapotranspiration (Hunsaker *et al., 2003;* Kamble *et al.*, 2013). This is because the K_c curve is designed to reflect ET_c for optimum and standard conditions, but when crop growth and water use deviate from the ‘’standard’’ conditions due to environmental factors such as crop stress from pests and disease, drought, nutrient deficiency, or variations in crop density for example, then conventional K_c curves and values become increasingly inaccurate as these environmental factors tend to vary considerably over space and time (Hunsaker *et al*., 2003). Hunsaker *et al.* (2003) point out that even under standard agronomic and weather conditions with minimal crop variability, applying tabulated crop coefficients will require some adjustment to account for local conditions. Remote sensing techniques offer a means of overcoming many of the shortcomings of conventional crop coefficient estimation, especially for variations in water use caused by these spatial and temporal variations in environmental factors. This is because satellite RS reflects the actual conditions that are present in the field as influenced by actual crop development patterns, local atmospheric conditions, and actual spatial variability of conditions in the field. It is widely accepted that remote sensing data is imperative for estimating spatio-temporal information on ET_c, and therefore, RS techniques have become a popular approach for estimating crop coefficients and evapotranspiration (Immerzeel *et al*., 2006; Al Zayed, 2016; El-Shirbeny *et al*., 2015; Ayyad *et al*., 2019). It has been found in several studies that similarities exist between the crop coefficient curve and that of satellite-derived vegetation indices such as the normalized difference vegetation index (NDVI) or the soil-adjusted vegetation index (SAVI) (Courault *et al*., 2005; Hunsaker *et al.,* 2003; Hunsaker *et al.,* 2005; Folhes *et al.*, 2009; Farg *et al.,* 2012; Kamble *et al*., 2013; Pereira *et al*., 2015; Zhang *et al.*, 2016; Reyes-Gonzalez *et al.* 2018; Cha *et al*., 2020). Linear regression models are typically used to estimate a relationship between the tabulated K_c values and the satellite reflectance values of crops to establish a new crop coefficient curve. Estimation of ET_c from remote sensing started in the 1970’s, and multispectral vegetation indices as near real-time surrogates specifically for crop coefficients was proposed in 1980 by Jackson *et al*. (1980) who demonstrated the close relationship between the seasonal pattern of a VI for wheat and that of the wheat crop coefficient. Bausch & Neale (1987) and Neale *et al*. (1989) established the VI-based K_c approach by deriving K_c curves for maize in Colorado based on

several VI's (Hunsaker *et al.*, 2003). Over the years, scholars developed and improved RS techniques that are replicable and useful for ET_c and K_c estimates. These improvements created less need for ground-based measurements and provided ET_c and K_c estimates at high spatio-temporal resolutions that can help decision-makers in agricultural management (Ayyad *et al*., 2019).

2.9. Crop growth stages

The FAO-56 document by Allen *et al.* (1998) provides average lengths of plant growth stages but explains that these typical growth stage lengths are only intended for use under standard crop densities and optimum farming and water management practices. Therefore, adjustment of these growth stage lengths according to local conditions is required so that the $K_{c(b)}$ curves more adequately reflect crop water use under local conditions (Hunsaker *et al.*, 2005). During the growing season, K_c generally increases from a minimum value at emergence until a maximum K_c is reached when the canopy cover is fully developed, generally during mid-season. The K_c curve tends to decline during the plant senescence phase after full cover has been reached until harvest time, depending on crop growth characteristics and management practices on the fields (Allen *et al*., 1998; Kamble & Irmak, 2008). This crop coefficient curve and seasonal distribution can be observed for most agricultural crops as K_c values depend primarily on the characteristics of canopies, such as light absorption capacity and canopy roughness, which change during the different crop growth stages (Kamble *et al.,* 2013). Justice & Townsend (2002) explain that the ratio of transpiration to evapotranspiration increases as the canopy cover develops until most of the ET comes from transpiration, and soil evaporation contributes the least amount.

2.9.1. Initial stage

The initial phase lasts from the date of planting until there is roughly 10% ground cover. The crop, the crop cultivar, the planting date, and the climate all have a significant impact on how long the initial period lasts. When roughly 10% of the ground surface is covered by green vegetation, the initial period is complete. During the initial period, the leaf area is small, and evapotranspiration is predominately in the form of soil evaporation. As a result, when the soil is moist from irrigation and rainfall, the K_c during the initial phase (Kc_{ini}) is high, and when the soil surface is dry, the K_c is low (Allen *et al*., 1998).

2.9.2. Crop development stage

The crop development stage runs from 10% ground cover to effective full cover. The start of flowering is when many crops experience effective full cover. Effective cover for row crops, such as maize, can be described as the point at which some leaves of plants in adjacent rows start to entwine so that soil shading becomes nearly complete or the point at which plants achieve nearly full size if no entwining takes place. A way to estimate the occurrence of effective full cover is when the Leaf Area Index (LAI) reaches three. LAI is defined as the average total area of leaves per unit area of ground surface (can be determined in remote sensing). Soil evaporation continuously decreases as the crop matures and progressively covers more and more of the ground, and plant transpiration gradually becomes the main process. The K_c value reflects the quantity of ground cover and plant development during the crop development stage. Depending on the crop, the frequency of wetting, and whether the crop requires more water at full ground cover than the reference crop, the K_c values will vary under different conditions (Allen *et al*., 1998).

2.9.3. Mid-season stage

Between effective full cover and the beginning of maturity is the mid-season stage. When the crop's evapotranspiration decreases in comparison to the reference ET_o, it frequently signals the beginning of maturity by the ageing, yellowing, or senescence of leaves, leaf drop, or browning of fruit. For maize specifically, the mid-season stage is the longest period in its growth cycles. Midway through the season, the K_c reaches its maximum value. For the majority of growing and cultural situations, the value of K_c ($K_{c\ mid}$) is mostly consistent. Differences in crop height and resistance between the agricultural crop and the grass reference surface, as well as weather conditions, would be the main causes of the $K_{c\ mid}$ deviating from the reference value (Allen *et al*., 1998).

2.9.4. Late season stage

The late season stage runs between the start of maturity and harvest or full senescence. At the end of this stage, the calculation for K_c and ET_c comes to an end (Allen *et al*., 1998).

2.10. Reference evapotranspiration (Et_o) and the Penman-Monteith method

Reference ET plays an important part in the Earth's water and energy cycles during crop growth as pointed out by Liu *et al.* (2016). Understanding the factors that determine reference ET and spatiotemporal variations of ET is paramount in terms of guiding water-saving irrigation, regulating agricultural production, evaluating climate aridity, understanding vegetation water consumption, and the balance of water supply and demand (Liu *et al.*, 2016).

According to Allen *et al.* (1998), reference evapotranspiration is the evapotranspiration rate from a well-watered hypothetical surface, usually, a grass reference crop such as Alfalfa that is about 20 inches tall with adequate soil moisture, free of disease, and absent of any physiological or environmental stresses is (Irmak, 2017). Since reference ET is only influenced by meteorological conditions, it represents the evaporative power of the atmosphere at a specific location and time of the year regardless of crop type, soil moisture or management practices that are present. In other words, Et_o represents the greatest evapotranspiration rate conceivable under given physical and meteorological parameters (Sello, 2019). By relating actual ET to a specific surface provides a reference to which ET from other surfaces, crop types and growth stages can be related (Allen *et al.,* 1998; Brown, 2000). Et_o is a climatic parameter estimated based on meteorological data, including solar radiation, air temperature, wind speed, and humidity from local weather stations (Reyes-Gonzalez, 2018). The FAO Penman-Monteith equation is the recommended standard for calculating Et_o from meteorological data as this method closely approximates Alfalfa Et_o (Allen *et al.*, 1998; Cai *et al.*, 2007; Djaman *et al.*, 2018). The equation is written as:

$$ETr = \frac{0.408\Delta(Rn - G) + \gamma(900/(T + 273))u2(es - ea)}{\Delta + \gamma(1 + 0.34u2)}$$

Equation 2.3: *The Penman-Monteith equation for calculating reference evapotranspiration.*

where R_n is the net radiation at the crop surface (MJ m^{-2} day^{-1}), G the soil heat flux density (MJ m^{-2} day^{-1}), T the air temperature at 2 m height (°C), u2 the wind speed at 2 m height (m s^{-1}), e_s the vapor pressure of the air at saturation (kPa), e_a the actual vapor pressure (kPa), Δ the slope of the vapor pressure curve (kPa $°C^{-1}$) and γ is the psychrometric constant (kPa $°C^{-1}$) (Cai *et al.*, 2007).

2.11. Optical remote sensing vegetation Indices

The energy reflected by the surface of biomass is calculated using remotely sensed reflectance data from satellite sensors as the difference between the incident energy and the energy directly absorbed by the leaf or canopy as well as the energy transmitted through the biomass surface to the ground or other underlying biomass (Jensen, 2000). The electromagnetic spectrum's visible, near-infrared (NIR), and mid-infrared bands (400–2500 nm) are the bands typically used for monitoring of vegetation biophysical characteristics. The proportionate amount of energy reflected by the biomass varies depending on the wavelength and area of the electromagnetic spectrum. Low values in the visible bands and high values in the NIR are typical characteristics of the leaf spectral reflectance pattern (Fig. 5) (Jensen, 2000; Pocas *et al.*, 2020).

With principal absorption bands for chlorophyll occurring at 0.43–0.45 m and 0.65–0.66 m, the leaf pigments in the palisade mesophyll are responsible for a strong absorption of incident energy in the visible spectrum, leading to low reflectance values in this spectral range. In contrast, the spongy mesophyll layer of the leaves, which is made up of many cells and intercellular air spaces where the oxygen and carbon dioxide exchanges associated with photosynthesis and respiration occur, is what causes NIR energy to be reflected (Jensen, 2000; Pocas *et al*., 2020).

Owing to the fact that different agricultural species exhibit different morphological and physiological characteristics, the leaves of different agricultural crop species have different spectral response patterns (Fig. 2.5). Additionally, spectral response patterns can vary throughout the length of a plant in response to senescence or other stress factors that affect the characteristics of the leaf, such as nutrition or water deficiencies (Carter, 1993). Generally, healthy green vegetation has high reflectance in the NIR range. As the vegetation canopy grows, more NIR energy is reflected, and less red radiant energy is absorbed for photosynthetic activities. As a result of reduced absorption by pigments and water, changes in the reflectance patterns, particularly increased reflectance at visible and infrared wavelengths, may be associated with crop stress. Furthermore, variations in the NIR reflectance pattern of healthy vegetation may be connected to the senescence, late phases of plant growth, or yellowing, of the leaves (Carter, 1993).

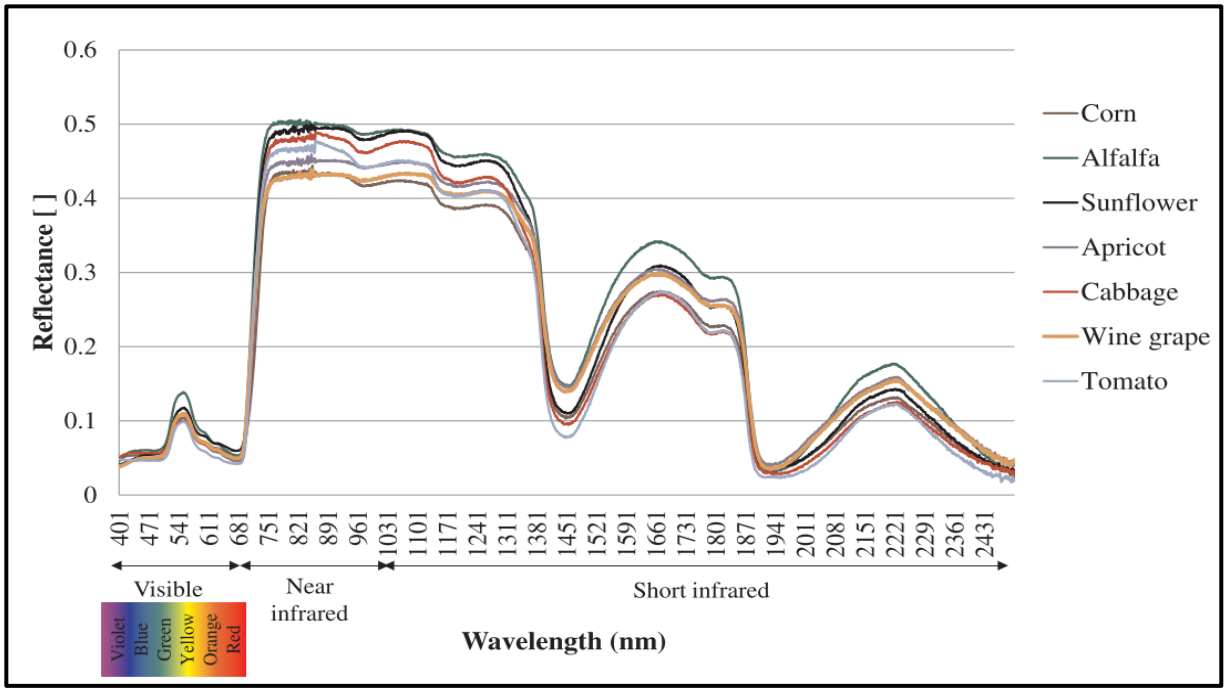

Figure 2.5: Typical leaf reflectance profiles for various types of agricultural crops (Hosgood et al., 1993).

A vegetation index is needed to make sense of these reflectance values and profiles and does so by quantifying vegetation biophysical parameters by combining a number of spectral bands in order to represent biomass and/or plant vigour for each pixel in a remote sensing image (Zhang & Kovacs, 2012; Liu *et al.,* 2016). This is primarily achieved by deriving the electromagnetic wave reflectance information from canopies and leaves using passive sensors (Xue & Su, 2017; Pocas *et al*., 2020). Many different VI's have been developed for different applications including environmental monitoring, biodiversity conservation, agriculture, and forestry (Xue & Su, 2017). In agriculture alone, many VI's have been developed to collect remotely sensed information about different aspects and types of plants and in different types of contexts. Examples include 'basic' vegetation indices such as the Difference Vegetation Index (DVI), the Ratio Vegetation Index (RVI), and the Normalized Difference Vegetation Index (NDVI); vegetation indices considering atmospheric effects include the Atmospherically Resistant Vegetation Index (ARVI), and the Atmospherically Effect Resistant Vegetation Index (AIVI); as well as adjusted-soil vegetation indices such the Soil-Adjusted Vegetation Index (SAVI), the Modified Soil-Adjusted Vegetation Index (MSAVI), and the Optimized Soil-Adjusted Vegetation Index (OSAVI) (Xue & Su, 2017; Sishodia *et al.*, 2020).

NDVI, which is one of two vegetation indices selected for this study, is calculated from multispectral information as the normalized ratio between the red and near-infrared bands. It has been used extensively for vegetation monitoring and is one of the most widely used indices for detecting variation in crop biomass, crop yield assessment and drought detection worldwide (Justice and Townsend, 2002; Kamble *et al*., 2013; Sishodia *et al.*, 2020). Generally, higher values of NDVI indicate a higher degree of photosynthesis.

$$NDVI = \frac{(NIR - RED)}{(NIR + RED)}$$

Equation 2.4: The equation for calculating Normalized Difference Vegetation Index

where:

NIR = The reflectance of near-infrared radiation

Red = The reflectance of visible red radiation

This study will include another popularly used Vegetation Index (VI), namely the Soil-Adjusted Vegetation Index (SAVI), to be compared to the Normalized Difference Vegetation Index (NDVI). The aim is to determine which of the two VIs has the strongest linear relationship with the

Food and Agriculture Organization's (FAO) tabulated crop coefficients. Thereby, the most robust parameter of the two can be identified for calculating actual crop evapotranspiration. The Soil-Adjusted Vegetation Index (SAVI) was designed to correct NDVI for the influence of soil reflectance/brightness because of differences in soil colour, soil moisture, and soil variability where vegetative cover is low by using a soil-reflectance correction factor (L) (Xue & Su, 2017).

$$SAVI = \frac{(R_{NIR} - R_{red})(1 + L)}{R_{NIR} + R_{red} + L}$$

Equation 2.5: The standard equation for calculating Soil-Adjusted Vegetation Index.

where:

NIR = The reflectance of near infrared radiation

Red = The reflectance of visible red radiation

L = The soil correction factor (related to the amount of green vegetation cover)

The range of *L* is from 0 to 1 and varies according to the amount of vegetative cover that is present. When the degree of vegetation cover is high, *L* is close to 0. Conversely, when vegetation cover is sparse, *L* is closer to 1 in order to correct soil reflectance (Xue & Su, 2017; Sishodia *et al.*, 2020).

2.12. International and South African Remote Sensing studies of evapotranspiration

2.12.1. International studies

Specific examples of where the above-mentioned methods/models of RS-based estimation of ET have been implemented in different areas of the world include that of Reyes-Gonzalez *et al.* (2018) in Comarca Lagunera, Mexico where the Crop Coefficient method ($Et_c = Et_o \times K_c$) was used to estimate ET for five irrigated silage corn fields in four different growing seasons using a satellite remote sensing-based vegetation index to calculate K_c values based on a relationship between NDVI and tabulated K_c values. Et_o was calculated from meteorological data from a weather station using the Penman-Monteith method (Reyes-Gonzalez *et al.*, 2018). Folhes *et al.* (2009) conducted a study in a semi-arid region in the northeast of Brazil where grain as well as tropical fruits are grown during two months of the growing season. In this study, the ET was estimated with the Mapping Evapotranspiration at High Resolution and with Internalized

Calibration (METOIC) model using Landsat imagery. This model uses the residual of the energy balance equation to estimate ET for each pixel in the image. A micrometeorological tower in the crop field measuring ET (eddy correlation flux measurements) was used to validate the ET values estimated by the METOIC model (Folhes *et al.*, 2009). An example of a study where the SEBAL model (a widely used RS-based model to estimate ET) was used includes that of Cha *et al.* (2020) in the Kai-Kong River Basin in North-western China, where wheat, corn, cotton, chilli, and pear is grown. Landsat images were incorporated into the Surface Energy Balance over Land (SEBAL) model to calculate daily ET values, which were then used to calculate seasonal ET estimates using the trapezoidal and sinusoidal methods (Cha *et al.*, 2020). The Disaggregated Atmosphere Land Exchange Inverse (ALEXI/DisALEXI) surface-energy balance model is often used in operational ET estimation applications. One such example is OPENET (https://openetdata.org/). OPENET is an operational ET portal that uses open-source data from multiple satellites and weather stations to provide ET estimates across the western United States. The platform provides free access to farmers, landowners, and water managers and uses both the Atmosphere-Land-Exchange Inverse (ALEXI) and DisALEXI models. These models are surface-energy balance models that work by considering time differences related to morning land surface temperature derived from geostationary satellites to surface moisture availability and latent heat flux (Knipper *et al.*, 2019). Another example where (ALEXI/DisALEXI) was implemented was part of the Grape Remote-Sensing Atmospheric Profile and Evapotranspiration experiment (GRAPEX), where evapotranspiration rates were monitored over two vineyards in central California in the United States (Knipper *et al.*, 2019).

2.12.2. South African studies

Many RS-based ET studies have been done in South Africa of which several focused on using energy balance models including Surface Energy Balance Algorithm over Land (SEBAL) and Surface Energy Balance System (SEBS) (Gibson *et al.*, 2013). Limited focus however has been placed on ET estimation of grain crops such as maize; even less so involving statistically derived relationships between ET and vegetation indices such as the Normalized Difference Vegetation Index (NDVI) in combination with the crop coefficient approach as explained by Allen *et al.* (1998).

According to Gibson *et al.* (2013), SEBAL is the most widely applied model in South Africa. However, this model is protected by intellectual property law and is not available for unaffiliated researchers to use. The Surface Energy Balance System (SEBS) model on the other hand which has been used in numerous studies in SA, is an open-source model (Gibson *et al.*, 2013). Various

types of applications for ET estimation using remote sensing techniques have been carried out in South Africa and at different spatial scales from field scale to catchment scale and regional scale (Kongo & Jewitt, 2006; Klaasse *et al*., 2008; Gibson *et al*., 2009; Gibson *et al.*, 2011; Klaasse *et al*., 2011; Jarmain *et al*., 2011a; Jarmain *et al*., 2011b; Hellegers *et al*., 2011; Jarmain & Klaasse, 2012; Ramoelo *et al*., 2014). Some examples of South African studies include Kongo & Jewitt (2006) who were the first to estimate ET using remote sensing data in South Africa at a catchment scale. This study involved a catchment's response to rainwater harvesting (Gibson *et al.*, 2013). Another study was by Gibson *et al*. (2009) who used the SEBS model to calculate annual ET for a quaternary catchment in the Western Cape province to assess the compliance of water users to water use legislation. Furthermore, SEBAL modelling was used to calculate ET by Hellegers *et al*. (2011) to assess water use competition in the transboundary Inkomati catchment shared between South Africa, Swaziland, and Mozambique. At a provincial scale, Jarmain & Meijninger (2012), using SEBAL, assessed the impact of invasive alien plant species and the clearing thereof on ET, and the availability of water resources in the Western Cape and KwaZulu-Natal provinces (Fig. 2.6).

Figure 2.6: Provincial map of South Africa.

In terms of ET studies of crops, ET and water-use efficiency were calculated for table and wine grape vineyards in the Western Cape by incorporating high-resolution Landsat imagery into the SEBAL model by Klaasse *et al*. (2008). This research was extended to include deciduous fruit-producing areas of the Western Cape and incorporated into an operational product called Fruitlook (Jarmain & Klaasse, 2012). This approach has also been used to measure water-use efficiency in sugarcane and some grain crops, where the data was disseminated on operational websites for users to view on SugarcaneLook and GrainLook (Jarmain *et al*., 2013). No similar ET studies were found to be conducted in the North-West province of South Africa on maize crops.

2.13. Literature review summary and concluding remarks

The literature review delves into different facets of evapotranspiration (ET), a key component of the hydrological cycle characterised by water loss from plant leaves and soil. This

process is influenced by a range of factors, including meteorological conditions such as solar radiation and air temperature, alongside soil characteristics and crop properties. These factors lead to temporal and spatial variations in ET rates, posing precise measurement and estimation challenges. This aspect is particularly critical in agricultural contexts, where accurate ET data is necessary.

Traditional methods for estimating ET, such as lysimeters and Eddy Covariance systems, offer accuracy but are limited by high costs and their point-based nature, restricting their use over large areas. As an alternative, satellite-based remote sensing techniques have emerged as popular because of their affordability, extensive coverage, and reasonable accuracy. These methods include Surface Energy Balance algorithms and vegetation indices (NDVI and SAVI), providing enhanced large-scale agricultural and environmental monitoring solutions. Additionally, integrating remote sensing technologies with the FAO56 crop coefficient method shows promise for improving ET estimation by considering spatial and temporal variations in plant growth and vigour.

The review concludes by highlighting the crucial role of ET in water resource management, particularly in agriculture, where it significantly impacts irrigation, crop yield, and water-use efficiency. Advanced remote sensing technologies, combined with traditional methods, offer improved ET estimation accuracy, necessary for sustainable agriculture and effective water management. While remote sensing models like SEBAL and SEBS have been widely used in South Africa, there remains a gap in utilising these methods for grain crops like maize, indicating an area for future research and development.

Chapter 3: Study area and methodology

3.1. Study area

The Mooi River catchment (Fig. 3.1) is located on the Highveld of South Africa, covering an area of 3,294 km^2. It forms part of the primary Vaal River basin and stretches from 16 km north of Potchefstroom towards Derby in the north and eastwards towards the Witwatersrand of the Gauteng province.

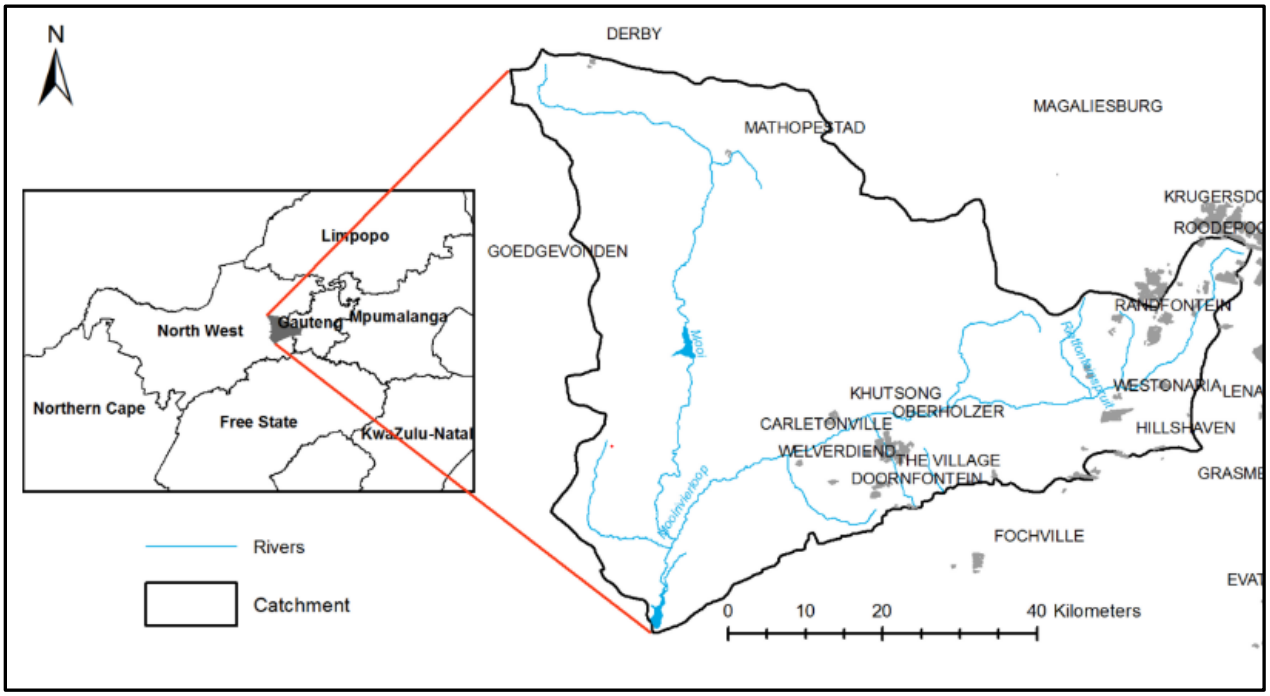

Figure 3.1:Location of the Mooi River catchment (adopted from Hauptfleisch, 2019).

3.1.1. Environmental setting and land use

The Mooi River catchment has a temperate climate with mild to warm summers. It experiences summer rainfall (Austral - October to March) with an average of 600 mm per year (Lynch *et al*., 2001; Schulze, 1997). Rainfall over the catchment has high spatial and temporal variability, with high-intensity convective storms during the summer months that frequently cause severe hail and flash flooding (Dyson, 2009). Land use of the catchment consists mainly of grazing areas, cultivated croplands, and urban areas. Main agricultural activities include rainfed agriculture of grain crops, particularly maize, as well as livestock farming and irrigated crop farming.

3.2. Methodology

The methods for this study are arranged in seven phases. Firstly, the identification of maize fields in addition to those collected during the site visit using MAXENT modelling. Secondly, the identification of maize fields with planting dates that are similar to those collected during the site visit using the Leaf Area Index (LAI). Thirdly, the reference evapotranspiration (ET_o) phase, during which the ET_o values for the isolated fields and the various satellite overpass dates were obtained from WAPOR. Fourthly, the growth stage classification where the growth stage lengths were calculated using growing degree days (GDDs) so that it could be determined which satellite overpass dates fall inside which growth stage, and thus which vegetation index values will be assigned to which tabulated K_c values. The fifth stage consisted of adjusting the tabulated crop coefficient values taken from the FAO-56 document to account for local relative humidity and wind speed conditions before they could be used in the regression analysis. The sixth stage involved the development of a linear regression model to find the relationship between the two vegetation indices (i.e., NDVI and SAVI) and the tabulated K_c values extracted and adjusted in phase 5. Lastly, phase seven calculated actual evapotranspiration (ET_c) for each field and produced the spatial and temporal maps for ET_c.

The Mooi River catchment contains 2808 cultivated areas/fields according to a shapefile obtained from the Department of Agriculture, Forestry, and Fisheries (DAFF). Several crops, including maize, soybeans, sunflowers, and lucerne, are grown on the 2808 fields and were planted at various times during the 2021–2022 growing season. During a site visit to the research area, a sample of 193 maize fields were identified by taking the GPS coordinates of each field's centre. Of these 193 fields, 28 had similar planting dates (from 10 November to 15 November 2021), while the remaining 165 were unknown. All other maize fields in the study area, besides those visually identified during the site visit, were identified by maximum entropy modelling in MAXENT. Furthermore, Leaf Area Index (LAI) was used to detect maize fields with similar growth patterns as the sample of 28 with known planting dates and were therefore considered to have been planted at a similar time.

Evapotranspiration rates of maize crops are strongly influenced by the various growth stages that the plant goes through from planting to harvest (Allen *et al*., 1998). Based on the sample that was taken during the site visit, this study concentrated on fields that had similar planting dates to focus on fields with aligned growth stages, thus making them spatially and temporally comparable in terms of ET_c when applying the FAO's Crop Coefficient Approach for calculating actual evapotranspiration.

This study will use the Crop Coefficient Approach to calculate evapotranspiration (ET). In this approach, the crop evapotranspiration (ET_c) is calculated by multiplying the reference crop evapotranspiration (ET_o), by a crop coefficient (K_c):

$$ET_c = K_c \times ET_o$$

Equation 3.1: The crop coefficient method for calculating evapotranspiration.

where:

ET_c = crop evapotranspiration
K_c = crop coefficient
ET_o = reference crop evapotranspiration

Reyes-Gonzalez *et al.* (2018) explain that a useful method to estimate ET_c for crops is to multiply reference evapotranspiration (ET_o) by a crop coefficient (K_c). The FAO has recommended the Crop Coefficient approach (Allen *et al.*, 1998). It has been used in numerous studies in combination with an empirical method to calculate K_c based on a statistically derived relationship (e.g., linear regression) between crop coefficients and Normalized Difference Vegetation Index (NDVI) values derived from satellite imagery along with other similar vegetation indices. Studies include that of Hunsaker *et al.* (2003); Hunsaker *et al.* (2005); Farg *et al.* (2012); Kamble *et al.* (2013); and Reyes-Gonzalez *et al.* (2018). Therefore, This study will incorporate the methodology by using Sentinel-2 imagery to estimate NDVI, K_c and ET_c values, whereas ET_o will be obtained from the FAO WAPOR website. Figure 3.2 is a workflow of the ET_c estimation methodology using satellite remote sensing-based vegetation index that will be used in this study, derived from Reyes-Gonzalez (2018). The following section will describe the various stages of the methodology for this study.

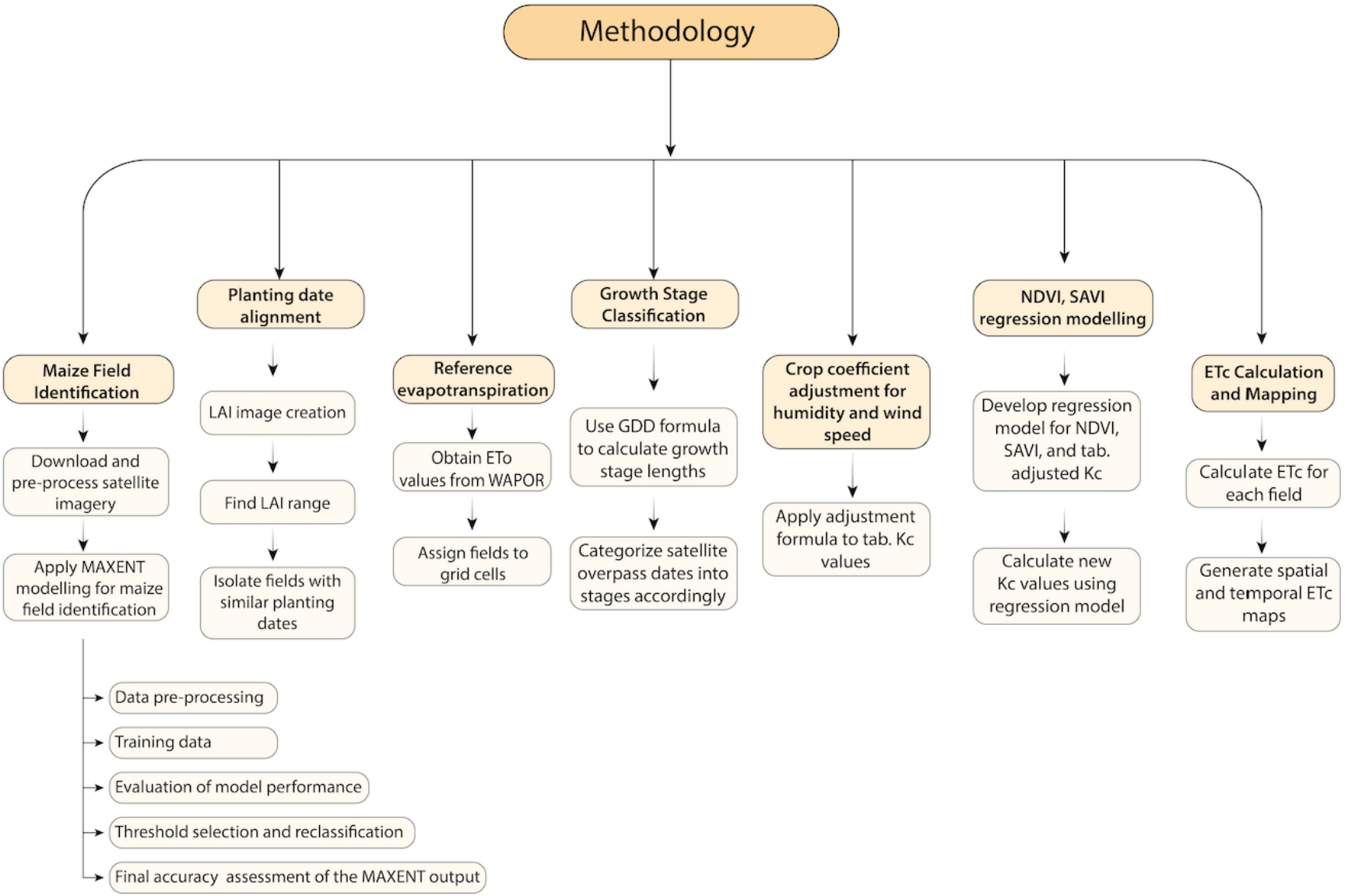

Figure 3.2: Flow diagram for project methodology.

3.3. Download and pre-processing of satellite imagery

Sentinel-2 satellite imagery tiles were downloaded in L1C (not atmospherically corrected) from Copernicus hub for all satellite overpasses between 15 November 2021 and 01 September 2022 with equal or lower than 30% cloud cover. The study area is spatially spread over four different Sentinel-2 tiles; therefore, the tiles for each date were merged before they could be clipped to the study area. Each merged image was then visually inspected for cloud cover over the study area, and those that had cloud cover over the fields in the study area were removed from the time series (the tiles are much larger than the study area; therefore, 30% cloud cover was selected with the possibility that the cloud cover will fall outside of the study area). The imagery was then pre-processed for atmospheric correction in the Sen2Cor package of R (programming language) and thereby converted to L2A format (Ranghetti, 2019).

3.4. NDVI and SAVI calculations

Vegetation index calculations were achieved by applying the mathematical equations for the Normalized Difference Vegetation Index (NDVI) and Soil Adjusted Vegetation Index (SAVI) to the downloaded imagery (Eq. 3.2 and 3.3). This process was conducted using the raster calculator in QGIS for each pixel in the downloaded imagery.

The vegetation index values for all the pixels within each identified maize field were computed to a mean value using the Zonal Statistics tool in QGIS. This was done to ensure that each field could represent an average Actual ET_c value in the study's final results, eliminating the presence of intra-field ET_c variability.

$$NDVI = \frac{(NIR - RED)}{(NIR + RED)}$$

Equation 3.2: The equation for calculating Normalized Difference Vegetation Index

where:

NIR = The reflectance of near-infrared radiation

Red = The reflectance of visible red radiation

$$SAVI = \frac{(R_{NIR} - R_{red})(1 + L)}{R_{NIR} + R_{red} + L}$$

Equation 3.3: The standard equation for calculating Soil-Adjusted Vegetation Index.

where:

NIR = The reflectance of near infrared radiation

Red = The reflectance of visible red radiation

L = The soil correction factor (related to the amount of green vegetation cover)

3.5. First phase: Identification of maize fields using MAXENT modelling.

Maximum Entropy (MAXENT) modelling was used to identify which fields in the study area had maize grown on them during the 2021-2022 growing season, in addition to those that were physically identified during a site visit to the area. Recent advances in remote sensing and geographic information system technology have made it possible to develop modelling tools such as species distribution models (SDMs), of which MAXENT is one example (Beck, 2013; Merow *et al*., 2013). Many studies in ecology, biogeography, and evolution use species distribution modelling. While there are alternative techniques, such as Grap, Bioclim, and Domain, for modelling species distributions, MAXENT is one of the crop science field's most extensively used strategies and has been utilised by agricultural enterprises for modelling crop plant distributions (Philips *et al.*, 2006; Peng *et al*., 2019). MAXENT is a multivariate approach that assesses the likelihood of the occurrence of field crops (as well as numerous other types of fauna and flora species) using historical or projected climate data at different scales. It frequently relies on general circulation models (GCMs) to forecast future climate conditions under certain change assumptions, such as rising carbon dioxide levels (Elith & Leathwick, 2009; Beck, 2013; Arajo *et al*., 2019). Utilising remotely sensed temporal series data, like vegetation indices, as the independent variable to simulate the distributions of crop varieties in any given area is a considerably more modern application of MAXENT's capability (Beck, 2013; Maguranyanga & Murwira, 2015).

Based on the presence records (point locations of verified maize fields) and environmental correlates (characteristics of the NDVI data) that have been fed into the model during the simulation, MAXENT uses the principle of maximum entropy to determine the likelihood of the occurrence of a specific spatial phenomenon (in this case, maize crops) (Philips *et al*., 2006). The model's eventual output is produced by calculating the contribution of each environmental variable. MAXENT has the benefit that it employs presence-only data, not relying on or requiring data of confirmed absences from specific locations, unlike some other SDMs that require absence data (alongside presence data) to predict species distribution (Li & Guo, 2011; Tchamba, 2018). MAXENT produces robust results with sparse, irregularly sampled data and minor location errors

(Elith *et al*., 2006). These features specifically justified the decision to use MAXENT for this study compared to other SDMs.

3.5.1. Maxent data pre-processing

Before using MAXENT, data pre-processing and geographic information system (GIS) processing were necessary to convert the data to a format compatible with the software and to make sure the model outputs would be as accurate as possible based on the input data. The environmental layers are one of the two input datasets that MAXENT needs. The model will be trained using the second type of data, which is the training data or presence data/points.

3.5.2. Environmental layers

Two more pre-processing procedures were needed before the downloaded Sentinel-2 satellite imagery could be used as environmental layer inputs in MAXENT. Firstly, to remove "noise" from the images originating from the areas in between the fields, such as roads, buildings, water bodies, grazing areas, trees, and other types of vegetation, the 11 images had first to be clipped to the field boundaries contained in the shapefile obtained from DAFF. These non-maize features would have a negative impact on the MAXENT model performance which can lead to inaccuracies.

Secondly, the 11 images had to be assessed for collinearity to remove those with high collinearity. Satellite imagery can be highly correlated, and it is essential to remove correlated variables before fitting a species distribution model to avoid overfitting the model with redundant variables. There are several ways to detect collinearity. The variance inflation factor (VIF), which measures how strongly the rest of the predictor variables can explain each predictor, is often used (Pradhan, 2016; Naimi & Araujo, 2016). To avoid overfitting, the collinear variables in this study were identified and excluded using the VIF (vifstep) approach in ‘R’ (Pradhan, 2016; Naimi & Araujo, 2016). The VIF stepwise technique calculates VIF measures, with values larger than a threshold of 10 indicating a strong correlation between variables, hence removing them owing to collinearity issues. The VIF values were recalculated as a stepwise process until all values were below the threshold. The VIF was applied and after accounting for variable multi-collinearity, seven NDVI images were left to train the models. Table 3.1 shows the NDVI images that were eliminated because they had a VIF score of greater than 10.

Table 3.1: VIF scores of all NDVI images with those highlighted in yellow being removed due to their VIF score being above 10.

Variables (image date)	VIF
12/30	1.999743
01/24	3.120391
02/13	2.923224
04/14	1.958753
05/04	3.757581
05/24	5.510512
05/29	38.238597
06/03	28.205871
06/08	28.984916
06/13	31.802195
06/18	2.477306

3.5.3. Training data/presence points

The training data consists of the coordinates of the maize fields, which have been physically validated during a field trip to the study area. Through spatial thinning, the original number of location points in this presence data was decreased from 193 to 86 (Fig. 3.3) to obtain a more equal and less cluttered spatial distribution of training datal. The programming language "R" was used to perform spatial thinning over several equal distances including 1 km and 2 km.

It frequently occurs that training data is collected only from geographical areas that are easily accessible (i.e., near major roads or towns), or as in the case with this study, from areas where it was possible to contact and visit farmers in the study area. This leads to geographic clusters of presence data (Hijmans *et al*., 2000; Boria *et al*., 2014). Such sampling biases artificially enhance the spatial autocorrelation among presence points in the study area. In such a case, the model may become overfit to environmental biases that correlate to these factors in geographic space. When a model fits calibration data too closely, overfitting occurs, which reduces the model's capacity to predict independent evaluation data and thereby affects model quality by inflating model accuracy (Veloz, 2009; Kramer-Schadt *et al*., 2013; Boria *et al*., 2014). A flawed model can result in omission errors (false negatives, where a species is falsely believed

to be absent) or commission errors (false positives, where a species is mistakenly thought to be present) (Rondinini *et al*., 2006). According to a study by Yackulic *et al*. (2013), 87% of MAXENT models were built on data that were probably subject to sample selection bias. A common technique to deal with sampling bias in presence records due to uneven sampling is the process of spatial thinning (as implemented in this study) (Kramer-Schadt *et al*., 2013; Boria *et al*., 2014). Spatial thinning reduces the number of sampling points to lessen the effects of sampling bias while keeping the most relevant data. This is achieved by placing an equal distance (selected by the user) between each presence point (Aiello-Lammens *et al*., 2015). Kramer-Schadt *et al*. (2013) recommend that spatial thinning of presence data should be implemented in situations with a strong sampling bias towards some regions (as in the case with this study).

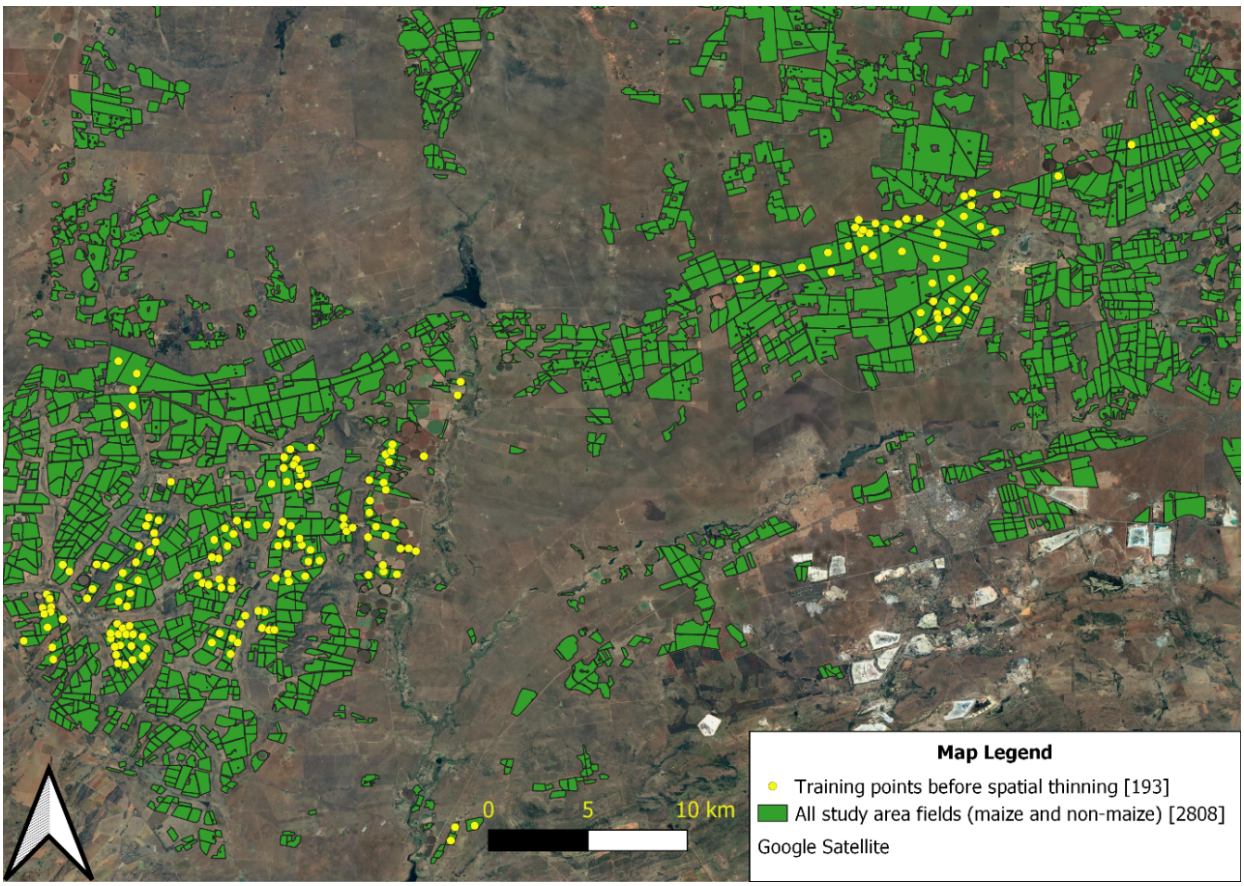

Figure 3.3: Map indicating all the training points (193) before applying spatial thinning.

The 193 training data points were processed in the 'spThin' package of 'R' using several different distance parameter values, including 1km and 2km, respectively, to determine how the MAXENT model performance will be affected by the number of training points provided. An equal

distance of 1 km was found to provide the best model performance. A similar distance of greater than 1km resulted in too few training points, therefore reducing the model performance. (Fig. 3.4).

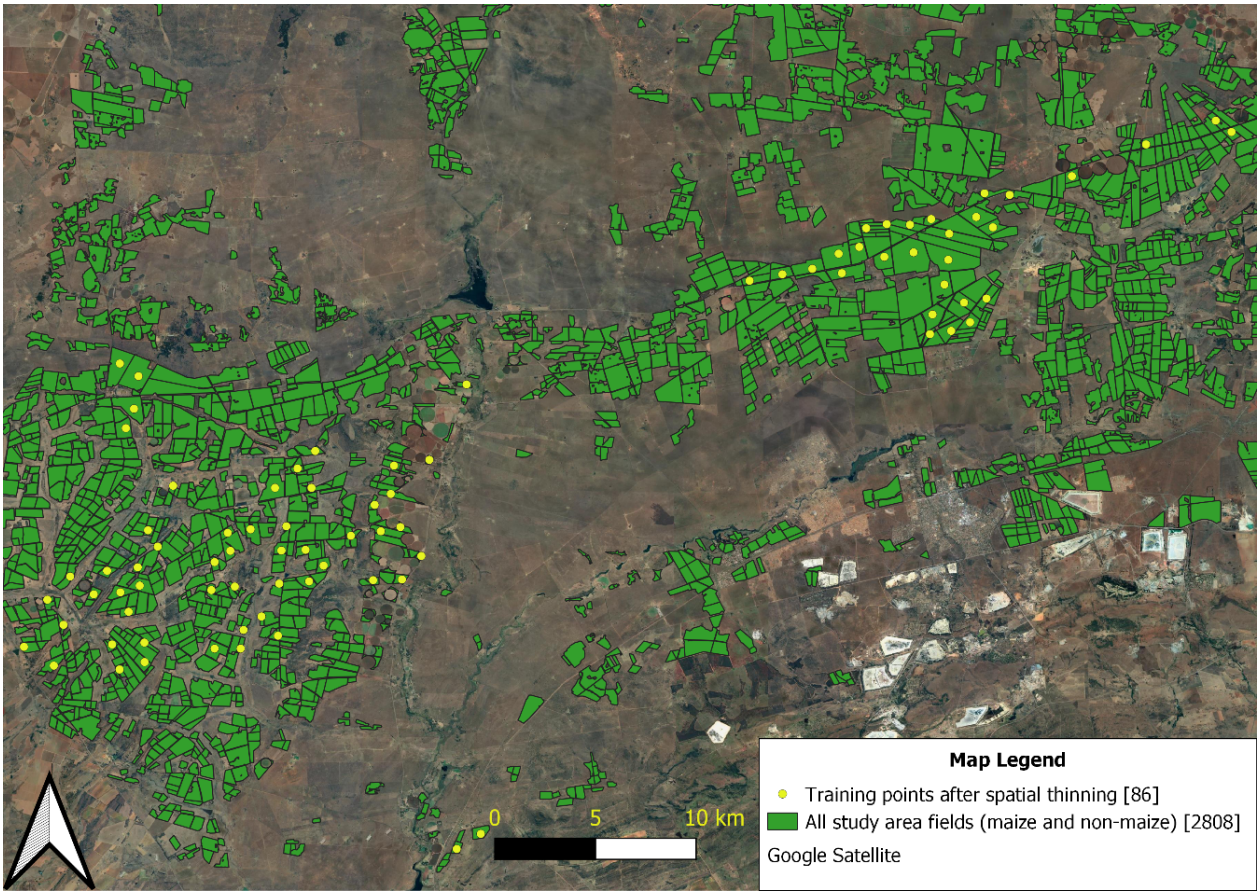

Figure 3.4: Map indicating the training points' spatial distribution (86) after applying spatial thinning.

3.5.4. Model settings and evaluation of model performance

K-fold cross-validation of the MAXENT algorithm was run with ten replicates to use all the data efficiently and to ensure a more realistic average output (Tchamba, 2018). This also helps to evaluate uncertainty in the model. For model convergence, the number of maximum iterations was set to 5,000 to provide the models adequate time for the intersection of input information to build up the models (a high number of iterations gives the models sufficient time to process the data because of avoiding over- or under-prediction of the species distribution). The number of background points for each analysis was set to 10,000 (default setting) to represent pseudo-absence locations, which the model uses to define probability distribution and estimates.

Overall validation of the model was evaluated using the threshold-independent area under the curve (AUC) of the receiver-operating characteristic (ROC), which is a plot of sensitivity

against specificity. This is a standard way of evaluating the performance of a model where the AUC graph (Fig. 3.5) shows the probability that a randomly chosen presence-only is ranked higher than a randomly selected or background location (Tchamba, 2018). AUC values range between 0 and 1, with larger values indicating a better model performance. The red curve accounts for the mean value, while the blue area represents plus or minus one standard deviation from the mean value. An AUC lower or equal than 0.5, therefore, indicates that the model predicted outcomes no better than random chance, whereas an AUC ≥ 0.7 indicate strong predictive power, and an AUC = 1.0 indicate a perfectly fitted model (Fielding & Bell, 1997; Casthilo, 2015; Maguranyanga, 2015; Peng *et al*., 2019; Tchamba, 2018; Dai *et al*., 2022). For the model run where spatial thinning of 1 km equal distance was used, the AUC was 0.743 compared to 0.711 using 2 km equal distance (Fig. 3.5). The model results using the 1km equal distance set of training points were therefore used for subsequent analysis and for identifying the rest of the maize fields in the study area.

It is generally understood that AUC < 0.7 indicates low accuracy of the model, and AUC > 0.9 indicates that the prediction results are ‘’excellent’’. Therefore, the probability of occurrence results can be adopted when AUC is 0.7–0.9 (Hosmer & Lemeshow, 2000; Dai *et al*., 2020). The jack-knife test, a built-in function of MAXENT, was used to calculate the test, training, and AUC gain that results from each variable in the model when it is present or absent from the model and when all other variables are present. These tests evaluate the variable contributions in the model explaining the distribution of maize in the study area (Philips *et al.*, 2006; Maguranyanga, 2015). According to the test, the NDVI images for the satellite overpass dates of 13 February 2022 and 30 December 2021 had the most significant contributions in predicting the probability of occurrence for maize in the study areas, whereas 05 April 2022 and 01 January 2022 had among the lowest contributions (Fig. 3.6).

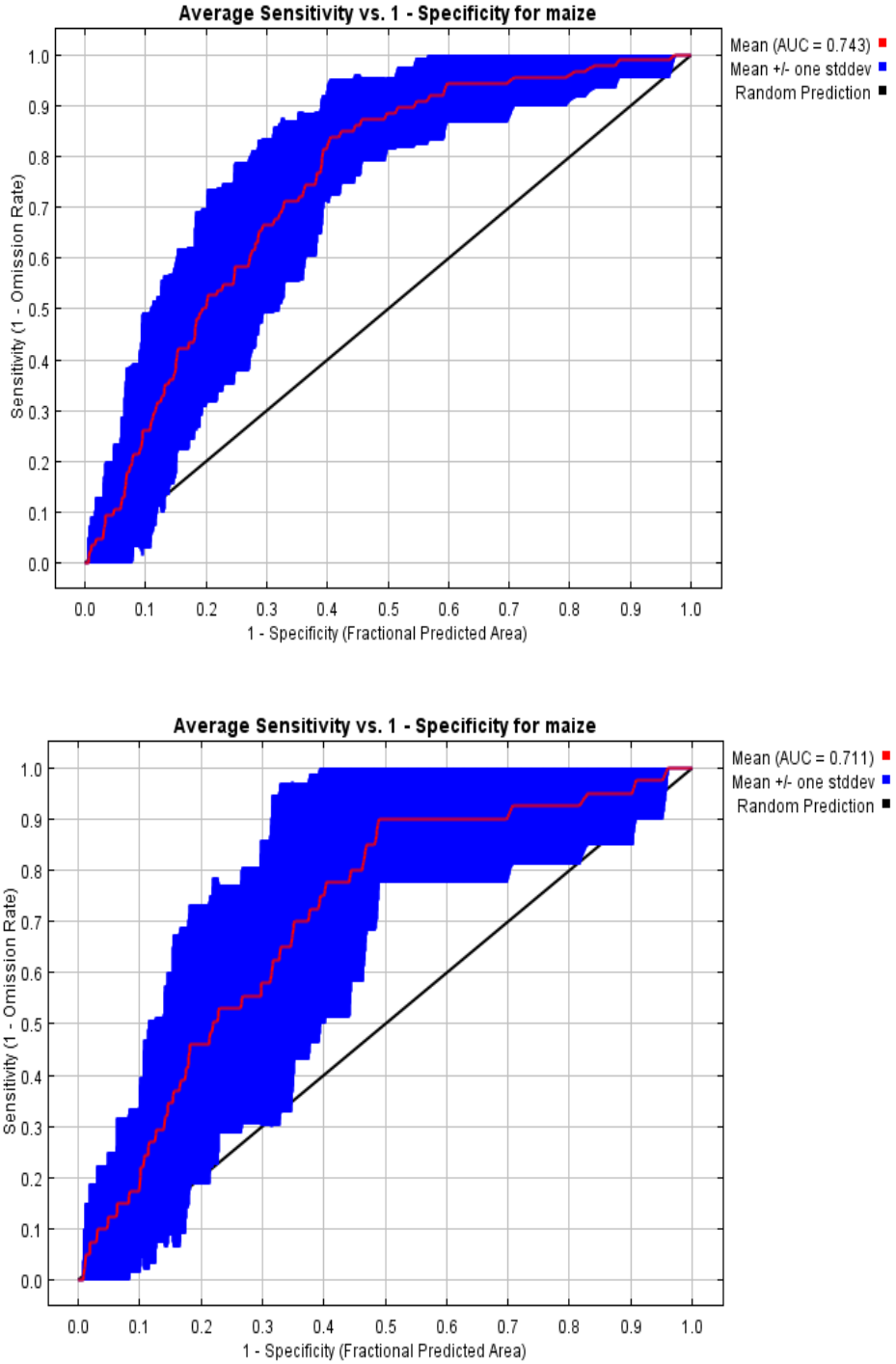

Figure 3.5: The difference in results of the AUC between using 1km (top) and 2km (bottom) equal distance spatial thinning.

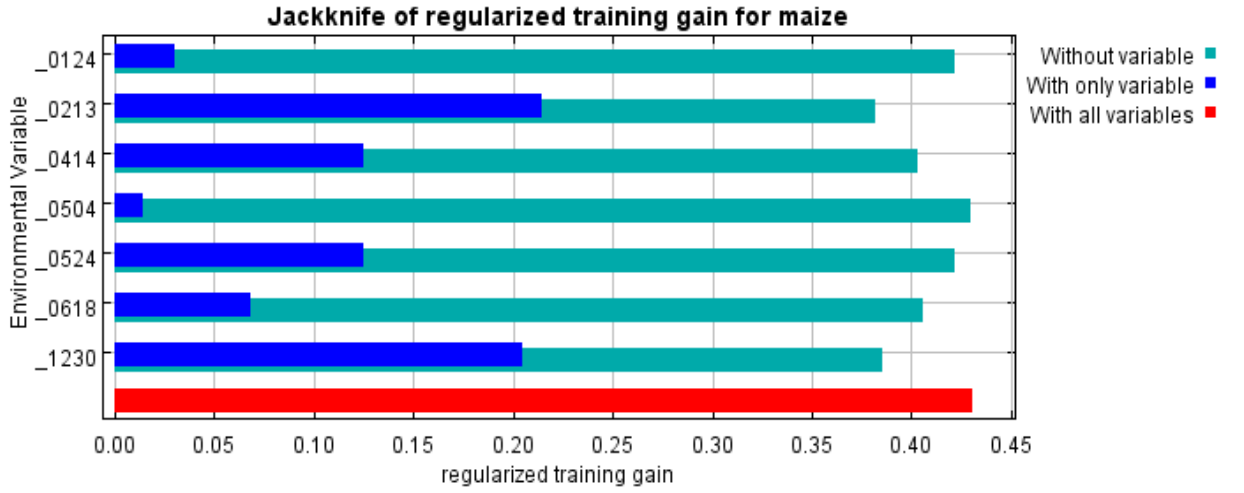

Figure 3.6: The Jackknife test results from the MAXENT model highlighting the significance of variables used in training the maize distribution.

3.5.5. Threshold selection and reclassification

MAXENT outputs include a variety of thresholds that can be used to produce a binary map, where areas and features that exceed a given threshold are deemed suitable. In contrast, those that fall below the threshold are deemed unsuitable (Casthilo, 2015). As in the 2019 study by Peng *et al.*, the "Maximum training sensitivity plus specificity" criterion was chosen for this study. A separate output is produced by each of the model's ten replicates, which results in a different threshold for maximum training sensitivity and specificity. The mean was taken from the ten different thresholds (0.52) and was used to classify the output map from MAXENT into a binary map where all pixels below 0.52 were not considered maize and those ≥ 0.52 were considered maize.

Since the MAXENT output used to produce the binary map is in raster format, the analysis above was performed at pixel level rather than field level. As a result, it was discovered that some fields only included a very small number of pixels with values below 0.52, while others were almost entirely occupied by these pixels. As a result, only those fields with at least 70% overlap with a minimum of 0.52 pixels were isolated and considered actual maize fields, with the remaining fields being rejected. The cause of this phenomenon is likely because of natural variation in the fields, which may be brought on by irregular spatial and temporal distribution of soil types, rainfall, and insect occurrence.

3.6. Second phase: Identification of fields with similar planting dates

During the second phase of the study, Leaf Area Index (LAI), a biophysical parameter of plants that can be remotely sensed, was used to find maize fields in the study area that had similar planting dates to those that were sampled during the site visit to the study area.

The different growth stages that the plant goes through during its life cycle significantly impact the evapotranspiration rates of maize crops. The size and shape of its leaves, as well as the percentage of the ground that a plant covers as it progresses through its several growth stages, from emergence to full senescence, determine the rate of evapotranspiration that takes place (Allen *et al*., 1998; Barbieri *et al*., 2012; Farg *et al.,* 2012). This study focused on fields with similar planting dates to those sampled during the site visit. This ensured that their actual evapotranspiration (ET_c) values were comparable. Analysing fields planted during the same period of time reduces variability and makes the comparisons more accurate and insightful. Comparing fields planted at different times would add unnecessary variability and complexity.

The Leaf Area Index (LAI) is one of several methods for observing the growth pattern of plants. The leaf area index is a biophysical parameter of plants that measures the one-sided green leaf area per unit ground area and is considered an indicator of canopy density and biomass (Fig. 3.7) (Wang *et al*., 2017).

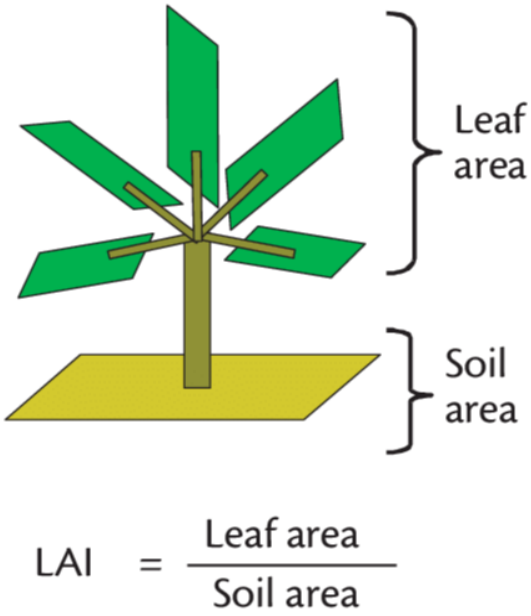

Figure 3.7: Leaf Area Index (Wang et al., 2017).

LAI tends to increase from emergence and peak at full effective cover, which is usually during the tasselling stage of maize, and then decrease again because of leaf loss in the later stage of the plant's life cycle (Allen *et al.*, 1998; Lu *et al*., 2020). According to Wang *et al*. (2017) and Luo *et al.,* (2020), LAI is one of the most widely used vegetation parameters for remote-sensing phenology extraction.

Only 28 of the 193 verified maize fields in the study area had planting dates recorded because only two local farmers could be reached to get this information. The 28 recorded planting dates were at most 5 days apart. Using LAI, it was possible to identify all the fields with planting dates that were similar (within 5 days) to the 28 fields sampled from the study area during a site visit. This was achieved by using the LAI range of values for those 28 fields from each satellite overpass date to identify fields outside the sample for which the LAI values fell within the same range. Additionally, after repeating this process for each LAI image, the resulting output layers were spatially intersected to find the overlapped fields. The remaining fields in this output were considered to have similar planting dates.

3.6.1. Leaf Area Index (LAI) image creation.

It was decided that only the first three cloudless Sentinel-2 images (12/30, 01/24, and 02/13) of the growing season would be used as the 4th image (04/14) may show signs of senescence. The biophysical processor plugin of the ESA SNAP software was used to produce LAI images at 10m spatial resolution from the L2A Sentinel-2 images. The identified maize fields produced by the MAXENT model in phase one were then used to clip the LAI images.

3.6.2. Finding the LAI range and isolating fields with similar planting dates.

The pixel values from all 28 fields with known planting dates were extracted to find the range for each of the satellite images (note that the analysis was done on pixel level for all the 28 fields together and not on field level for each individual field as an average or median). It was found that the ranges for each image were very large because of natural variation occurring on the fields, leading to extreme outliers. Many of the outliers were found to be around the edges of fields as those crops tend to be more exposed and affected by weather elements, as well as dust when they are next to gravel roads and encroachment of surrounding weeds and pests compared to those that are located further away from the boundaries of the fields. To reduce the outliers resulting from this phenomenon, all the fields were equally reduced in size by using a negative buffer of 20 m, thereby disregarding the edges of the fields. To further reduce outliers occurring closer to the centre of the fields, the upper and lower 25% of the datasets were removed by only using the interquartile range (IQR) from each satellite image.

The LAI analysis was carried out at the pixel level, similar to the *Threshold Selection and Reclassification* section of the first phase of the methodology; therefore, certain fields that had less than 70% of their area covered by pixels in the IQR were also removed. The procedure was performed for the four images, followed by a spatial intersection of the four outputs. The fields that overlapped were considered to have had the same growth pattern and, hence, similar planting dates. Only these remaining fields with similar planting dates became the subject of further analysis for determining the spatial and temporal variation of evapotranspiration over the Mooi River catchment.

3.7. Third phase: Reference Evapotranspiration (ET_o)

For this phase, a 9km (per cell) grid was placed over the study area to divide the area into different ET_o 'zones'. This allowed for fields spaced closely together to be grouped into ET_o zones. Daily ET_o values for each satellite overpass date were obtained from The Food and Agriculture Organization of the United Nations' (FAO) WaPOR (database) -portal to monitor Water Productivity through Open access of remotely sensed derived data. This was done for each cell and can be viewed in Appendix A. The ET_o values corresponding to each grid cell were assigned to those fields located within the respective grid cell.

3.8. Fourth phase: Growth stage classification

To calculate new crop coefficients, two linear regression models were developed in the fifth phase of the project (after this phase) using the tabulated crop coefficient (K_c) values from the FAO document on evapotranspiration (Allen *et al*., 1998) and two vegetation indices (NDVI and SAVI) for the fields in the study area. The satellite images used in the study and their associated vegetation index values had to be aligned with the FAO tabulated K_c values related to the different maize growth phases (i.e., initial, development, mid, and late) (see Appendix B) of maize growth to generate these regression models. The lengths of these different growth stages determined which satellite overpass dates (and their VI values) fell inside which growth stage and which vegetation index values were assigned to which tabulated K_c values.

As a result, the fourth phase of the study dealt with classifying the growth stage lengths. Generic lengths for different maize growth stages are provided by the FAO literature (Doorenbos & Pruitt, 1992; Smith, 1977; Allen *et al*., 1996 cited in Annandale *et al*., 1999), but according to Allen *et al*., 1998 and Hunsaker *et al*., 2005, these lengths should be adjusted per local conditions for K_c curves/values to reflect crop water use behaviour more adequately.

To adjust these generic growth stage lengths to reflect local conditions better, the Growing Degree Days (GDD) method was used to calculate each stage's length. The well-known GDD technique uses temperature data to identify crop development phases (Wang, 1960; McMaster & Wilhelm, 1997, cited in Pandzi *et al*., 2020). The following formula calculates it:

$$GDD = \frac{Tmin+Tmax}{2} - T_{\text{base}}$$

Equation 3.4: The formula for calculating Growing Degree Days.

where:

T_{min} = daily minimum temperature

T_{max} = daily maximum temperature

T_{base} = base temperature for a specific crop

For maize, T_{base} = 10 °C. When calculating GDD for maize, an extra restriction states that if either T_{min} or T_{max}, or both, are below 10 °C, the value of 10 °C is substituted in their place. Additionally, 30 °C is used in place of T_{max} if it is higher than 30 °C (McMaster & Wilhelm, 1997). According to McMaster & Wilhelm (1997), the growth rate of maize does not change below and above 10 °C and 30 °C, respectively.

The GDD system, also known as heat units, has roots that go back more than 250 years due to the long-standing recognition of air temperature as a crucial factor in crop development (Moeletsi, 2017). Temperature, and more specifically sums of daily temperatures, directly impact how long it takes a plant to reach a given growth stage. The amount by which the mean daily temperature exceeds a specific base temperature is typically used to define heat units. Cooler temperatures tend to inhibit growth, while warmer ones hasten maturity. Growing degree days (GDD), an indicator based on air temperature, were therefore created to identify the phenological characteristics of crops. A maize plant must accumulate a particular number of GDDs to reach each growth phase, regardless of how many calendar days it takes for the GDDs to collect.

Maize closely follows the accumulation of average daily temperatures throughout its lifetime (Moeletsi, 2017; Djaman *et al*., 2018; Pandzi *et al*., 2020; Pereira *et al*., 2021). It makes agronomic sense to define crop development period in terms of heat units rather than days since climatic conditions might lead a crop to mature early in certain regions while delaying maturation in others. Even while it might not always take the same number of days to achieve maturity or

another growth stage, the crop will always need the same number of heat units. GDD has frequently been used to estimate the lengths of maize's growth stages, even though many several factors (such as cultivar, environmental pressures, and soil qualities) can affect how long a plant takes to reach a particular stage of development (Moeletsi, 2017; Pandzi *et al*., 2020). To calculate the accumulated GDD, daily GDDs are added together starting at zero. The crop is projected to start the next phase of its development when a certain number of accumulated GDD is attained (Pandzi *et al*., 2020).

The daily air temperature data to calculate the cumulative growing degree days was obtained from the South African Weather Service (SAWS) for the Zuurbekom Automatic Weather Station (AWS) located to the east of the Mooi River catchment (Fig. 3.8). This is the closest AWS to the study area with daily air temperature data that could be obtained from SAWS.

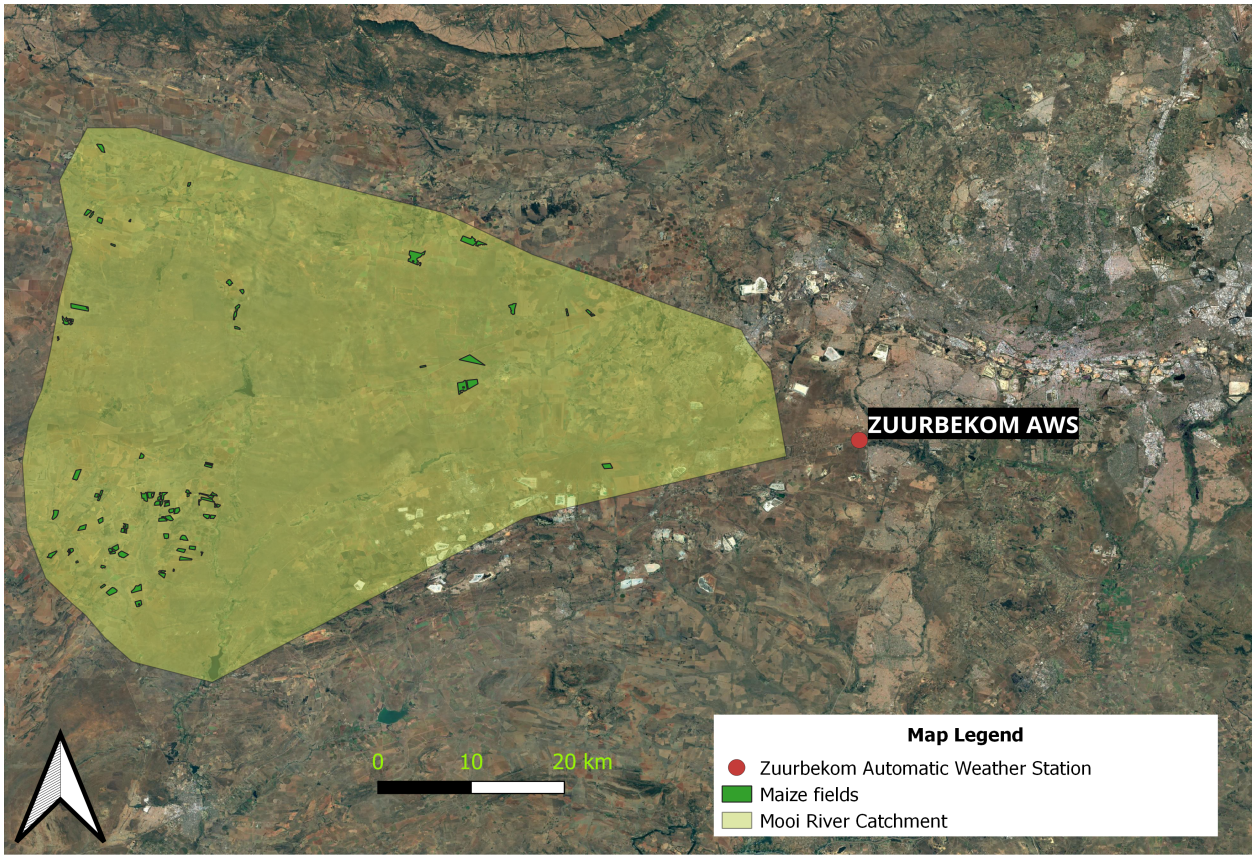

Figure 3.8: Location of the Zuurbekom automatic weather station relative to the Mooi River Catchment.

Maize growth stages are often classified into smaller sub-stages by agronomists and seed companies, as seen in Figure 3.9 (i.e. V0 to R6). However, the classification system provided by the FAO literature (Doorenbos & Pruitt, 1977; Smith, 1992; Allen *et al*., 1996 cited in Annandale

et al., 1999) (Table 3.2) was used in this study since it has been used widely in many different evapotranspiration studies that use the crop coefficient method.

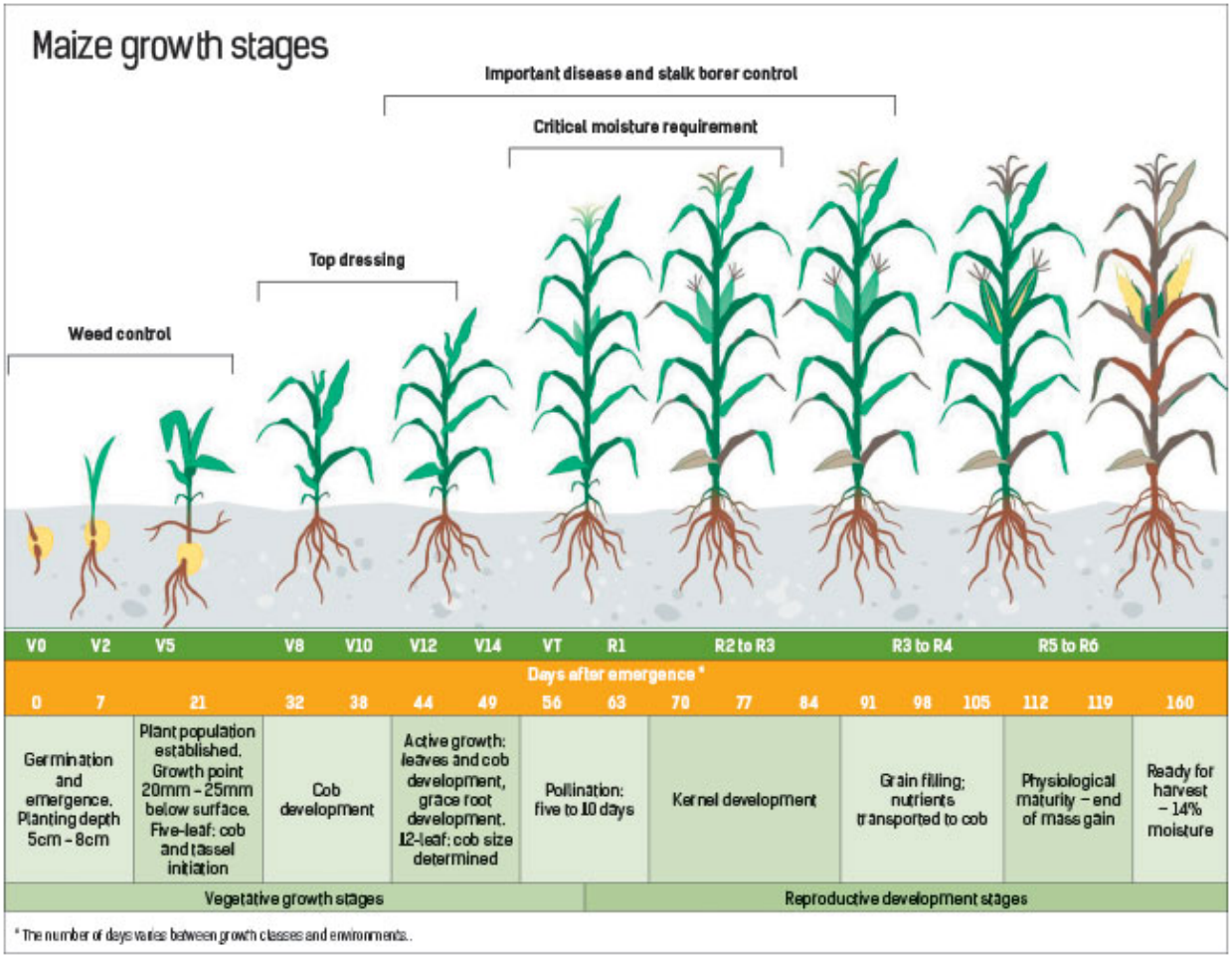

Figure 3.9: Commonly used growth stage classification used by agronomists and seed companies in South Africa (Farmer's Weekly, 2017).

Table 3.2: Broader growth stages for maize provided by the FAO (1996) cited in Annandale et al., 1999).

Crop		Maize 1	Maize 2 (cv. PNR 6552)	Maize 3 (cv. PNR 6479, Ermelo)	Maize 3 (cv. PNR 6479, Kroonstad)	Maize (cv. PNR 473, Setlagole)
Period (days)	Initial stage	20	20	20	20	20
	Development stage	50	50	50	50	50
	Mid-season stage	40	40	40	40	40
	Late-season stage	40	40	40	40	40

To estimate how many GDDs are required to complete each growth stage provided by the FAO literature, a South African study by Haarhoff (2020) conducted near Ottosdal, Northwest Province, approx. 100 km southeast of the Mooi River catchment was used (Fig. 3.10) in conjunction with an article published in Farmer's Weekly (2017). In these sources, maize growth stages are classified into smaller sub-stages (Fig. 3.9 and 3.10), unlike those provided by the FAO. Using these sub-stages (i.e., V0 to R6) as a guideline, it was determined in which of the broader FAO stages these sub-stages belonged, and thereby estimated how many GDDs were required for each of the FAO stages (i.e., initial, development stage, mid-season, and late-season stage) by using the graph in Haarhoff (2020) as a guideline. Note that both articles use Days After Emergence (DAE) compared to Days After Planting (DAP) used in this study. As a result, ten days were added to the DAE to account for the time it takes for the maize to emerge.

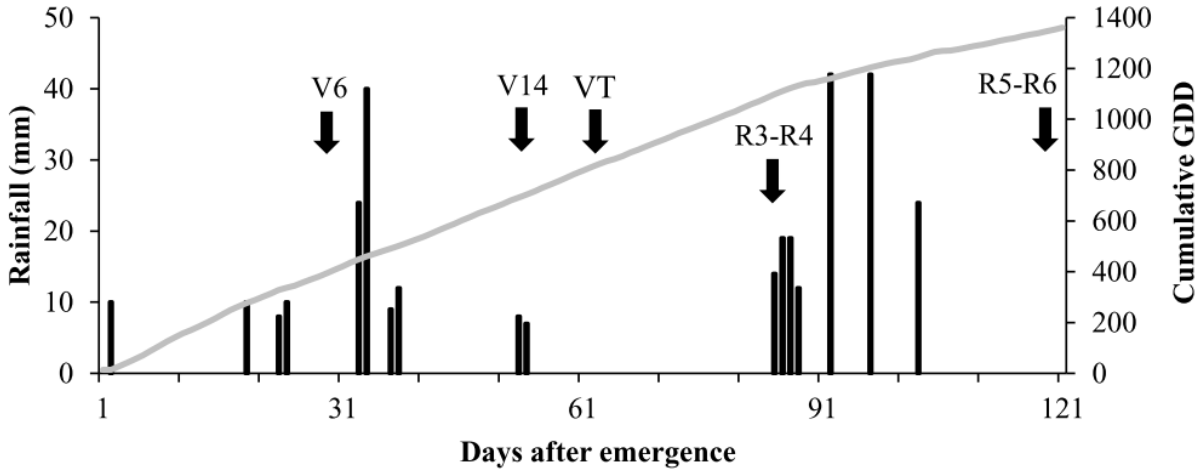

Figure 3.10: South African study near the Mooi River catchment providing the amount of GDDs it (Farmer's Weekly, 2017).

3.9. Fifth phase: Adjustment of tabulated crop coefficient values for local relative humidity and wind speed

The FAO-56 document, from which the tabulated crop coefficient (K_c) values for this study were taken, states that in climates where RH_{min} deviates from 45% or where u2 is greater or less than 2.0 m/s, the K_{cmid} (mid-season) values should be adjusted to account for local daily minimum relative humidity and daily wind speed conditions during the growth stage (Allen et al., 1998). Equation 3.5 considers the relationship between crop height and the relative impact of weather on the K_c (Pereira *et al*., 2015; Djaman *et al*., 2018). Table 4.2 displays the tabulated K_c values for maize from the FAO-56 publication.

$$Kc\ Stage = KcStage + [0.04(u2 - 2) - 0.004(RHmin - 45)]\left(\frac{h}{3}\right)^{0.3}$$

Equation 3.5: The formula for adjusting Kc_{mid} according to local weather conditions and crop height.

where:

K_cStage = standard value according to FAO-56 document

u_2 = value for daily wind speed at 2m (m/s)

RH_{min} = the value for daily minimum relative humidity during the growth stage (%)

The daily wind speed data that was received from SAWS was measured at 10 m height and, therefore, had to be converted to the standard height of 2 m before it could be used in the adjustment formula in Eq. 3.6. The graph in Figure 3.11 and the accompanying equation was used to do the conversion.

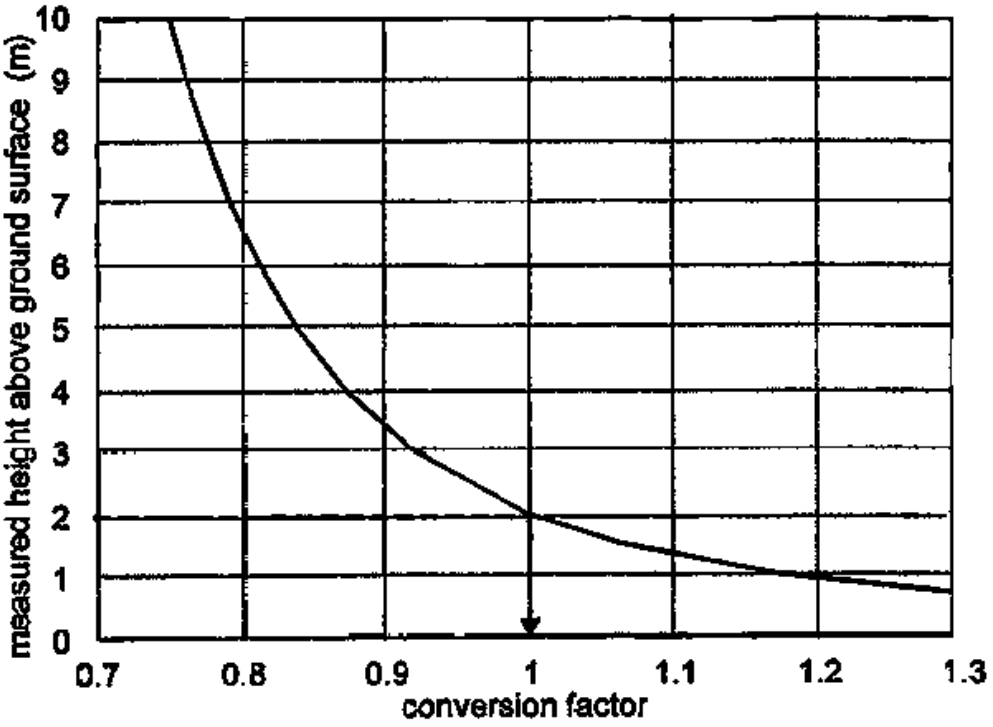

Figure 3.11: Graph showing the conversion factor to convert wind speed measured at a certain height above ground level to wind speed at the standard height (2 m) (Allen et al., 1998).

$$u2 = uz \frac{4.87}{(67.8z - 5.42)}$$

Equation 3.6: The formula for converting wind speed measured at a certain height to wind speed at 2 m.

where:

u_2 = wind speed at 2 m above ground surface (m s^{-1})
u_z = measured wind speed at z m above ground surface (m s^{-1})
z = height of measurement above ground surface (m)

The K_c values for the development stage (after the initial stage) were calculated by linear interpolation between the initial stage K_c (0.3) and the mid-season stage K_c (1.14). The K_c values between the mid-season stage K_c (1.14) and the late-season/end K_c (0.35) were also calculated by linear interpolation.

3.10. Sixth phase: Regression analysis for NDVI, SAVI and tabulated K_c values

The sixth phase aimed to determine the relationship between the Normalized Difference Vegetation Index (NDVI), the Soil-Adjusted Vegetation Index (SAVI), and the tabulated crop coefficient values. For this purpose, simple linear regression was used, with the vegetation indices (NDVI and SAVI) extracted from satellite imagery as independent variables and the tabulated K_c values functioning as the dependent variable (Table 3.3). The vegetation index with the strongest relationship, identified by the highest correlation coefficient with the tabulated K_c values, was selected, and the corresponding linear regression model was applied to generate the new K_c values. These newly derived K_c values played a crucial role in subsequent calculations as they were used to compute actual evapotranspiration (ET_c) by multiplying them with the Reference Evapotranspiration (ET_o) in phase 7 of the study.

Table 3.3: The acquisition dates, day after planting (DAP), growth stage, and satellite used for providing the NDVI and SAVI data used in the regression model.

Acquisition Dates	DAP	Growth Stage	Satellite
2021/11/30	20	Initial	Sentinel-2
2021/12/10	30	Development	Sentinel-2
2021/12/25	45	Development	Sentinel-2
2021/12/30	50	Development	Sentinel-2
2022/01/24	75	Development	Sentinel-2
2022/02/03	85	Mid-season	Sentinel-2
2022/02/13	95	Mid-season	Sentinel-2
2022/02/28	110	Mid-season	Sentinel-2
2022/03/26	136	Late-season	Landsat-7

3.11. Seventh phase: Calculation of actual evapotranspiration (ET_c) for each field and production of spatial and temporal maps

The seventh phase of the study involved the calculation of actual evapotranspiration for each field, identified as maize, within the Mooi River catchment. This was accomplished by multiplying the calculated crop coefficient value (new K_c) - derived from the NDVI-tabulated K_c regression model, determined in phase six - by the corresponding reference evapotranspiration (ET_o) value for each field, which was determined in phase three. Following this, actual evapotranspiration (ET_c) maps were produced using QGIS. These maps demonstrate the spatial and temporal variation of ET_c across the Mooi River catchment.

Chapter 4: Results

The results for each phase, as indicated in Chapter 3, are presented in this chapter. The initial phase utilised maximum entropy (MAXENT) modelling to pinpoint maize fields during the 2021-2022 growing season, while the second phase employed the Leaf Area Index (LAI) to identify fields with similar planting dates. In the third phase, the daily reference evapotranspiration values (ET_o) were obtained from the Food and Agriculture Organization of the United Nations (FAO) WaPOR database and assigned to corresponding grid cells. The fourth phase entailed classifying maize growth stage lengths using the Growing Degree Days (GDD) method. In the fifth phase, the FAO-56 documented K_{cmid} value was adjusted to reflect local humidity and wind speed conditions. The sixth phase developed regression models exploring the differences in the relationship between SAVI and NDVI and the tabulated K_c values. Lastly, the seventh phase entailed the computation of actual evapotranspiration for each maize field, ultimately producing spatiotemporal ET_c maps.

4.1. First phase

In the first phase, maximum entropy (MAXENT) modelling was used to identify all the fields in the study area that had maize grown on them during the 2021-2022 growing season based on NDVI satellite imagery and a ground-truthed sample of maize fields identified during a site visit (Fig 4.1).

Even though MAXENT conducts internal evaluations of model performance and accuracy, an external evaluation was carried out to ensure that the model correctly recognises fields of planted maize. This was accomplished by using the 107 validated maize field points that were removed by the spatial thinning analysis (where only 86 of the 193 points were kept for training data in the model) as testing points and overlaying them with the fields layer produced in the *Threshold Selection and Reclassification* section of the first phase of the methodology. Only 19 of the 107 testing points did not spatially match a maize field, indicating that the maize field map produced by the MAXENT modelling was 82% accurate.

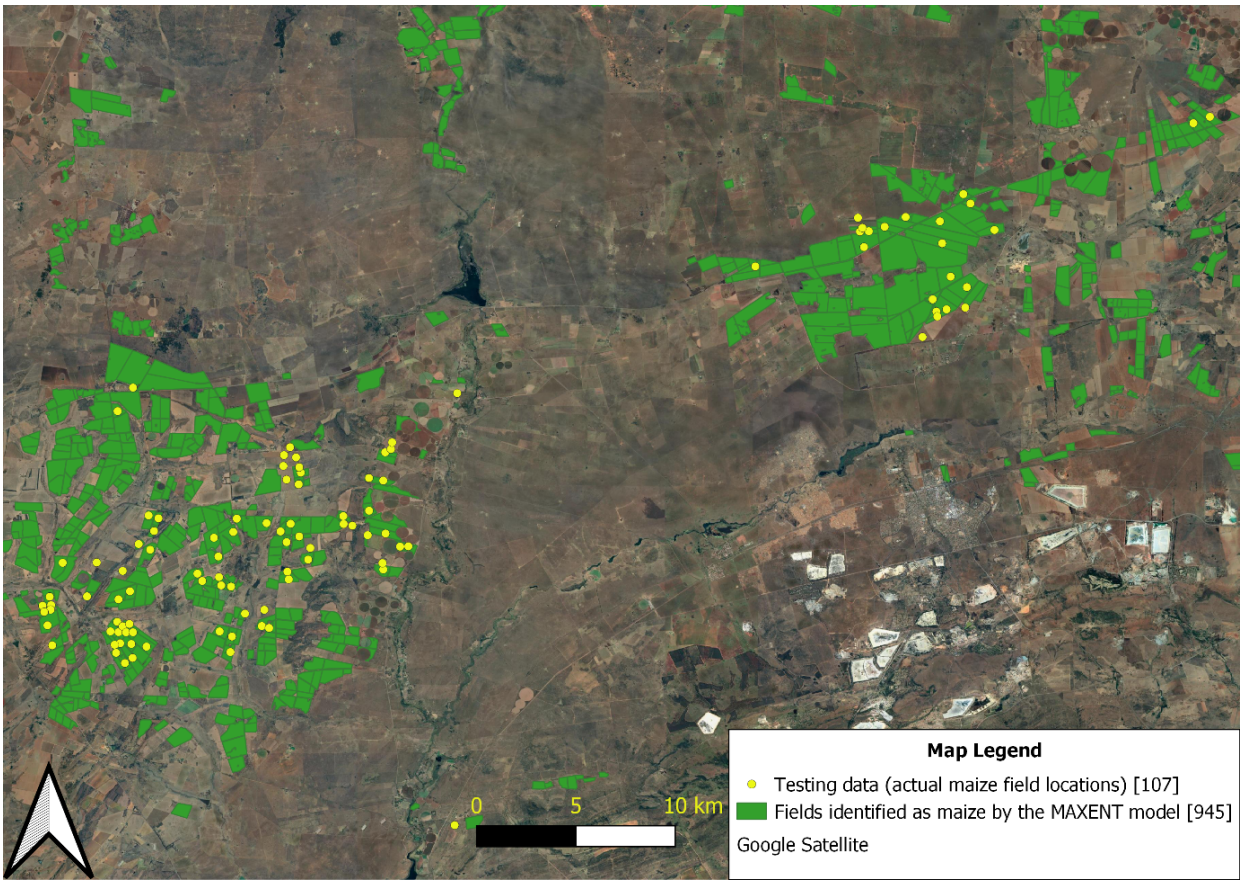

Figure 4.1: Map indicating the 88 testing points spatially matching the fields identified as maize by the MAXENT model, and the 19 that did not (the areas where no fields appear underneath testing points).

4.2. Second phase

In the study's second phase, the Leaf Area Index (LAI) was employed to identify maize fields within the study area that shared similar planting dates with the fields sampled during the site visit to the study area. Of the 945 maize fields identified by the MAXENT model, 87 were found to have similar planting dates (between 10 and 15 November 2021) (Fig. 4.2). As a result, only these 87 fields were considered for analysis in the subsequent phases of the study.

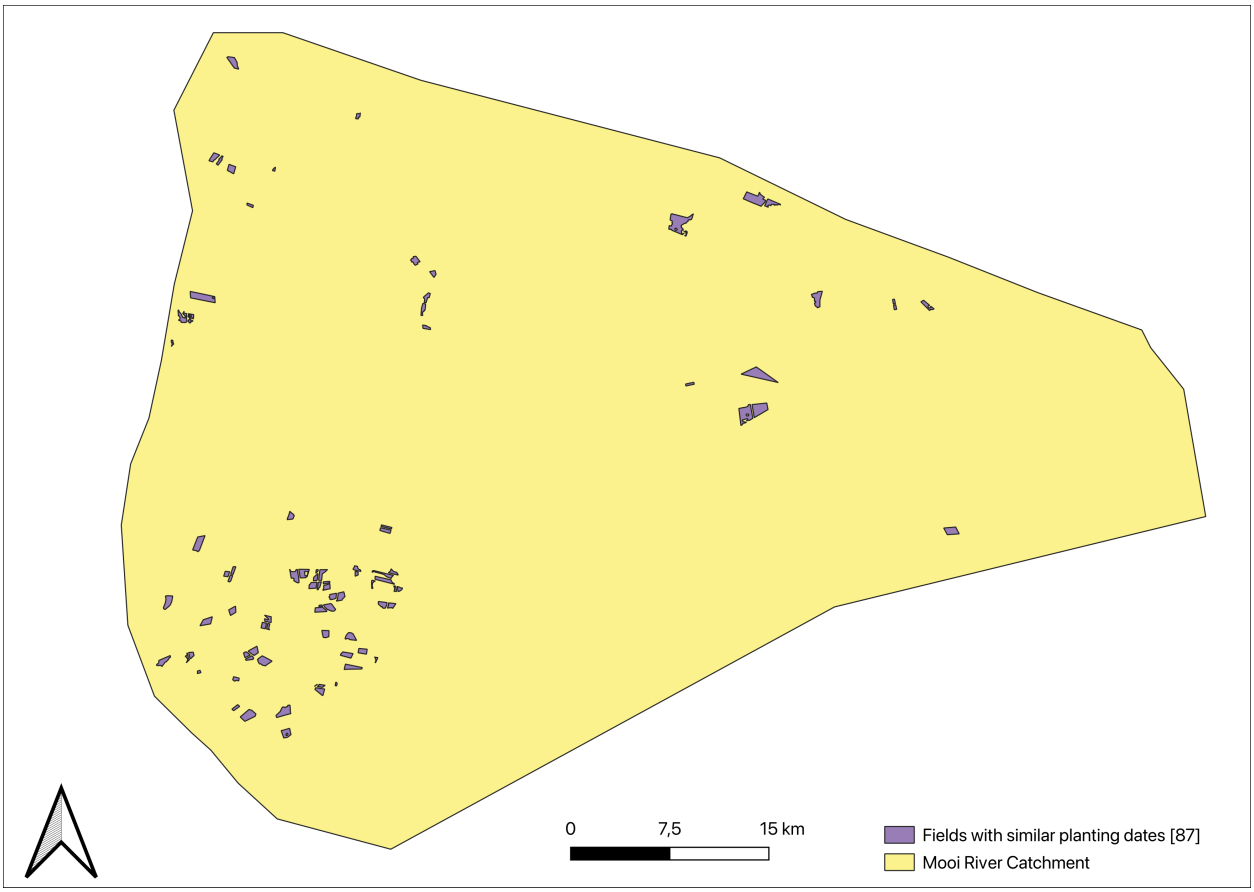

Figure 4.2: Maize fields with similar planting dates.

4.3. Third phase

Daily reference evapotranspiration values (ET_o) were obtained for each of the satellite overpass dates from The Food and Agriculture Organization of the United Nations (FAO) WaPOR database and assigned to each of the fields' corresponding grid cells so that fields that are spaced closely together share the same ET_o value (Fig 4.3). The table indicating the ET_o values for each respective grid cell and field can be viewed in Appendix A.

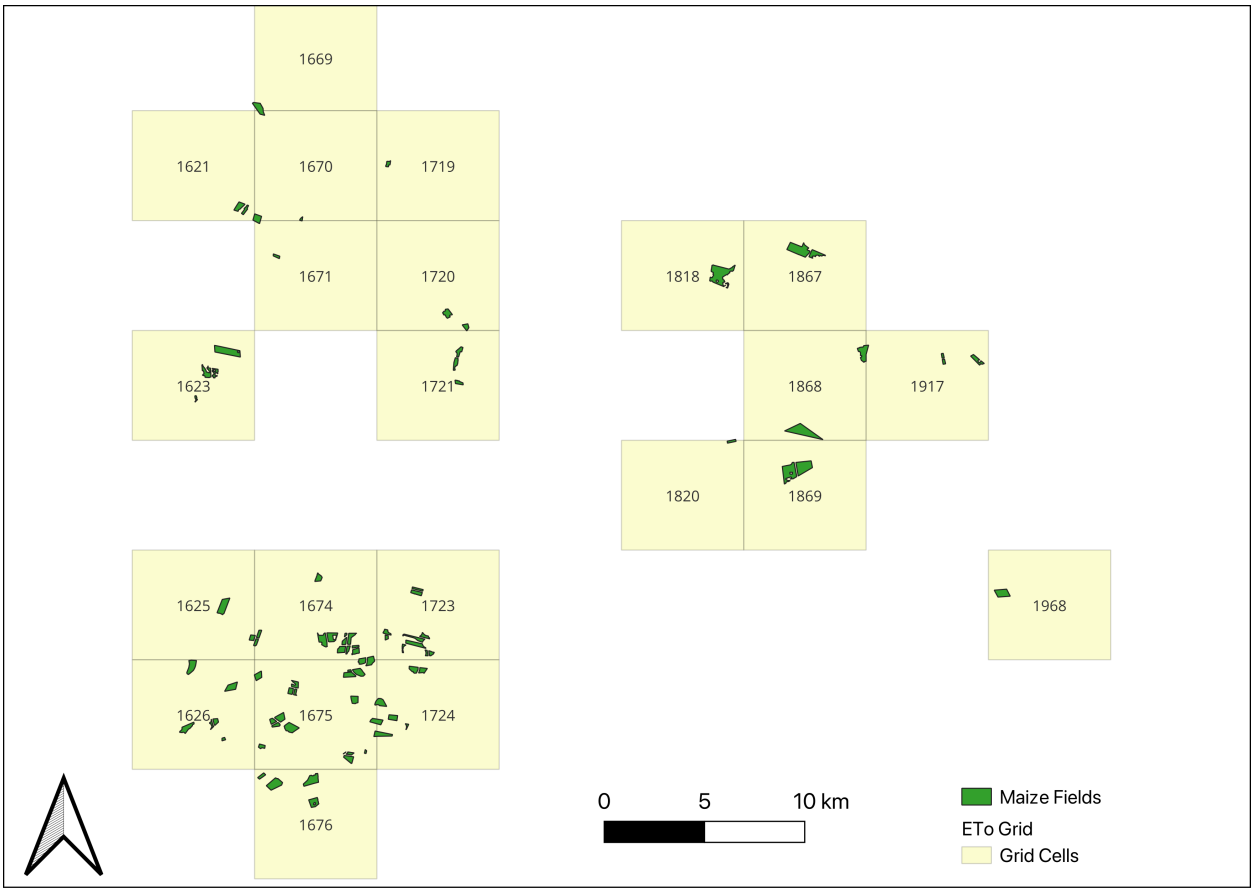

Figure 4.3: ET_o zones represented by the 9 km grid cells over the maize fields in the study area and the IDs of each of the cells.

4.4. Fourth phase

During the fourth phase of the study, maize growth stage lengths were classified and adjusted to local conditions, following the recommendations of Allen *et al*. (1998) and Hunsaker *et al*. (2005). To do this, the study utilised the Growing Degree Days (GDD) method (Wang, 1960; Cross & Zuber, 1972; McMaster & Wilhelm, 1997, cited in Pandzi *et al*., 2020) to calculate the duration (length) of each growth stage. To estimate how many GDDs are required to complete each growth stage provided by the FAO literature, the South African study by Haarhoff (2020) conducted approximately 100 km southeast of the Mooi River catchment was used in conjunction with an article published in Farmer's Weekly (Anon, 2017). This allowed for a more accurate estimation of the GDDs required for each stage. Appendix B presents the classification of growth stages based on the GDDs calculated from the temperature data provided by SAWS. As per Haarhoff's study (2020), it took 280 GDDs to complete the initial stage, 860 GDDs for the development stage, 1260 GDDs for the mid-season stage, and 1400 to conclude the late-season

stage (refer to Appendix B). These values were applied to establish the cut-off dates for each stage using the GDD formula, thereby tailoring the growth stage lengths to local conditions as advised by Allen *et al*. (1998).

The growth stage lengths and dates were identified in Table 4.1. after all deductions and GDD calculations were completed:

Table 4.1: Final growth stage lengths for the Mooi River Catchment after all calculations.

	Initial stage	**Development stage**	**Mid-season stage**	**Late-season stage**
Start date	2021/11/11	2021/12/09	2022/02/04	2022/03/14
End date	2021/12/08	2022/02/03	2022/03/13	2022/03/30
Total duration (days)	28	57	38	27

4.5. Fifth phase

In the fifth phase of the study, the tabulated Kc_{mid} (mid-season) value (1.20) taken from the FAO-56 document (Allen *et al*., 1998) was adjusted to account for local humidity and wind speed, which varied from standard conditions. An equation (Eq. 3.5) linking crop height and weather impact on K_c was employed for the adjustment. Wind speed data, initially recorded at 10m height, was adapted to the standard 2m height for the adjustment formula. The adjusted K_{cmid} value can be seen in Table 4.2.

K_c values for the development stage were determined by linear interpolation between initial (K_c 0.3) and mid-season stage values (K_c 1.14). Likewise, K_c values between mid-season (K_c 1.14) and late-season (K_c 0.35) were derived using linear interpolation (Fig. 4.4).

Table 4.2: Tabulated K_c values for maize extracted from FAO-56 (Allen et al., 1998) and the adjusted K_{cmid} using Eq.3. 5 and 3. 6.

	Initial Stage	**Mid-season Stage**	**Late-season Stage (end)**
K_c	0.3	1.20 1.14 (adjusted)	0.35

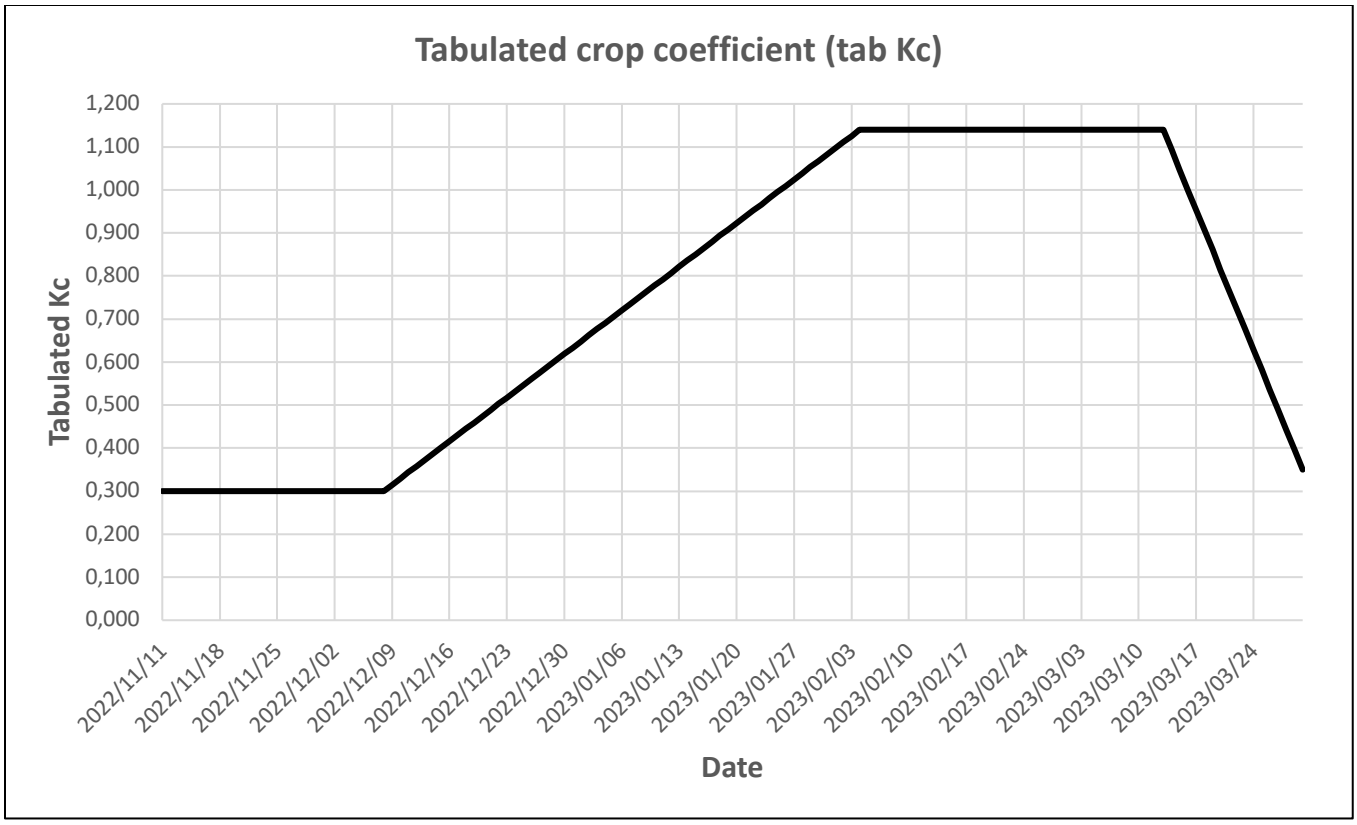

Figure 4.4: Graph showing the tabulated Kc curve after Kc_{mid} was adjusted.

4.6. Sixth phase

The sixth phase of the study involved the development of two regression models: one involving NDVI and tabulated K_c values and the other involving SAVI and tabulated K_c values. The aim was to ascertain which vegetation indices have a stronger relationship with the tabulated K_c values.

The resultant regression analysis showed marked differences in the relationship dynamics between each index and the tabulated crop coefficient (K_c) values. A notably robust correlation was detected for NDVI, indicated by a coefficient of determination (R^2) of 0.90 (Fig. 4.5). This model exhibited an exceptional predictive relationship between NDVI and K_c values, with 90% of the variation in K_c values being accounted for by changes in NDVI. The relationship was statistically significant, as evidenced by a p-value below the pre-determined significance level of 0.05 ($p < .00001$), underscoring the improbability of such a relationship emerging by chance.

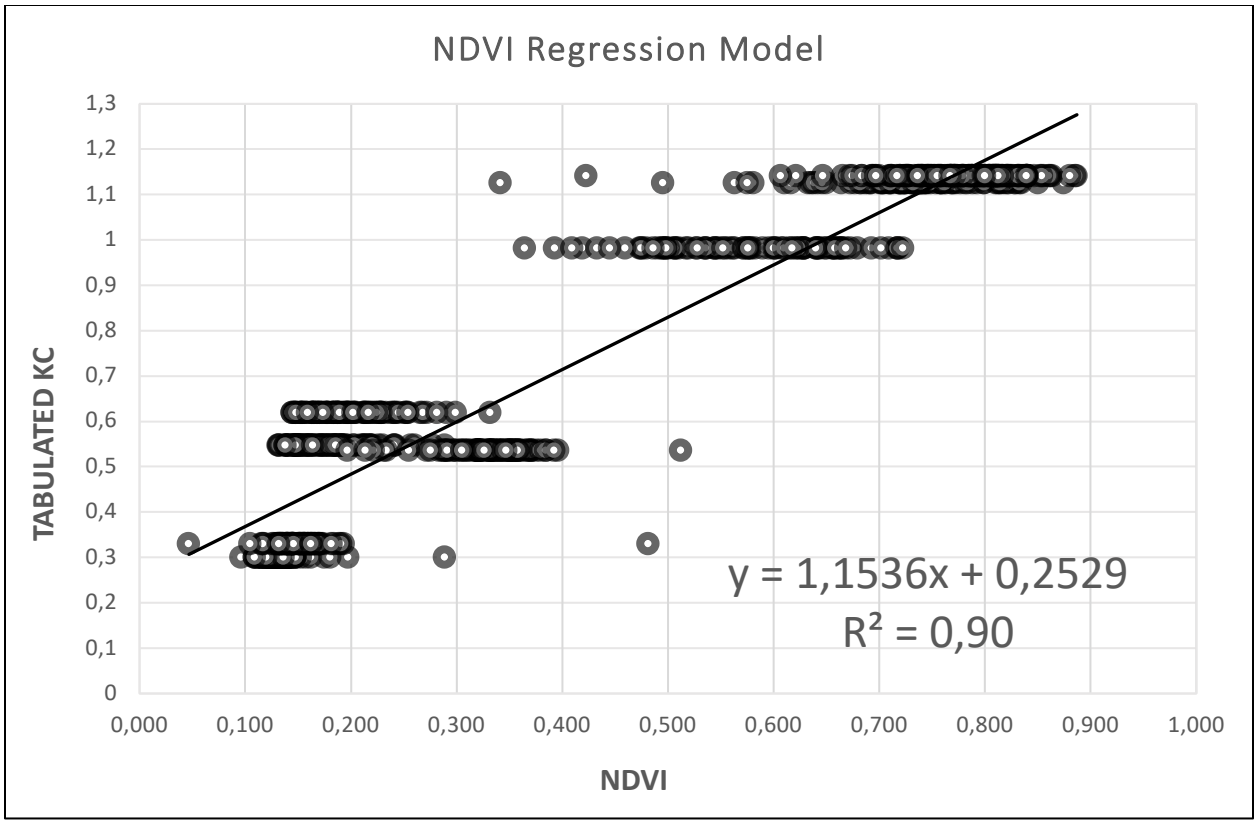

Figure 4.5: Linear relationship between NDVI and tabulated Kc for all satellite imagery indicated in Table 3. 3.

Conversely, the relationship for SAVI was weaker, indicated by a notably lower R^2 of 0.68 (Fig. 4.6). Even though the relationship was also statistically significant ($p < .00001$), it accounted for a somewhat lower proportion of the variance in K_c values. This implies that, although SAVI predicts K_c values, it does so with less precision than NDVI.

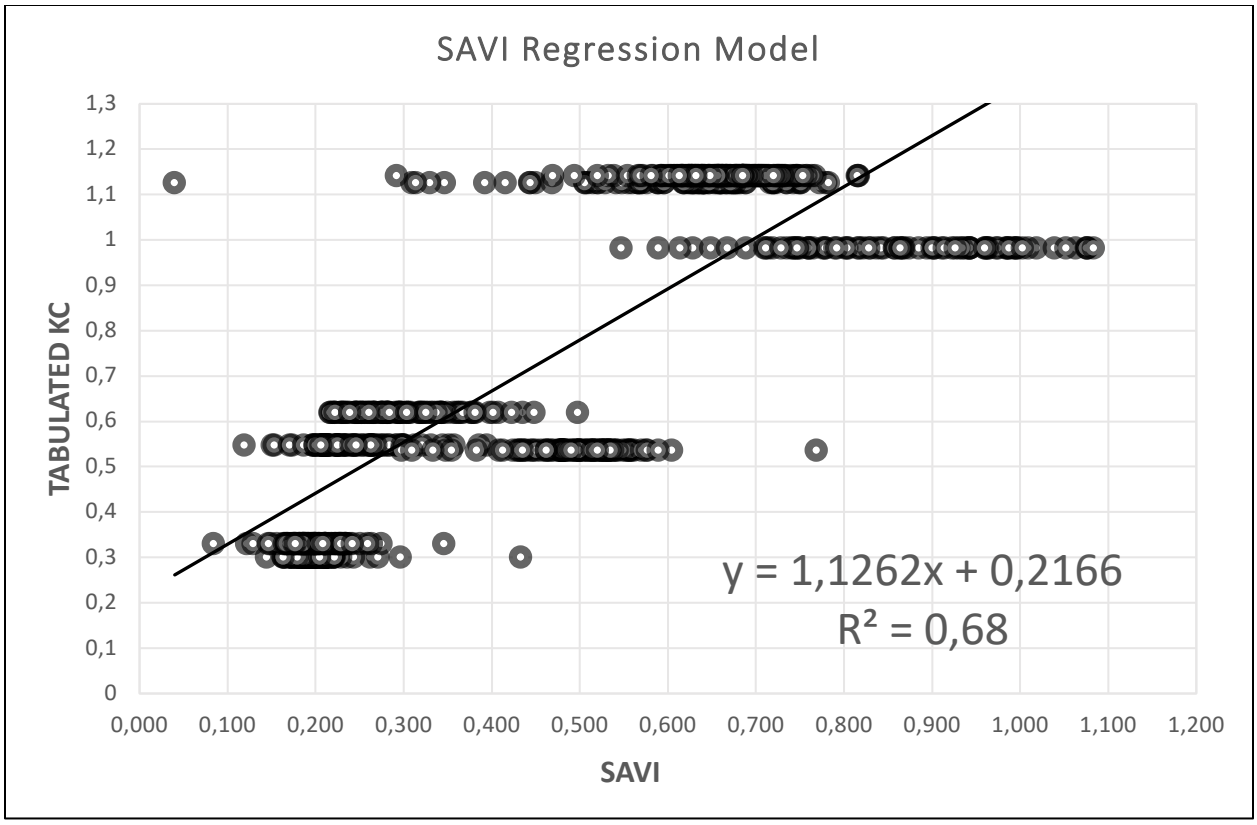

Figure 4.6: Linear relationship between SAVI and tabulated K_c for all satellite imagery indicated in Table 3. 3.

Because of these analyses, the K_c values extracted from NDVI (Fig 4.7) were identified as more reliable because of their stronger correlation with tabulated K_c. This led to the selection of NDVI for the computation of the final ET_c values within this study. Accordingly, spatial and temporal ET_c maps were produced utilising these final ET_c values, illustrating the spatial and temporal variability of actual evapotranspiration across maize fields within the Mooi River catchment. This provided essential insights into the variability of water usage across these fields.

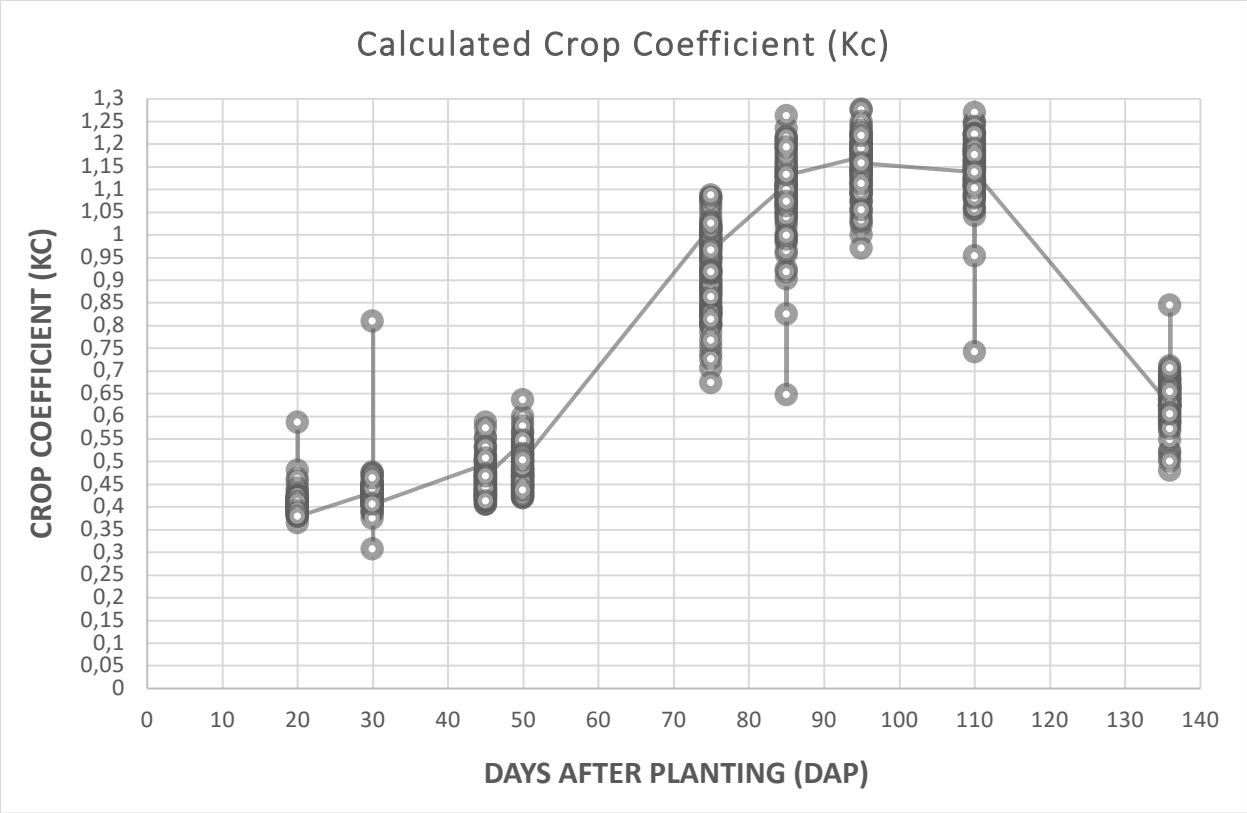

Figure 4.7: Graph showing the calculated Kc (new Kc values) curve from the NDVI-tabulated Kc regression model.

Figure 4.8 presents the average NDVI values for the 87 isolated maize fields throughout various growth stages of the growing season. From December to early January (DAP 0-50), NDVI readings were typically low, fluctuating between 0.1 and 0.2. As the crop matures, the NDVI values rise, peaking at 0.6 to 0.9 in the mid-season, then plateauing from mid-February to mid-March (DAP 85-110). Toward the end of the season, the NDVI levels had decreased to 0.2-0.4 by the beginning of April (DAP 135). Other researchers have observed similar seasonal NDVI curves for maize (Kamble *et al*., 2013; de Souza *et al.,* 2015; Toureiro *et al.,* 2017). All NDVI curves developed by these researchers showed low values at early stages, followed by an increase at mid-season stages, and a decline at late stages.

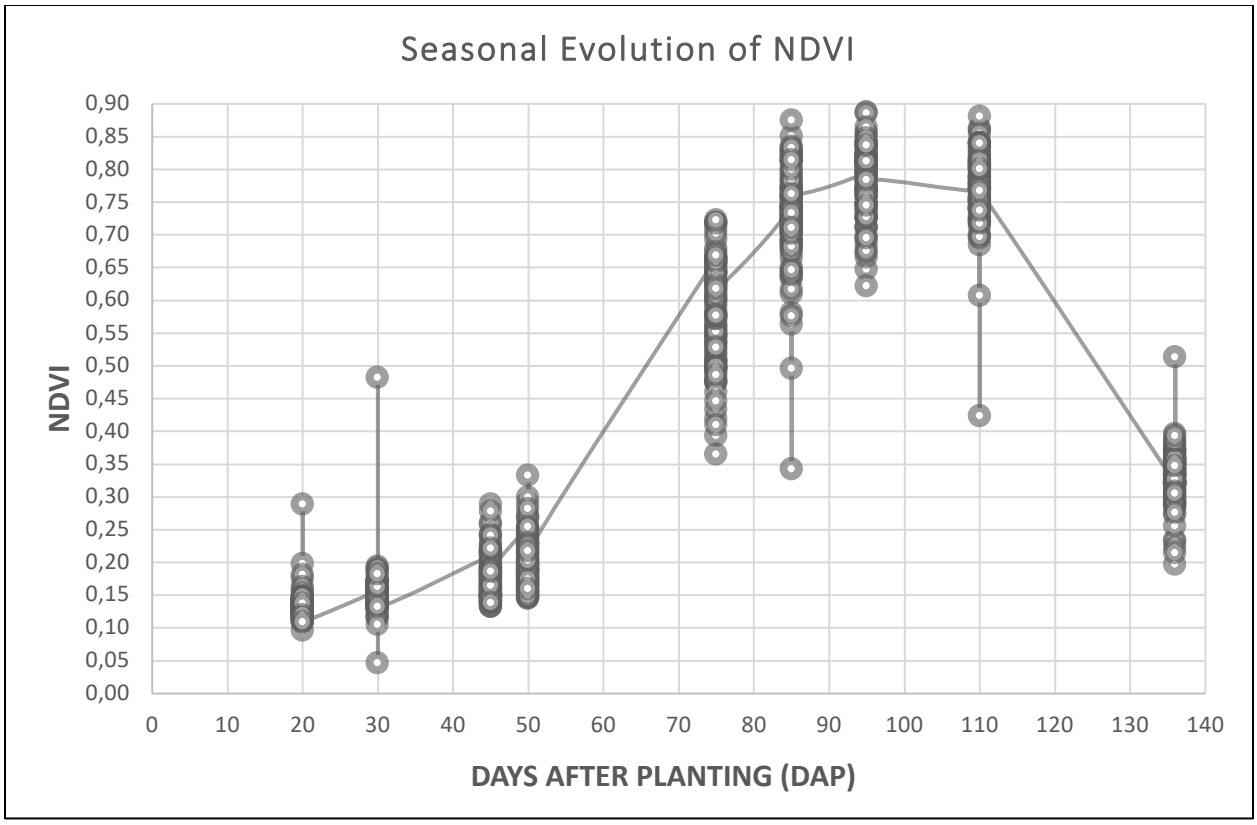

Figure 4.8: Seasonal evolution of NDVI at the 87 isolated maize fields within the Mooi River catchment.

4.7. Seventh phase

In the seventh phase of the study, the task of computing the actual evapotranspiration (Fig. 4.9 and 4.10) for each maize field of the Mooi River catchment was undertaken along with the production of the spatiotemporal ET_c maps. This calculation was enabled by a multi-step process in which a new crop coefficient value (K_c) was derived using the NDVI-tabulated K_c regression model determined in the preceding sixth phase. The newly calculated K_c was then paired and multiplied by the associated reference evapotranspiration (ET_c) value for each field.

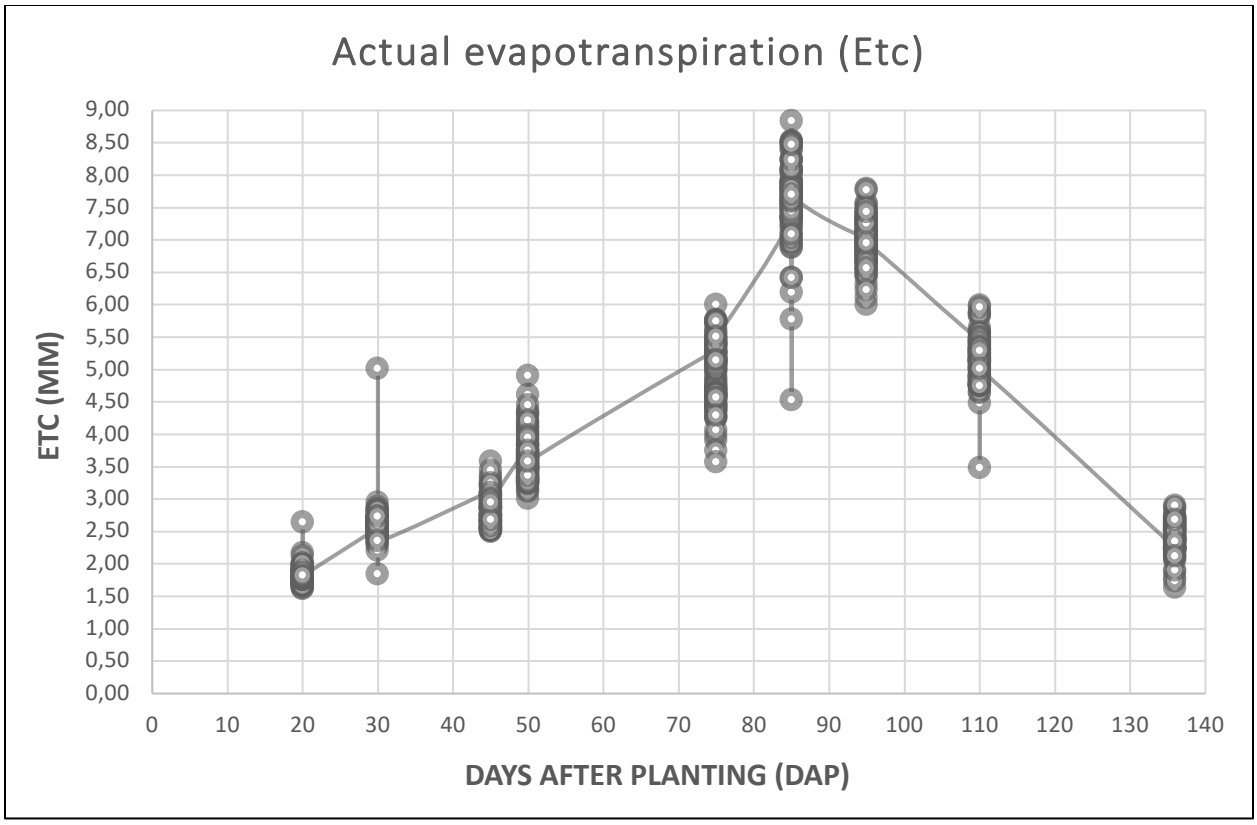

Figure 4.9: Line graph showing seasonal evolution of actual evapotranspiration (ET_c) at the 87 isolated maize fields within the Mooi River catchment.

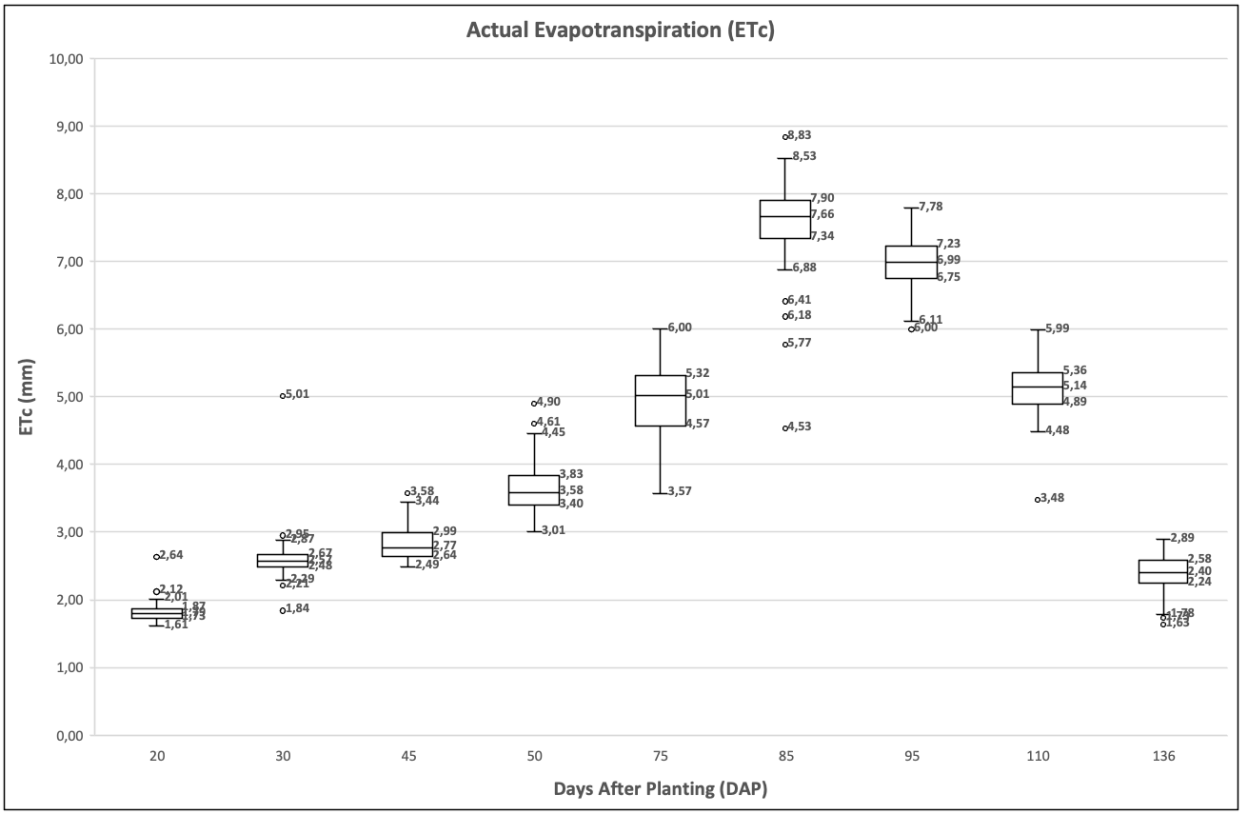

Figure 4.10: Box and whisker plot showing seasonal evolution of actual evapotranspiration (ET_c) at the 87 isolated maize fields within the Mooi River catchment.

Following this computational procedure, maps of the actual evapotranspiration (ET_c) were generated using QGIS (Fig 4.11- 4.19). The ET_c data for each time slice (DAP) was classified into four classes using the natural breaks (Jenks) method, resulting in a distinct map for each time slice. The Natural Breaks (Jenks) method was chosen because it is suitable for datasets characterized by uneven distributions and noticeable clusters. It was observed by viewing each dataset (time slice) as a histogram. The intent behind employing the Natural Breaks (Jenks) method for the ET_c maps was to accentuate the intra-variability present in the spatial distribution of actual evapotranspiration for each specific time slice during the growing season. The decision to use four classes in the classification was strategic; while increasing the number of classes could reduce data generalisation—a desirable trait—it could also hinder map clarity, heightening the potential for reading inaccuracies. Thereby, four classes were deemed optimal to effectively depict spatial variability without compromising map legibility.

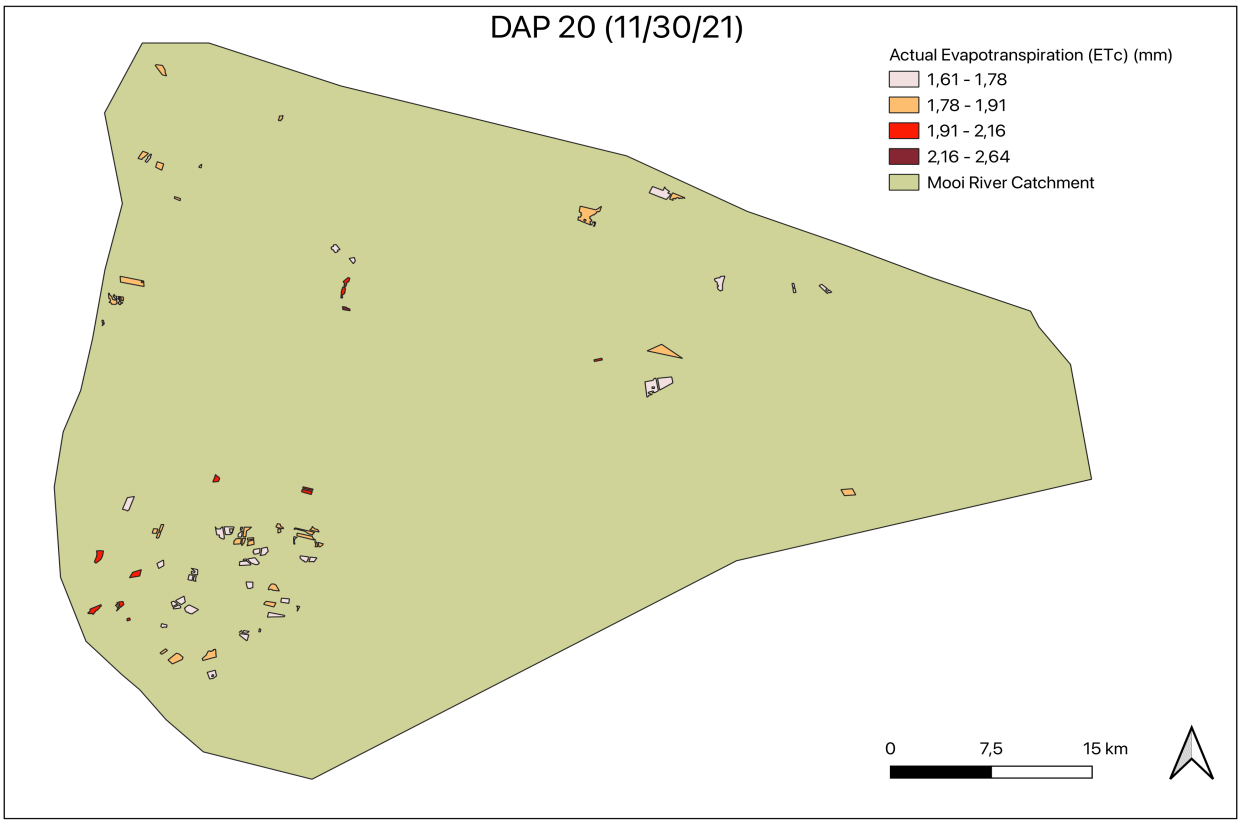
DAP 20 (11/30/21)
Actual Evapotranspiration (ETc) (mm)
1,61 - 1,78
1,78 - 1,91
1,91 - 2,16
2,16 - 2,64
Mooi River Catchment
0
7,5
15 km

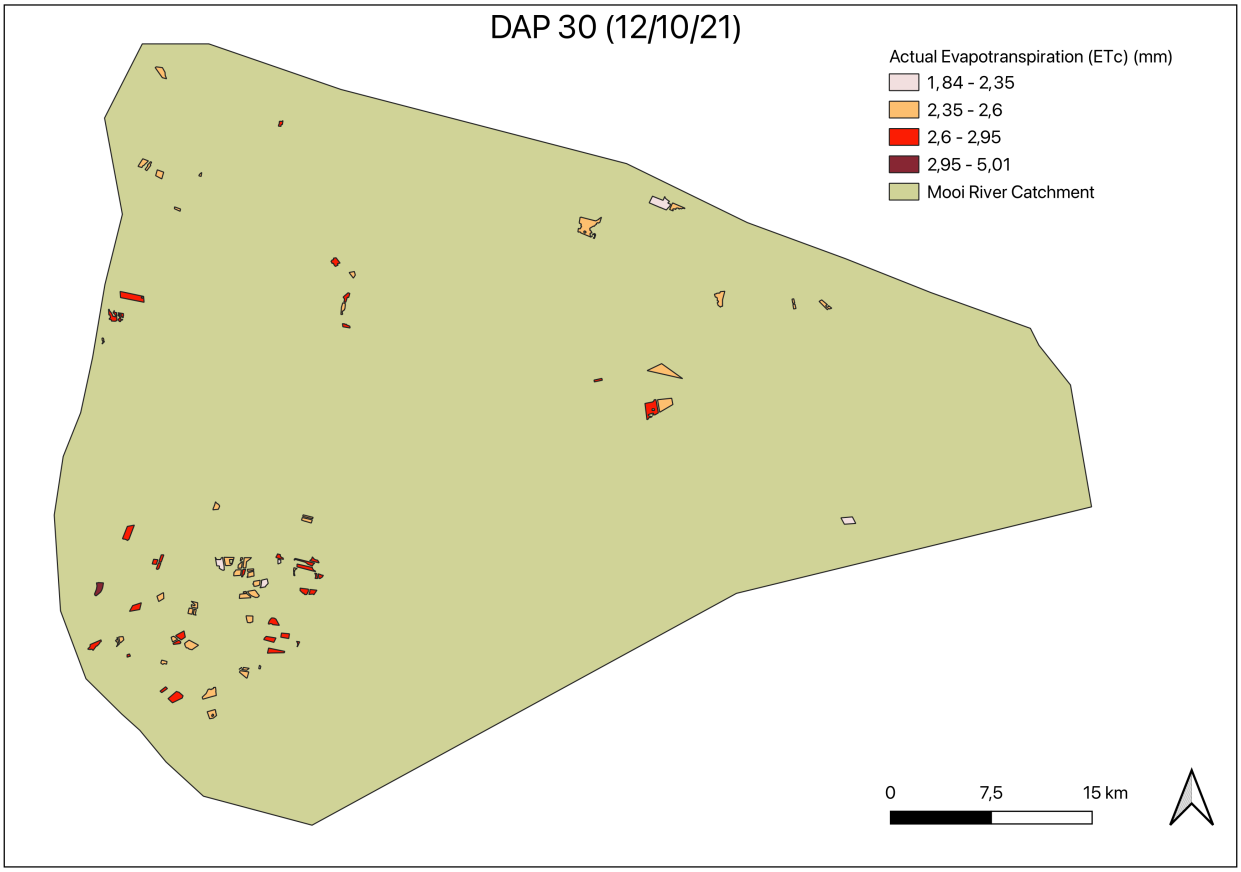
DAP 30 (12/10/21)
Actual Evapotranspiration (ETc) (mm)
1,84 - 2,35
2,35 - 2,6
2,6 - 2,95
2,95 - 5,01
Mooi River Catchment
0
7,5
15 km

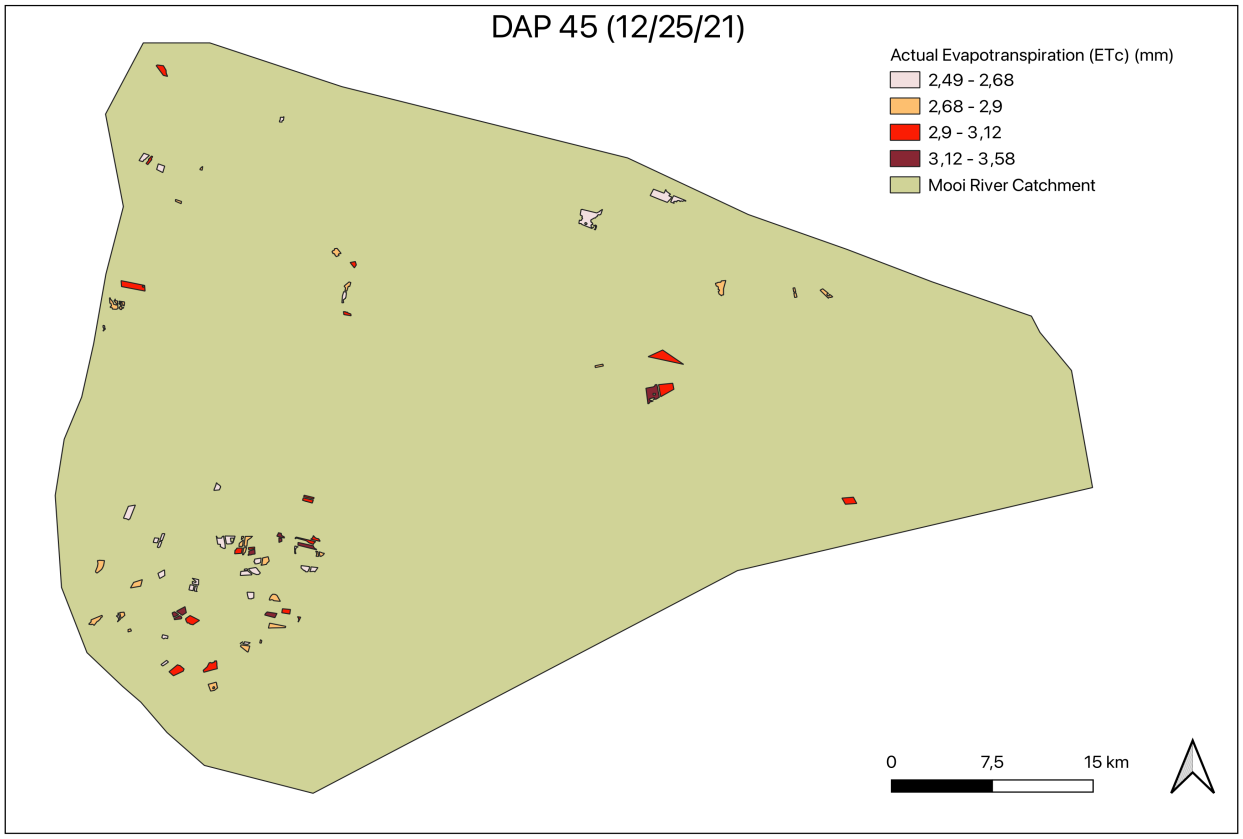
DAP 45 (12/25/21)
Actual Evapotranspiration (ETc) (mm)
2,49 - 2,68
2,68 - 2,9
2,9 - 3,12
3,12 - 3,58
Mooi River Catchment
0
7,5
15 km

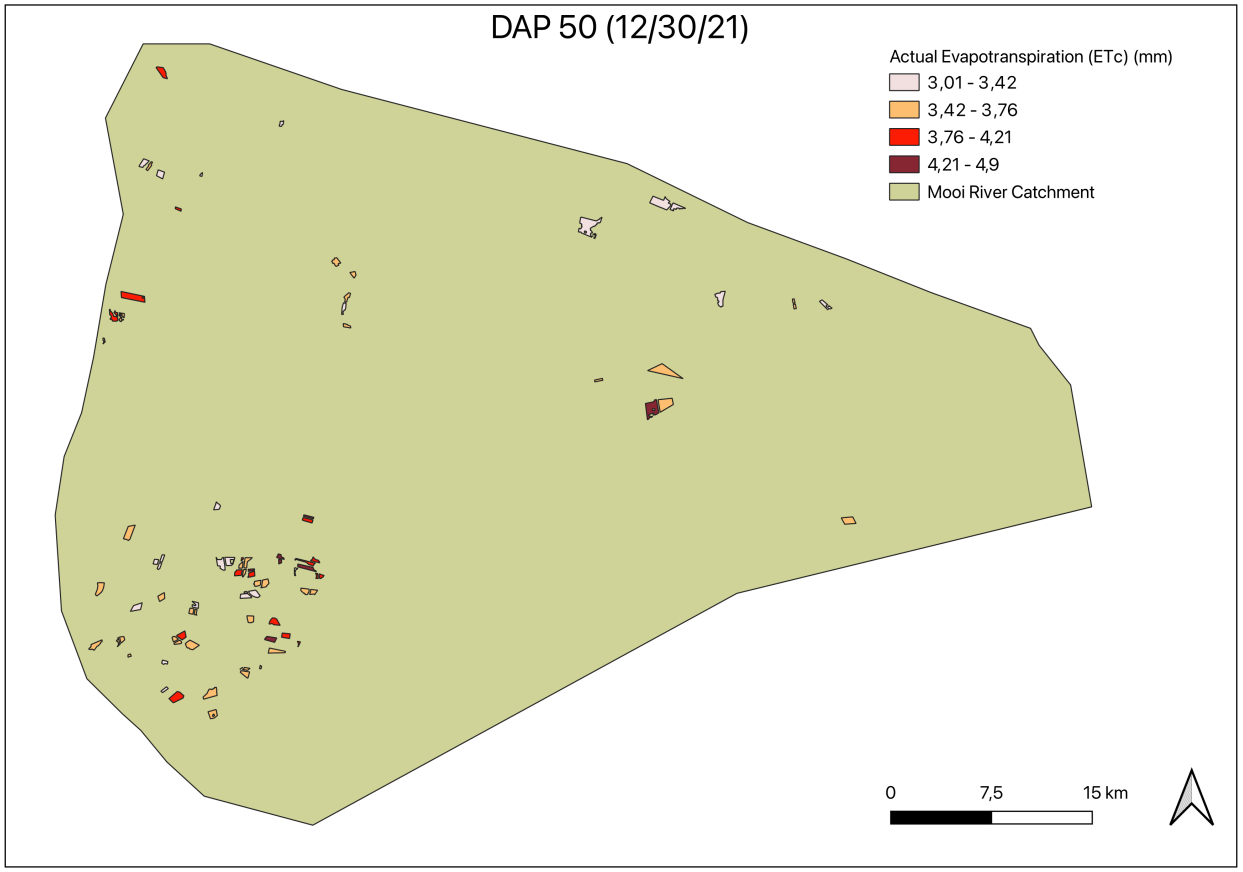
DAP 50 (12/30/21)
Actual Evapotranspiration (ETc) (mm)
3,01 - 3,42
3,42 - 3,76
3,76 - 4,21
4,21 - 4,9
Mooi River Catchment
0
7,5
15 km

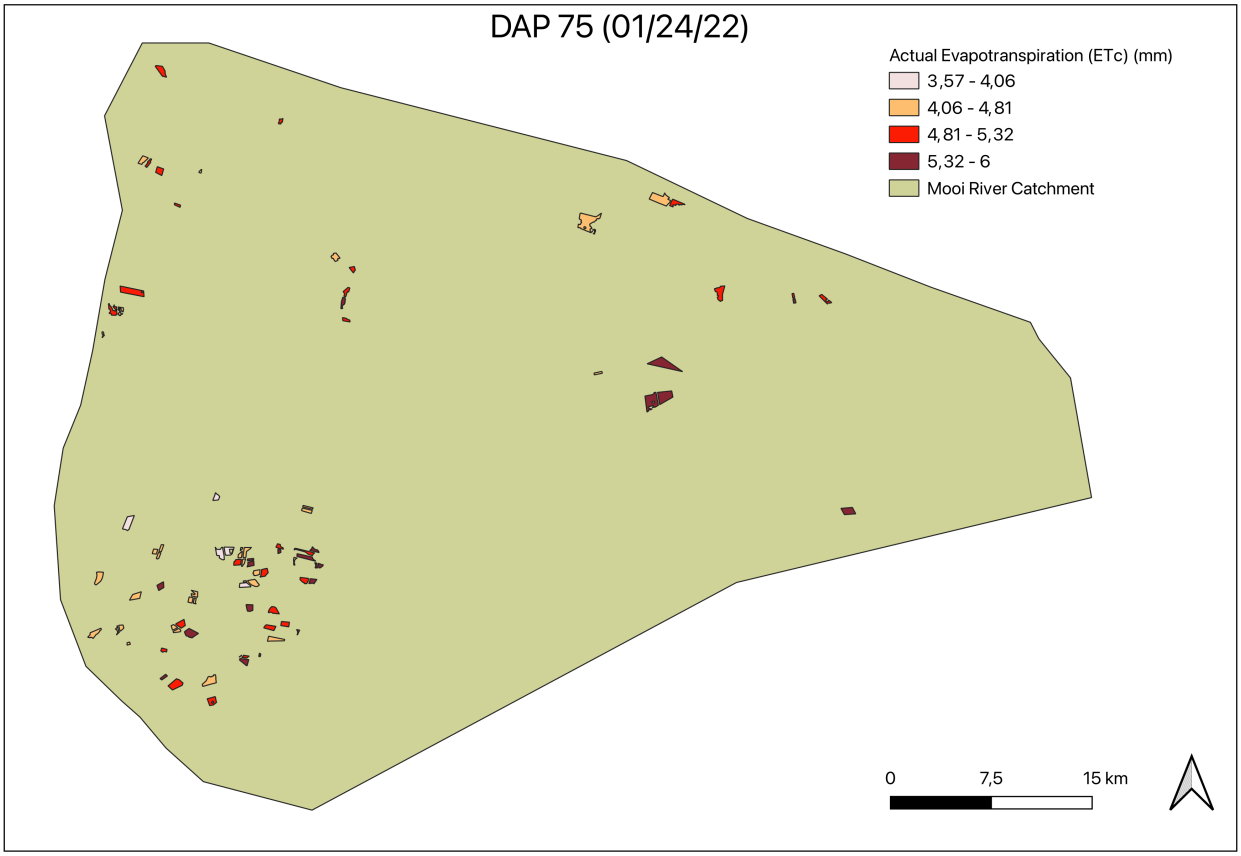
DAP 75 (01/24/22)
Actual Evapotranspiration (ETc) (mm)
3,57 - 4,06
4,06 - 4,81
4,81 - 5,32
5,32 - 6
Mooi River Catchment
0
7,5
15 km

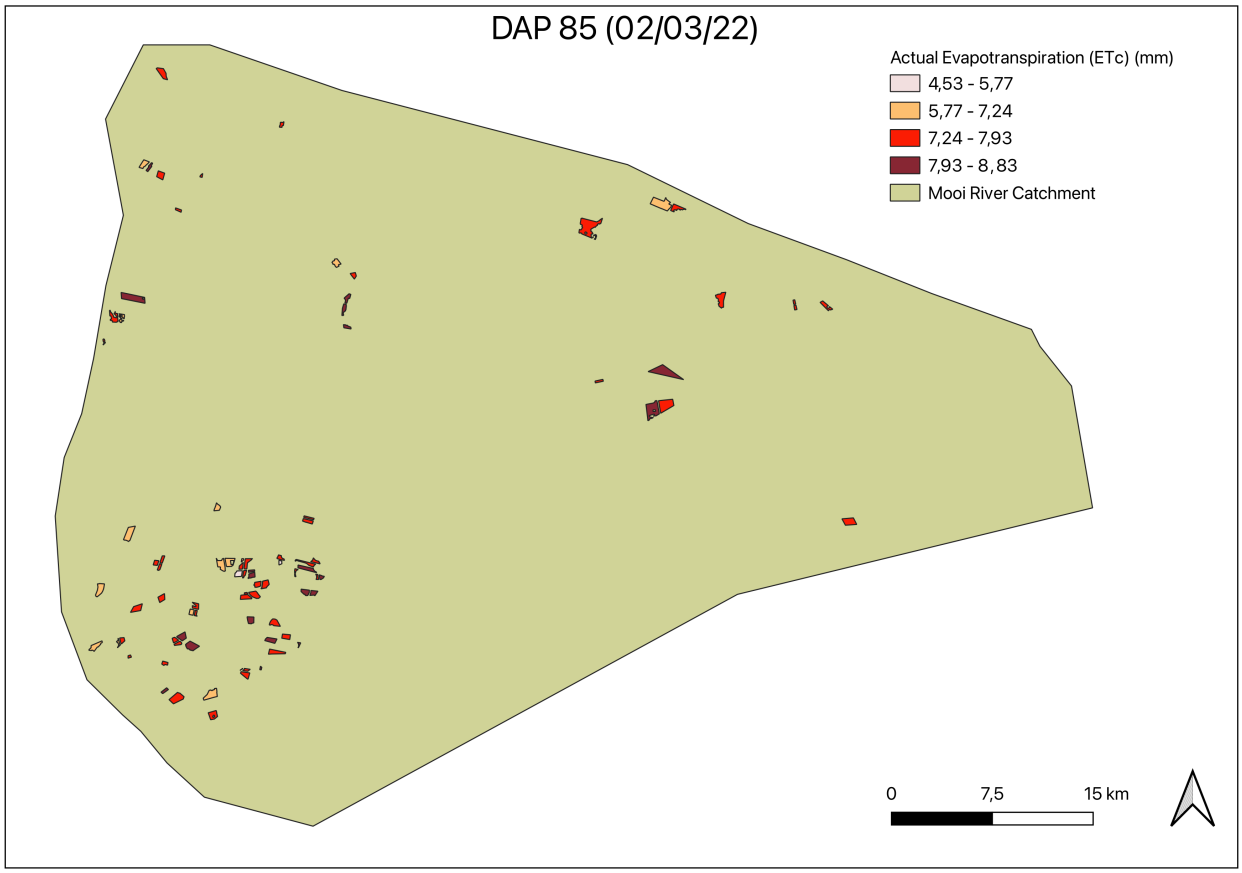
DAP 85 (02/03/22)
Actual Evapotranspiration (ETc) (mm)
4,53 - 5,77
5,77 - 7,24
7,24 - 7,93
7,93 - 8,83
Mooi River Catchment
0
7,5
15 km

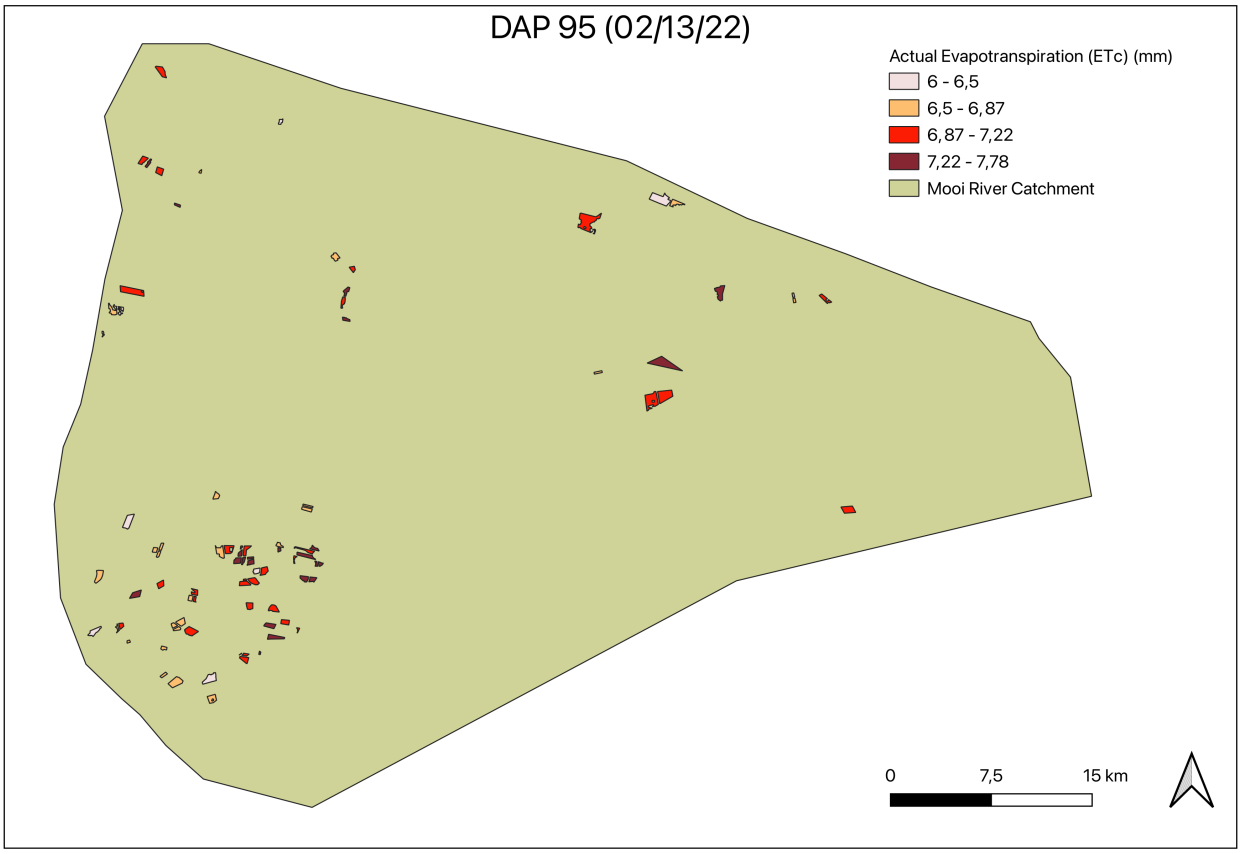
DAP 95 (02/13/22)
Actual Evapotranspiration (ETc) (mm)
6 - 6,5
6,5 - 6,87
6,87 - 7,22
7,22 - 7,78
Mooi River Catchment
0
7,5
15 km

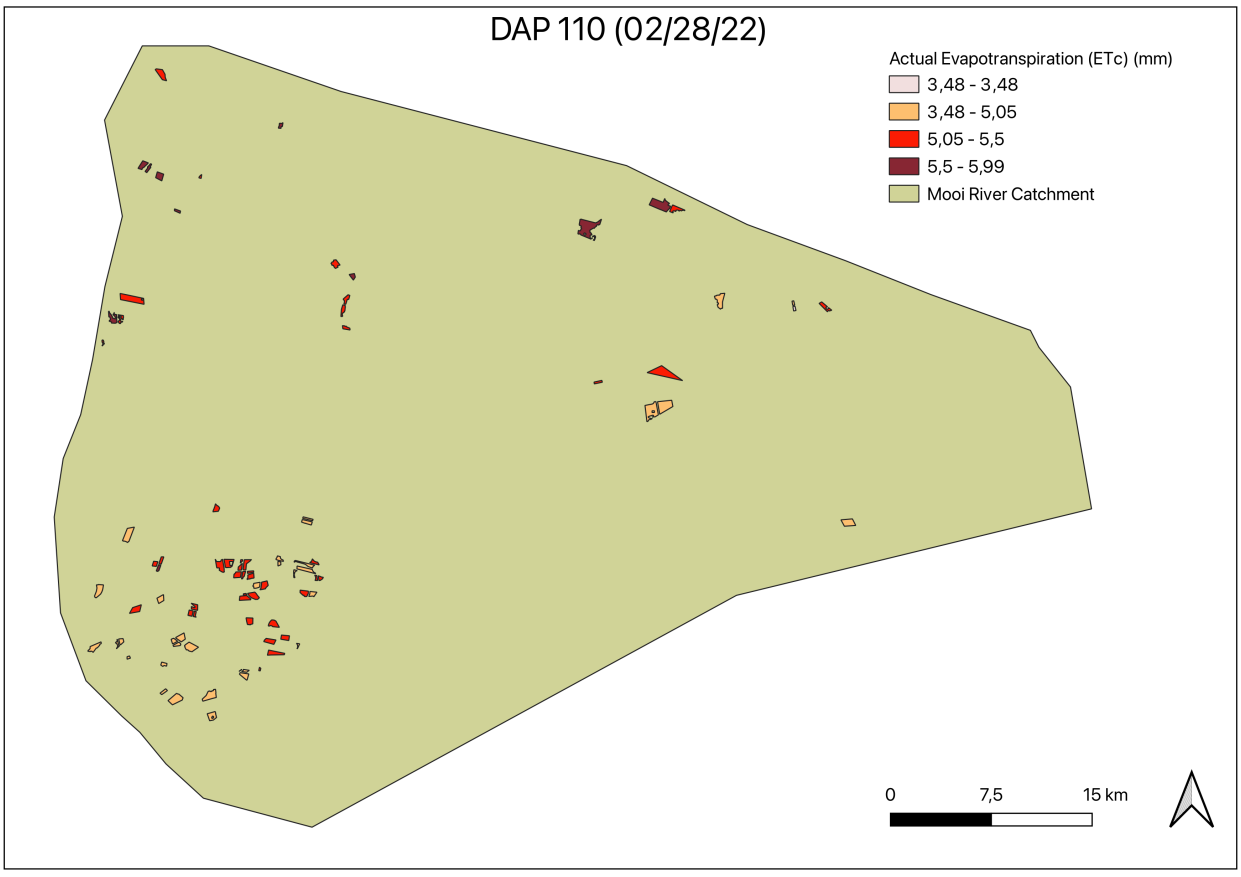
DAP 110 (02/28/22)
Actual Evapotranspiration (ETc) (mm)
3,48 - 3,48
3,48 - 5,05
5,05 - 5,5
5,5 - 5,99
Mooi River Catchment
0
7,5
15 km

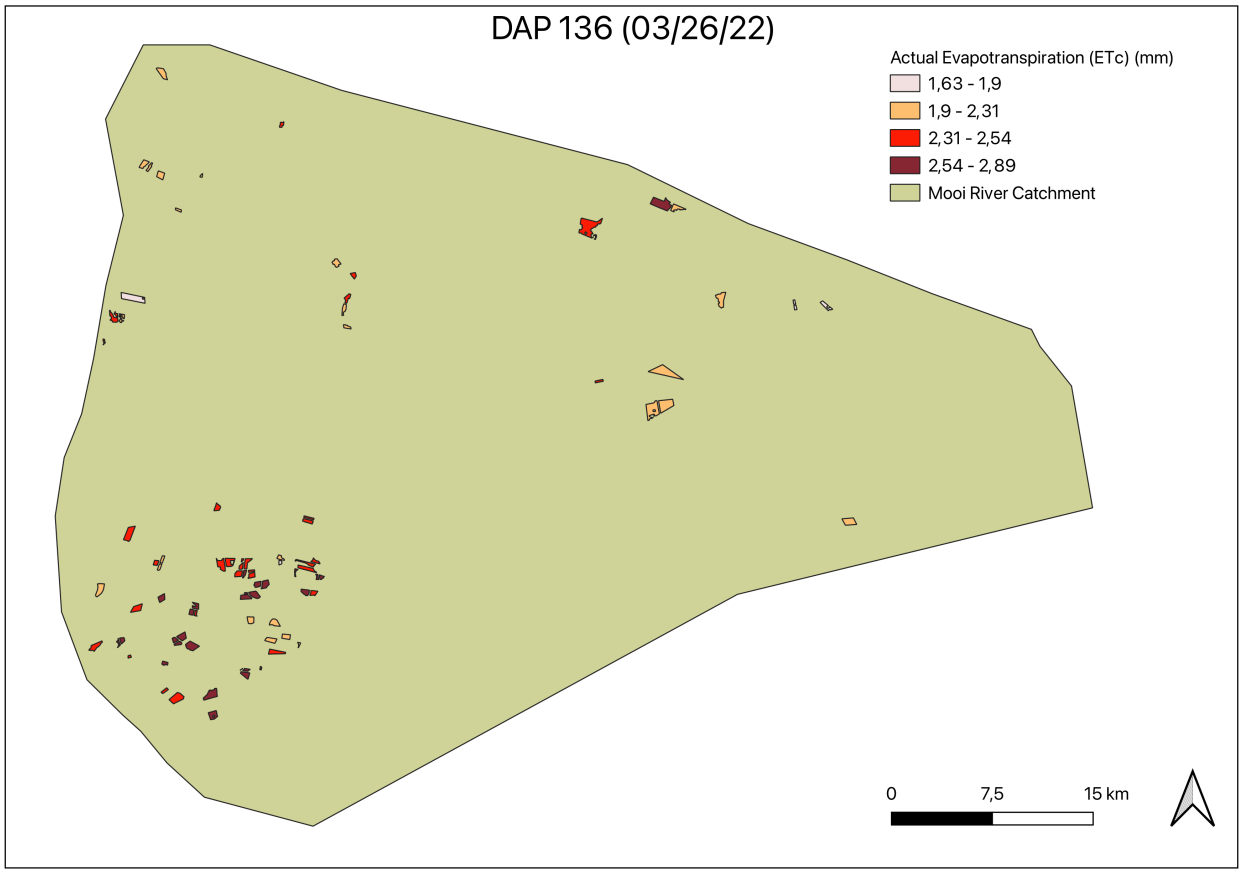

Figure 4.11-4.19: Maps indicating the spatial distribution of ET_c at 20-136 days after planting in the Mooi River catchment.

Chapter 5: Discussion

The study successfully used the Maximum Entropy (MAXENT) model to identify remaining maize fields among the 2808 total fields in the Mooi River catchment that were not noted during an initial visit. With external evaluation, the MAXENT model demonstrated an 82% accuracy in identifying maize fields, thus showcasing its potential for crop identification within complex agricultural landscapes in future research.

5.1. LAI analysis

Following the MAXENT modelling, the study employed the LAI analysis, which identified 87 out of the 945 maize fields in the Mooi River Catchment as having been planted between the 10th and 15th of November. It is essential to note that these 945 fields belong to various farmers within the catchment. The fields selected for analysis significantly influence the spatiotemporal variability of ET_c in the catchment, as incorporating different fields would naturally yield different results. Comparing fields with varying planting times would be a flawed approach because the planting dates would differ and be at different growth phases. Growth phases directly influence evapotranspiration rates as they relate to factors like plant size and other traits impacting water usage. If the study's primary aim were to quantify the cumulative water usage (among other things) for each field during the growing season, then including all maize fields in the catchment would be logical. However, to effectively capture and map the spatial and temporal inter and intra-variability of ET_c throughout the growing season, it becomes imperative to focus on fields with similar planting dates to ensure comparability. A significant concentration of fields with aligned planting dates was observed in the southwest corner of the study area, contrasting with a more dispersed distribution elsewhere in the catchment. The clustered planting dates in the southwest can be attributed to the ownership of many of those fields by a single farmer, from whom planting dates were also sourced. This clustering poses an analytical challenge: the region may have distinct soil or climatic conditions or particular farming practices that could skew results. Such a skew might introduce a bias, which can be considered a shortcoming in the study. Unfortunately, acquiring planting dates from all farmers in the catchment was not feasible.

5.2. Reference evapotranspiration

To ascertain the reference evapotranspiration values for the fields, the study area was divided using a grid consisting of 9km by 9km cells. Given the close proximity of many fields, there were minimal variations in their reference evapotranspiration values. Fields close to each other were consolidated within a single grid, all sharing the same evapotranspiration value. On the other

hand, more isolated fields were typically situated within their unique grid cells. The grid layout influenced the derived Et_c values and, in turn, affected the spatiotemporal patterns seen across the catchment. Within a grid cell, reference evapotranspiration values remained uniform but differed across separate cells. This grid configuration and its dimensions inherently shaped the resolution of the evapotranspiration dataset and, hence, the spatiotemporal variability seen in the data.

5.3. Corresponding trends in parameters

The study identified a substantial correlation among the trends of actual evapotranspiration (ETc), averaged season evolution of NDVI, tabulated crop coefficient, and calculated crop coefficient curves (Fig. 5.1 and 5.2). The correlation between these parameters during the growing season is primarily influenced by intertwined factors that shape each of these parameters. This is most prominently observed in phase seven's results, where ET_c, NDVI, calculated K_c, and tabulated K_c predominantly display an aligned trajectory, peaking around 80-110 days after planting (DAP). ET_c, however, deviates from the correlation slightly during this phase by descending sharply after peaking shortly after DAP 80. Such patterns underscore the potential of vegetation indices, particularly NDVI, in serving as reliable indicators for gauging actual ET_c.

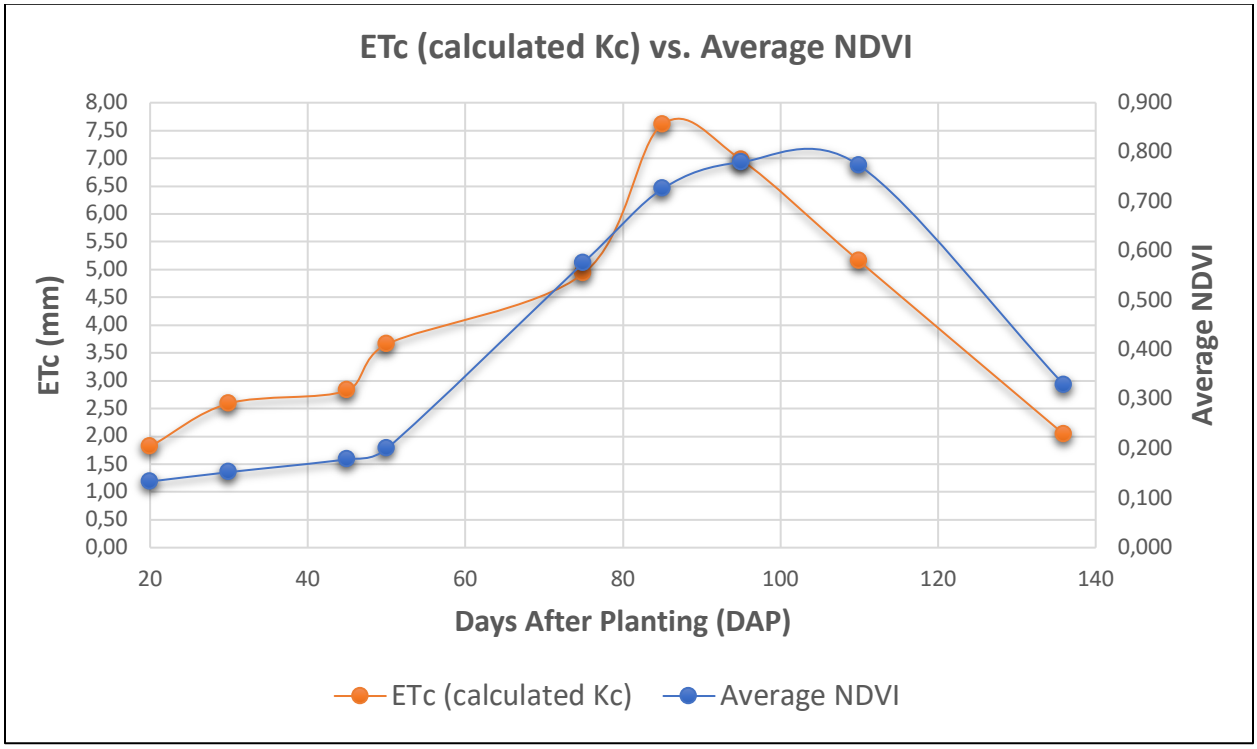

Figure 5.1: Line graphs showing a similar trend in ET_c calculated from the NDVI-tabulated K_c regression model and the seasonal evolution of averaged NDVI within the Mooi River catchment.

The alignment results from the mutual influences of the crop's aerodynamic properties, stomatal behaviour, canopy structure, and root characteristics that collectively steer water uptake, evaporation, and transpiration mechanisms, thereby dictating both ET_c rates and the crop coefficient. NDVI values, which resemble the crop's green biomass volume and photosynthetic vigour, also display variations throughout the growing season, mirroring these influences. In the early stages of the growing season, the low amounts of green biomass yield lower NDVI values. However, as the crop matures and intensifies its near-infrared light reflection, NDVI readings surge, culminating during the peak of the crop's developmental phase. Transitioning into the senescence stage, crops experience diminished chlorophyll levels, leading to reduced red light absorption and near-infrared light reflection, prompting a decrease in NDVI values. The foundation of such patterns can be attributed to several determinants, encompassing crop type, climate, soil characteristics, and the crop's growth trajectory.

In addition, drawing a distinction between K_c calculated and K_c tabulated is imperative. While tabulated K_c values stem from well-irrigated reference crops like alfalfa, calculated K_c readings rely on the actual crop growth scenarios, bridging the gap between tabulated K_c and the tangible crop growth conditions, ensuring a refined ET_c estimation (Reyes-Gonzalez *et al.*, 2018).

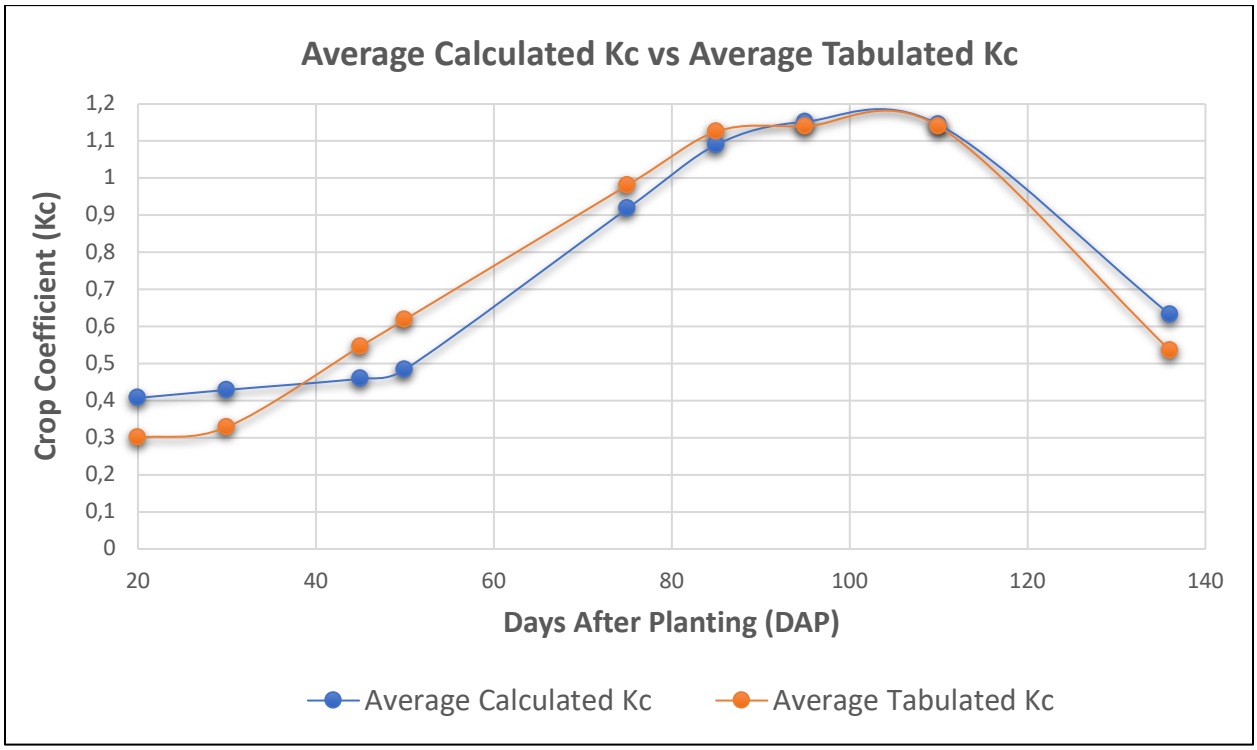

Figure 5.2: Line graphs showing a similar trend between calculated Kc and tabulated Kc during the growing season.

In essence, the correlation in the trends of crop coefficient, ET_c, and NDVI throughout maize's growing phase in this study is not incidental. These parameters are intrinsically interconnected and moulded by consistent factors with regard to the crop's physical attributes, ambient conditions, and developmental phases. Understanding these interrelationships allows for more accurate prediction and interpretation of these vital agricultural parameters.

5.3.1. ETc (calculated K_c) vs ETc (tabulated K_c)

Figure 5.3 illustrates the discrepancies between actual evapotranspiration (ET_c) calculated using two distinct methods: the conventional method, which employs tabulated crop coefficients multiplied by reference evapotranspiration (ET_o), and an alternative approach using crop coefficients derived from the Normalized Difference Vegetation Index (NDVI) in this study. The NDVI-based method accounts for both spatial and temporal variability in crop coefficients, thereby reflecting the natural fluctuations in crop conditions within the Mooi River catchment area.

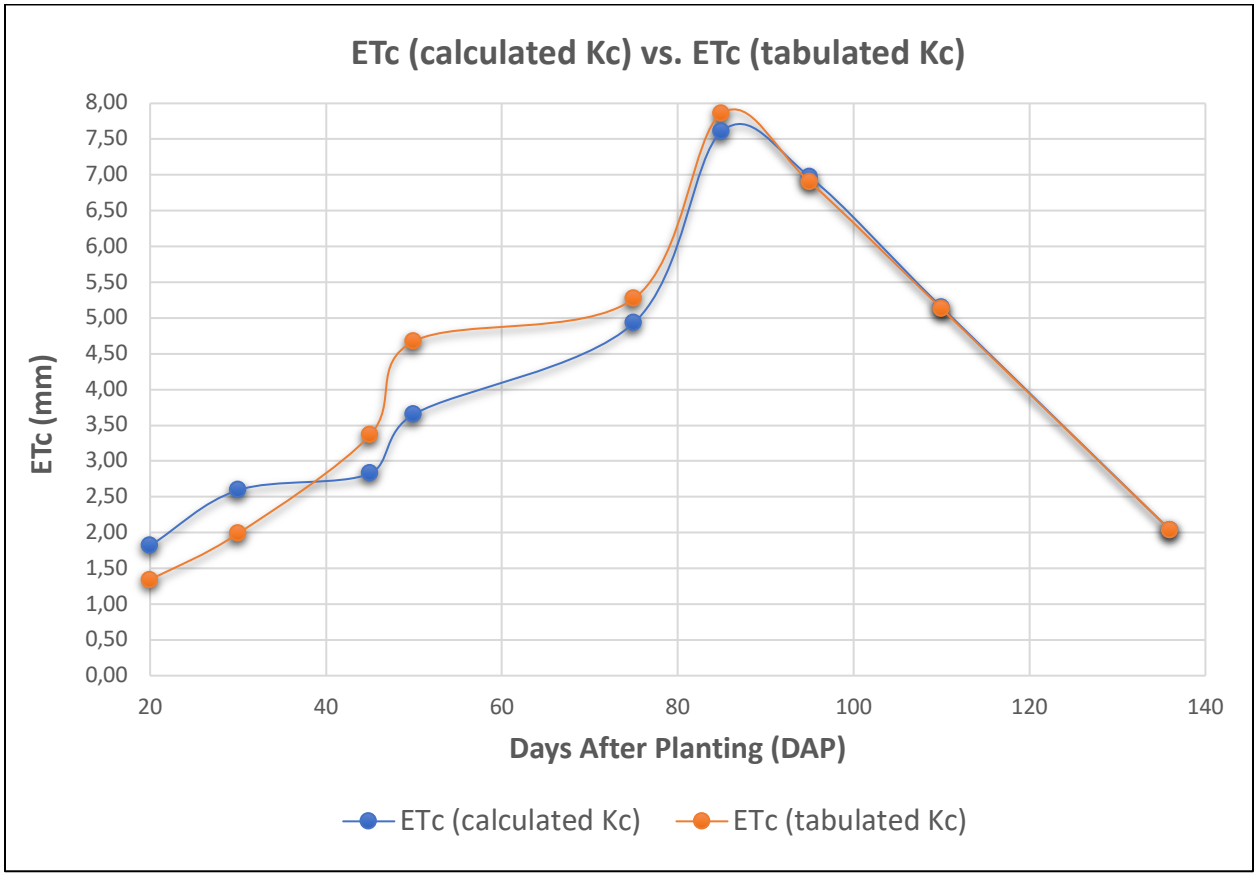

Figure 5.3: Line graphs showing differences in ET_c calculated from the NDVI-tabulated Kc regression model, ET_c calculated from tabulated crop coefficient values.

In Figure 5.3, it is evident that approximately 20 to 40 days after planting, ET_c values calculated with NDVI-based crop coefficients indicate higher levels of ET_c compared to those derived using conventional tabulated crop coefficients. From around 40 to 95 days after planting, the ET_c values using NDVI-based coefficients drop to levels lower than those obtained through traditional methods. Beyond approximately 95 days after planting until the end of the season, the two ET_c curves closely align.

The most significant divergence between ET_c calculated using tabulated coefficients and ET_c calculated using NDVI-based coefficients occurs during the initial to developmental stages of maize growth. Conversely, the mid to late-season stages exhibit almost identical ET_c levels between the two methods. This suggests that employing crop coefficients calculated from a vegetation index like NDVI is most critical during the initial to developmental phases of the maize's growth cycle, particularly for rainfed maize.

5.4. Growth stage lengths

The growth stage-length analysis utilised the growing degree days (GDD) formula in conjunction with literature-based insights to discern the duration of each maize field's four growth stages for that year based on temperature data from a nearby weather station. This was instrumental in assigning the correct satellite imagery and corresponding vegetation index data with the tabulated crop coefficient values for each growth stage, aiding the linear regression analysis. For the initial growth stage, the analysis indicated a span of 28 days. Given this, the sole available cloud-free satellite image for this phase was dated 2021/11/30. Being early in the season, the associated NDVI values were on the lower spectrum, reflective of maize in very early stages of growth with small leaves. Correspondingly, these initial 28 days exhibited minimal ET_c values (Fig. 4.9). The development stage was discerned to last 57 days. As a result, four distinct cloud-free satellite images from 2021/12/10 to 2022/01/24 were assigned for ET_c computations within this period. The associated NDVI values, particularly towards the latter part of this phase, presented a gradual linear increment (see Fig. 4.8). This upward trend in NDVI was paralleled by a consistent increase in ET_c values during this segment of the season (Fig. 4.9). The mid-season stage spanned 38 days, corresponding with three cloud-free images from 2022/02/03 to 2022/02/28. This segment displayed the peak of NDVI values for the season (see Fig. 4.8). There was also a pronounced plateau in the NDVI data for about thirty days, from DAP 80 to DAP 110. However, the correlation between this phase's NDVI and Et_c values wasn't as consistent as in other stages. While both NDVI and ET_c values peaked during this time, the latter witnessed a rapid descent soon after its peak. The concluding late-season stage endured for 27 days. This

period was characterised by a sharp decrease in ET_c values, consistent with the declining NDVI values captured in the sole accessible cloud-free image dated 2022/03/26. As maize transitioned to its senescence phase, a pronounced drop in greenness would have been observed, leading to lowered NDVI values. Given that there is no growth during this phase, water consumption notably diminished, as illustrated in Figure 4.9.

5.5. Regression analysis

Utilising a simple linear regression model, it was found that NDVI values, derived from satellite imagery, had a significantly stronger correlation with the FAO's tabulated crop coefficient values compared to the SAVI values. This revealed a strong correlation with NDVI (R^2=0.90), compared to SAVI's R^2 of 0.68, corroborating previous studies and validating NDVI's effectiveness as a reliable tool for improving crop coefficients utilised in evapotranspiration estimations. For example, Reyes-Gonzalez *et al*. (2018) discovered an average R^2 of 0.97 for NDVI, Kamble *et al*. (2013) reported an R^2 of 0.90, and Hay *et al*. (2015) found an R^2 of 0.97. In contrast to other studies, this research found that the Soil-Adjusted Vegetation Index (SAVI) had a relatively lower correlation (R^2=0.68) with the tabulated crop coefficient (K_c). For example, in a study by Gontia & Tiwari (2010), a linear relationship between wheat crop coefficients and SAVI resulted in an R^2 of 0.90, with NDVI exhibiting an R^2 of 0.80.

Similarly, Parmar & Gontia (2016) reported an R^2 of 0.96 for SAVI in their assessment of groundnut crop coefficients, significantly higher than the R^2 of 0.74 observed for NDVI. As a result, SAVI has a weaker linear relationship with maize crop coefficients compared to wheat and groundnut. At the same time, NDVI demonstrates a stronger correlation with maize crop coefficients. This suggests that spectral characteristics of wheat and groundnut crops may influence the relationship between vegetation indices and crop coefficients differently. Additionally, factors such as the volume of satellite imagery, the spatial resolution of the imagery, and environmental parameters like climate and soil conditions may also contribute to these disparities in correlation.

As a result, the NDVI-tabulated K_c regression model was selected, leading to the generation of newly adjusted crop coefficients. The use of satellite-derived NDVI in the crop coefficient approach for estimating actual evapotranspiration enabled the adjustment of the FAO's standard crop coefficient values to more accurately represent the varying crop conditions in the maize fields, factoring in the inherent spatiotemporal variations in crop growth and conditions. Upon multiplying these adjusted values with a reference evapotranspiration value, an estimation

of the actual evapotranspiration of maize crops was achieved, effectively considering the spatial and temporal variations of crop water use in the study area. The computation of the actual evapotranspiration of each maize field led to the creation of spatiotemporal ET_c maps. These maps offer valuable insights into the spatial and temporal variations of ET within the Mooi River catchment, facilitating crop yield assessments and predicting potential drought impacts on crop productivity, particularly in semi-arid regions like the Mooi River catchment where annual precipitation can fall below evapotranspiration demands.

5.5.1. Limitation of the regression analysis

The study observed a distinct shortage of cloud-free satellite images during the initial and late-season growth stages. This limitation led to a reduced volume of NDVI and SAVI data available for the linear regression during these periods compared to the more abundant data during the development and mid-season stages. A primary reason for this difference in data availability is the duration of each growth stage. Longer growth phases, such as the development stage, which spanned 57 days and the mid-season stage, which lasted 38 days, provide more opportunities to capture cloud-free images because of the extended duration. In contrast, the initial growth phase, lasting only 28 days, and the late-season stage, spanning 27 days, had fewer chances to obtain clear images. Another factor contributing to this data disparity was the pervasive cloud cover throughout the 2022 growth season, which limited the number of suitable images for the study. A linear regression model's accuracy depends heavily on the volume and quality of its input data. Consequently, this study's regression model might exhibit biases stemming from the limited data available. Even though the NDVI-tabulated K_c model, derived from this regression, was solely used to calculate evapotranspiration (ET) using the training NDVI data and was not extrapolated to new datasets, the limitation is relevant.

Motulsky & Christopoulos (2004) explain that fewer data points could expand confidence intervals for estimated coefficients. This expansion introduces more uncertainty, complicating determining genuine relationships in a dataset. With a limited dataset, validating essential regression assumptions, such as linearity and homoscedasticity, becomes harder, as noted by James *et al*. (2013). Such a limitation may introduce biases or misinterpretations. Additionally, a sparse dataset could weaken the model's statistical power, potentially missing significant patterns. Overfitting, or the model's tendency to capture random variations rather than genuine trends, is another concern with limited data, as pointed out by Kuhn & Johnson (2013).

The quality and volume of input data play a crucial role in shaping regression outcomes. For ET calculations, the resulting estimates could be less accurate if the NDVI values fail to accurately represent the ground conditions during crucial growth stages. While the mid-season and development stages likely yield more accurate estimates due to their richer data sets, the lack of data during the initial and late-season stages due to cloud cover is a shortcoming in the study.

5.6. Spatiotemporal variability of maize ET_c in the Mooi River catchment

In Figures 4.9 and 4.10, the depiction of actual evapotranspiration provides a more comprehensive representation of the inter-variability of ET_c throughout the maize's growth cycle, spanning from 20 days after planting (DAP) to 136 DAP. This chronological portrayal reveals how Et_c fluctuates temporarily over distinct time intervals. In contrast, Figures 4.11 through 4.19 offer a deeper insight into the intra-variability of ET_c, highlighting the spatial variability within each specific day or time slice post-planting. To accurately showcase these spatial distinctions, the ET_c scale for each map is adjusted according to the data range for that specific day, ensuring that the nuances of actual evapotranspiration within every individual time slice are captured and understood.

It can be observed that the actual evapotranspiration (ET_c) commences at a relatively low point in the early phases of maize crop development, registering its lowest value of 1.614 mm. As the maize progresses through its growth stages, the ET_c gradually rises until it peaks at 8.83 mm at 85 days after planting (DAP). As the maize then transitions into its senescence phases, the ET_c begins a gradual descent until it reaches 2.89 mm just prior to the commencement of the maize harvest. This pattern indicated minimal water use during the early stages, a surge during the mid-growth phases, and a reduction in the late stages as harvesting approached. This trend in ET_c is consistent with other studies, including Ko & Piccinni, 2008; Gontia & Tiwari, 2010; Johnson & Trout, 2015; Reyes-Gonzalez *et al*., 2015, and Reyes-Gonzalez *et al*., 2018.

From a spatial perspective, it can be observed in Figures 4.11 to 4.19 that specific fields consistently maintain either a lower or higher level of ET_c than other fields. However, it is also worth noting that some fields do not conform to a predictable pattern in certain instances, thereby exhibiting a more complex ET_c behaviour. The spatial ET_c maps depict significant variation in evapotranspiration across the Mooi River catchment, with lower ET_c rates particularly evident in the southwest compared to the east of the study area throughout the growing season. This

variation highlights the catchment's diversity and the complex interaction of factors influencing ET_c rates. Climate conditions vary within the catchment, including temperature, humidity, wind speed, and solar radiation, potentially impacting evaporation and transpiration rates. Soil properties, such as texture, structure, and water-holding capacity, also significantly influence ET_c rates. Environmental factors, including vegetation cover and topography, contribute to these disparities.

Adding to the understanding of this variability is the study of Van Loggerenberg (2016), which highlights the high spatial and temporal variability of rainfall across the Mooi River catchment. This high variability can lead to varying soil moisture conditions, thereby affecting ET_c rates. Moreover, the diversity in land use, vegetation cover, and farming practices can further intensify the spatial variability of actual evapotranspiration. In essence, the spatial variations in ET_c rates within the Mooi River catchment, as expressed in the ET_c maps, underscore the intricate interplay of multiple factors, including climate, soil, vegetation, topography, and human activities present in the catchment.

Chapter 6: Conclusion

6.1. Summary

The study set out to determine how the evapotranspiration of maize crops varies over space and time within the Mooi River catchment using satellite multispectral vegetation indices and the crop coefficient approach. The first and second research objectives have drawn conclusions about the effectiveness of using a species distribution model (SDM)—specifically, the Maximum Entropy (MAXENT) model in this study. This model proved to be a robust and valuable tool in identifying maize crops through NDVI, demonstrating an accuracy of 82%. In this instance, 945 maize fields were discerned among 2808 cultivated fields. Moreover, the study concluded that the LAI vegetation index effectively monitors plant growth patterns and extracts maize crop phenology from remote sensing images. It was employed to isolate 87 fields from the 945 identified by the MAXENT model. These fields were specifically chosen as they were planted between November 10th and 15th, ensuring uniformity in planting dates for the analysed maize fields. This was crucial for accurate assessments of actual evapotranspiration's spatiotemporal variability.

The third objective of the study was to determine the lengths of maize growth stages in the Mooi River catchment, employing the growing degree days (GDD) formula. This enabled categorising the total growth period of satellite imagery into four distinct maize growth stages. By doing so, the appropriate FAO (tabulated) crop coefficient value could be aligned to each satellite image, allowing for precise linear regression analysis and enabling the accurate correlation of NDVI values with corresponding crop coefficient values. Following this, objectives four and five were completed by extracting reference evapotranspiration (ET_o) values from the FAO's WaPOR database using a 9km-per-cell grid over the study area to create different ET_o 'zones', grouping proximate fields, whereafter NDVI and SAVI values were averaged for each of the 87 fields from the respective satellite image pixels within each of the field's boundaries.

The final three objectives involved adjusting the FAO's tabulated crop coefficients using a linear regression model derived from the relationship between these tabulated crop coefficient values and the NDVI values extracted from satellite imagery. These objectives also included calculating the actual evapotranspiration values (ET_c) and creating spatiotemporal maps of ET_c.

The regression analysis revealed that NDVI had a remarkably stronger relationship with tabulated K_c compared to SAVI, with an R^2 of 0.90 compared to an R^2 of 0.68 with SAVI.

Consequently, the NDVI-tabulated K_c regression model was selected for actual evapotranspiration calculations.

It was ultimately found that the average ET_c across the Mooi River catchment starts at a low, registering its minimum at 1.614 mm during the initial growth phase of maize. It experiences a gradual increase, peaking at 8.83 mm at 85 days after planting (DAP) and subsequently descends to 2.89 mm nearing harvest. This trend in ET_c aligns consistently with findings from other studies, including those by Ko & Piccinni (2008), Gontia & Tiwari (2010), Johnson & Trout (2015), and Reyes-Gonzalez *et al.* (2015, 2018). Spatial examination revealed considerable ET discrepancies across the Mooi River catchment, delineating the intricate interplays of diverse climatic, environmental, and soil conditions affecting ET_c levels during the growth cycle. Figures 4.11 to 4.19 depict these disparities, illustrating how specific fields sustain divergent ET_c levels, with some presenting unpredictable patterns and displaying intricate ET_c behaviours. The catchment's variability is further emphasized by lower ET_c rates in the southwest, contrasting with those in the east, throughout the growing season. The multifaceted influences of climate, soil properties, vegetation cover, and topography all significantly contribute to the variations observed in evapotranspiration within the catchment.

6.2. Importance of study findings and recommendations for future studies

The findings of this study are of significant importance as they reveal noticeable discrepancies at certain times of the year between ET_c calculated from tabulated K_c and ET_c derived from adjusted (new) K_c values by a vegetation index like NDVI. These discrepancies are crucial as NDVI more accurately reflects the real-time crop growth conditions and incorporates various environmental and climatic variables impacting crop growth. The most marked divergence between the ET_c calculated using tabulated coefficients and NDVI-based coefficients is observed during the initial to developmental stages of maize growth, underlining the need for more accurate assessment methods during these phases. This difference implies that to achieve the most precise and reliable ET_c estimates, particularly during the early growth phases of rainfed maize, it is necessary to utilise crop coefficients calculated from a vegetation index like NDVI, ensuring the estimates are more reflective of the actual field conditions and environmental variables. Interestingly, both methodologies display almost identical ET_c levels in the mid to late-season stages.

The in-depth spatiotemporal variability study in the Mooi River catchment has revealed the significant variations in ET_c throughout the maize growth cycle, reinforcing the imperative to incorporate diverse factors, including climate, soil, and human activities, in understanding and measuring agricultural parameters. The maps and models that resulted from this study can serve as essential resources for farmers, water managers, and policymakers, facilitating optimized water use and sustainable management of scarce water resources in semi-arid regions, thereby increasing food security.

In addressing future avenues of research, extending this methodology to different crop species and varied regions is imperative to substantiate its extensive applicability in managing agricultural water use and understanding how different types of agricultural landscapes affect evapotranspiration. An accurate estimation of crop evapotranspiration is fundamental not only for irrigation management in irrigated areas but also for crop yield assessments in rainfed regions, particularly pertinent in arid regions. It has profound implications on maize-soybean systems and other crop variants, offering insights into water-related stress impacts on crop development and yields. In addition, continuous measurement of ET_c throughout the growing seasons in semiarid regions is necessary in predicting potential drought impacts on crop yields. These enhanced methodologies and insights are not merely beneficial for the Mooi River region but extend to similar agricultural contexts, paving the way for sustainable water resource management and enhanced food security.

References

Aiello-Lammens, M.E., Boria, R.A., Radosavljevic, A., Vilela, B. & Anderson, R.P., 2015: spThin: An R package for spatial thinning of species occurrence records for use in ecological niche models. *Ecography*, 38(5), 541-545.

Allen, Richard G., Pereira, L.S., Raes, D., & Smith, M., 1998: Crop evapotranspiration: Guidelines for computing crop requirements. *Irrigation Drainage*, Paper No. 56, FAO 300.

Al Zayed, I.S., Elagib, N.A., Ribbe, L. & Heinrich, J., 2016: Satellite-based evapotranspiration over Gezira Irrigation Scheme, Sudan: A comparative study. *Agricultural Water Management*, 177, 66–76.

Annandale, J.G., Benadé, N., Jovanovic, N.Z. & du Sautoy, N., 1999: Facilitating irrigation scheduling by means of the soil water balance model. *WRC Report* No. 753/1/99, p. 285.

Araújo, M.B., Anderson, R.P., Barbosa, A.M., Beale, C. M., Dormann, C.F., Early, R., Garcia, R.A., Guisan, A., Maiorano, L., Naimi, B., O'hara, R.B., Zimmermann, N.E. & Rahbek, C., 2019: Standards for distribution models in biodiversity assessments. *Science Advances*, 5(1). #4858.

Ayyad, S., Al Zayed, I.S., Ha, V.T.T. & Ribbe, L., 2019: The performance of satellite-based actual evapotranspiration products and the assessment of irrigation efficiency in Egypt. *Water (Switzerland)*, 11(9), #1913,

Barbieri, P., Echarte, L., della Maggiora, A., Sadras, V. O., Echeverria, H., & Andrade, F. H., 2012: Maize evapotranspiration and water-use efficiency in response to row spacing. *Agronomy Journal*, 104(4), 939–944.

Bargaoui, Z. & Chebbi, A. 2009: Comparison of two kriging interpolation methods applied to spatiotemporal rainfall. *Journal of Hydrology*, 365(1–2), 56–73.

Bausch, W.C. & Neale, C.M.U., 1987: Crop coefficients derived from reflected canopy radiation: A concept. *Transactions of ASAE*, 30(3), 703–709.

Beard, J.B., Green R.L. & S.I. Sifers, S.I., 1992: Evapotranspiration and leaf extension rates of 24 well-watered turf-type Cynodon genotypes. *HortScience*, 27(9), 986-998.

Beck, J., 2013: Predicting climate change effects on agriculture from ecological niche modeling: Who profits, who loses? *Climatic Change,* 116(2), 177-189.

Boria, R.A., Olson, L.E., Goodman, S.M. & Anderson, R.P., 2014: Spatial filtering to reduce sampling bias can improve the performance of ecological niche models. *Ecological Modelling*, 275, 73–77.

Brown, P. 2000: Cooperative extension basics of evaporation and evapotranspiration turf irrigation management series. *Turf Irrigation Management Series*, 1, 1–4.

Cai, J., Liu, Y., Lei, T., & Pereira, L.S., 2007: Estimating reference evapotranspiration with the FAO Penman-Monteith equation using daily weather forecast messages. *Agricultural and Forest Meteorology*, 145(1–2), 22–35.

Carter, G.A., 1993: Responses of leaf spectral reflectance to plant stress. *American Journal of Botany*, *80*(3), 239–243.

Cascone, S., Coma, J., Gagliano, A. & Pérez, G., 2019: The evapotranspiration process in green roofs: A review. *Building and Environment*, 147, 337–355.

Castilho, R., 2015: *Species Distribution Modeling 101 Basics Hands-On Experimental work notes*. Available at: http://protea.eeb.uconn.edu:3838/wallace/

Cha, M., Li, M., & Wang, X., 2020: Estimation of seasonal evapotranspiration for crops in arid regions using multisource remote sensing images. *Remote Sensing*, 12(15), #2398.

Cook, C., Reason, C.J. & Hewitson, B.C., 2004: Wet and dry spells within particularly wet and dry summers in the South African summer. *Climate Research*, 26, 17–31.

Courault, D., Seguin, B., & Olioso, A. 2003: Review on estimation of evapotranspiration from remote sensing data: From empirical to numerical modelling approaches. *Irrigation and Drainage Systems*, 19(3–4), 223–249.

Dai, X., Wu, W., Ji, L., Tian, S., Yang, B., Guan, B., & Wu, D., 2022: MaxEnt model-based prediction of potential distributions of Parnassia wightiana (Celastraceae) in China. *Biodiversity Data Journal*, *10*, #e81073.

Denmead, O.T., & Shaw, R.H. 1960: The effects of soil moisture stress at different stages of growth on the development and yield of corn. *Agronomy*, 52(5), 272–274.

Djaman, K., O'Neill, M., Owen, C.K., Smeal, D., Koudahe, K., West, M., Allen, S., & Lombard, K. 2018: Crop evapotranspiration, irrigation water requirement and water productivity of maize from meteorological data under semiarid climate, *Water (Switzerland)*, 10(4), #405.

Doorenbos, J. & Pruit, W.O., 1977: Guidelines for Predicting Crop Water Requirements. *FAO Irrigation and Drainage Paper, 24.* Food and Agriculture Organization of the United Nations.

Dye, P. 2013: A review of changing perspectives on eucalyptus water-use in South Africa. *Forest Ecology and Management*, 301, 51–57.

Dyson, L. 2009: Heavy daily-rainfall characteristics over the Gauteng Province. *WaterSA*, 35(5), 627-637.

El-Shirbeny, M.A., Alsersy, M.A., Saleh, N.H. & Abu-Taleb, K.A., 2015: Changes in irrigation water consumption in the Nile Delta of Egypt assessed by remote sensing. *Arabian Journal of Geosciences*, 8, 10509–10519.

Elith, J., Graham, C.H., Anderson, R.P., Dudik, M., Ferrier, S., Guisan, A., Hiimans, R.J., Huettmann, F., Leathwick, J.R., Lehmann, A., Li, J., Lohmann, L.G., Loiselle, B.A., Manion, G., Moritz, C., Nakamura, M., Nakazawa, Y., Overton, J.M.M., Peterson, A.T., Phillips, S.J., Richardson, K., Scachetti-Pereira, R., Schapire, R.E., Soberon, J., Williams, S., Wisz, M.S. & Zimmermann, N.E., 2006: Novel methods improve prediction of species' distributions from occurrence data. *Ecography*, 29(2), 129–151.

Elith, J. & Leathwick, J.R., 2009: Species distribution models: Ecological explanation and prediction across space and time. *Annual Review of Ecology, Evolution, and Systematics,* 40, 677-697.

Evett S.R., Mazahrih, N.T., Jitan, M.A., Sawalha, M.H., Colaizzi, P.D. & Ayars J.E., 2009: A weighing lysimeter for crop water use determination in the Jordan Valley, Jordan. *Transactions of the ASABE*, 52(1), 155-169.

Farg, E., Arafat, S.M., Abd El-Wahed, M.S. & El-Gindy, A.M., 2012: Estimation of evapotranspiration ETc and Crop Coefficient in of wheat in south Nile Delta of Egypt using integrated FAO-56 approach and remote sensing data. *The Egyptian Journal of Remote Sensing and Space Science*, 15(1), 83–89.

Fielding, A.H. & Bell, J.F., 1997: A review of methods for the assessment of prediction errors in conservation presence/absence models. *Environmental Conservation*, 24, 38–49.

Folhes, M.T., Soares, J.V., & Renno, C.D., 2009: Remote sensing for irrigation water management in the semi-arid Northeast of Brazil. *Agricultural Water Management,* 96(10), 1398–1408.

Frezghi, M.S. & Smithers, J.C., 2008: Merged rainfall fields for continuous simulation modelling (CSM). *WaterSA*, 34(5), 523–528.

Gibson, L.A., Jarmain, C., Su, Z. & Eckardt, F.E., 2013: Estimating evapotranspiration using remote sensing and the surface energy balance system - A South African perspective. *WaterSA*, 39(4), 477–484.

Gibson L.A., Munich Z., Engelbrecht J., Petersen, N. & Conrad J.E. 2009: *Remote sensing as a tool towards resource assessment and determination of the legal compliance of surface and groundwater use.* WRC Report No. 1690/1/09. Water Research Commission, Pretoria.

Gibson, L.A., Münch, Z., Carstens, M. & Conrad, J. 2011: *Remote sensing evapotranspiration (SEBS) evaluation using water remote sensing*. Report to the Water Research Commission by ARC – Agricultural Research Council – Institute for Soil, Climate and Water, Stellenbosch.

Gontia, N.K. & Tiwari, K.N. 2010. Estimation of spatially and temporally distributed crop coefficient and evapotranspiration of wheat (Triticumaestivum) in an irrigation command using remote sensing and GIS. *Water Resources Management*, 24, 1399-1414.

Grace, J., 1974: The effect of wind on grasses. I. Cuticular and stomatal transpiration. *Journal of Experimental Botany*, 25(3), 542-551.

Grace, J. & Russell, G., 1977: The effect of wind on grasses. III. Influence of continuous drought or wind on anatomy and water relations in Festuca Arundinacea Schreb*. Journal of Experimental Botany*, 28(2), 268-278.

Gonzalez-Dugo, M.P., Neale, C.M.U., Mateos, L., Kustas, W. P., Prueger, J. H., Anderson, M. C. & Li, F., 2009: A comparison of operational remote sensing-based models for estimating crop evapotranspiration. *Agricultural and Forest Meteorology*, 149(11), 1843–1853.

Haarhoff, S. J., 2020: *New perspectives on plant population and row spacing of rainfed maize*. Unpublished PhD Thesis, Stellenbosch University, South Africa.

Hassan-Esfahani, L., Torres-Rua, A., Ticlavilca, A.M., Jensen, A. & McKee, M., 2014: Topsoil moisture estimation for precision agriculture using unmanned aerial vehicle multispectral imagery. *International Geoscience and Remote Sensing Symposium (IGARSS)*, 3263–3266.

Hauptfleisch, R. 2019: *Characterising rainfall using a high-density rain gauge network in the Mooi River catchment*, MSc Dissertation, North-West University, South Africa.

Hellegers P.J.G.J., Jansen, H.C. & Bastiaanssen, W.G.M., 2011: An interactive water indicator assessment tool to support land use planning. *Irrigation and Drainage*, 61(2), 143–154.

Hijmans, R.J., Garrett, K.A., Huaman, Z., Zhang, D.P., Schreuder, M. & Bonierbale, M.,2000: Assessing the geographic representativeness of genebank collections: the case of the Bolivian wild potatoes. *Conservation Biology*, 14(6), 1755–1765.

Hosmer, D. W. & Lemeshow, S. 2000: *Applied logistic regression* (*2nd edition*). New Jersey: Wiley.

Hosgood, B., Jacquemound, S., Andreeoli, G., Verdebout, J., Pedrini, A., & Schmuck, G., 1993: *Leaf Optical Properties Experiment Database* (LOPEX93). Cambridge: Cambridge University Press.

Hu, C. H., Ran, G., Li, G., Yu, Y., Wu, Q., Yan, D. & Jian, S. 2021: The effects of rainfall characteristics and land use and cover change on runoff in the Yellow River basin, China. *Journal of Hydrology and Hydromechanics*, 69(1), 29–40.

Hunsaker, D.J., Pinter, P.J., Barnes, E.M. & Kimball, B.A., 2003: Estimating cotton evapotranspiration crop coefficients with a multispectral vegetation index. *Irrigation Science*, 22(2), 95–104.

Hunsaker, D.J., Pinter, P.J. & Kimball, B.A. 2005: Wheat basal crop coefficients determined by normalized difference vegetation index. *Irrigation Science*, 24(1), 1–14.

Hussain, M.Z., Hamilton, S.K., Bhardwaj, A.K., Basso, B., Thelen, K.D. & Robertson, G.P., 2019: Evapotranspiration and water use efficiency of continuous maize and maize and soybean in rotation in the upper Midwest U.S. *Agricultural Water Management*, 221, 92–98.

Immerzeel, W.W., Droogers, P., & Gieske, A., 2006: Remote sensing and evapotranspiration mapping: State of the art. *FutureWater*, Report 55, 1-37.

Irmak, S. 2017: Evapotranspiration basics and estimating actual crop evapotranspiration from reference evapotranspiration and crop-specific coefficients. *Crops, Irrigation Engineering*, G1994, 1–9.

James, G. Witten, D. Hastie, T. & Tibshirani, R., 2013: *An Introduction to Statistical Learning*. New York: Springer.

Jato-Espino, D., Charlesworth, S.M., Perales-Momparler, S., & Andrés-Doménech, I., 2017: Prediction of evapotranspiration in a Mediterranean region using basic meteorological variables. *Journal of Hydrologic Engineering,* 22(4), #040160.

Jackson, R.D., Idso, S.B., Reginato, R.J., & Pinter, P.J. Jr., 1980: Remotely sensed crop temperatures and reflectances as inputs to irrigation scheduling. *Irrigation and drainage special conference proceedings, 23–25 July, Boise, Idaho. ASCE, New York*, 390–397.

Jarmain C., Klaasse A., Basson F.C., Meijninger W., Wilmink, S. & Bastiaansen W., 2011a: *Developing an operational remote sensing system for monitoring of efficient crop water and nitrogen use of grapes, Western Cape Province*. Final Report, Western Cape Provincial Department of Agriculture, Cape Town.

Jarmain C., Singels A., Obando E., Paraskevopoulos A. & Mthembu, I. 2011b: *Water use efficiency of irrigated agri- cultural crops determined with satellite imagery*. WRC Project No. K5/2079//4, Progress Report, December 2011, Water Research Commission, Pretoria.

Jarmain, C. & Klaasse, A. 2012: Fruitlook: *An operational service to improved crop water and nitrogen management in grapes and other deciduous fruit trees using satellite technology for the season of 2011-12*. Progress Report, Western Cape Provincial Department of Agriculture, Cape Town.

Jarmain, C., & Meijninger W.L. 2012: *Assessing the impact of Invasive Alien Plants on South African water resources using remote sensing techniques*. In: Neale, C.M.U. & Cosh, M.H. (eds.) Proceedings of a Symposium organized by the International Commission on Remote Sensing of IAHS, held at Jackson Hole, Wyoming, USA, 27-30 September 2010. IAHS Publication No. 352. IAHS Press, Oxfordshire. 388–392.

Jarmain, C, Singels, A., Obando, E., Paraskevopoulos, A., Olivier, F., Munich, Z., Van der Merwe. B., Walker. S., Van der laan, M., Messehazion. M., Savage. M., Pretorius. C., Annandale. J. & Everson, C. 2013: *Water use efficiency of irrigated agricultural crops determined with satellite imagery.* WRC Project No. K5/2079//4, Deliverable 6, Water Use Efficiency Report 2012/13, 15 January 2013. Water Research Commission, Pretoria.

Jensen, J.R., 2000: *Remote Sensing of environment. An earth resource perspective*. New Jersey: Prentice Hall.

Jensen, M.E., Burman, R.D. & Allen, R.G., 1990: *Evapotranspiration and irrigation water requirements. Manual of Practice No. 70*. New York: ASCE, p. 331.

Jovanovic, N., Mu, Q., Bugan, RD. & Zhao, M., 2015: Dynamics of MODIS evapotranspiration in South Africa. *WaterSA*, 41(1), 79–90.

Johnson, L.F. & Trout, T.J. 2012. Satellite NDVI assisted monitoring of vegetable crop evapotranspiration in California's San Joaquin valley. *Remote Sensing*, 4(2), 439–455.

Justice, C.O. & Townshend, J.R.G., 2002: Special issue on the Moderate Resolution Imaging Spectroradiometer (MODIS): A new generation of land surface monitoring. *Remote Sensing of Environment,* 83(1-2), 1–2.

Kamble, B. & Irmak, A., 2008: Assimilating remote sensing-based ET into SWAP Model for improved estimation of hydrological predictions. *In Proceeding of the 2008 IEEE International Geoscience and Remote Sensing Symposium, Boston, MA, USA, 7–11 July 2008,* 3, 1036-1039.

Kamble, B., Kilic, A. & Hubbard, K. 2013: Estimating crop coefficients using remote sensing-based vegetation index. *Remote Sensing*, 5(4), 1588–1602.

Kim, K.S. & Beard, J.B., 1988: Comparative turfgrass evapotranspiration rates and associated plant morphological characteristics. *Crop Science*, 28(2), 328-331.

Klaasse A., Bastiaanssen W., Jarmain, C., & Roux, A. 2008*: Water use efficiency of table and wine grapes in Western Cape, South Africa*. WaterWatch Report, Wageningen, The Netherlands. 68 pp.

Knipper, K.R., Kustas, W.P., Anderson, M.C., Alfieri, J.G., Prueger, J.H., Hain, C.R., Gao, F. & Yang, Y. 2019: Evapotranspiration estimates derived using thermal-based satellite remote sensing and data fusion for irrigation management in California vineyards. *Irrigation Science*, 37(3), 431–449.

Ko, J. & Piccinni, G., 2009: Corn yield responses under crop evapotranspiration-based irrigation management. *Agricultural Water Management*, 96(5), 799–808.

Kongo V.M. & Jewitt G.P.W. 2006: Preliminary investigation of catchment hydrology in response to agricultural water use innovations: A case study of the Potshini catchment - South Africa. *Physics and Chemistry of the Earth,* 31(15-16), 976–987.

Kramer-Schadt S., Niedblla J., Pilgrim J.D., Schroder B., Lindenborn, J., Reinfelder, V., Stillfried, M., Heckmann, I., Scharf,A. K., Augeri, D.M., Cheyne, S.M., Hearn, A.J., Ross, J., Macdonald, D.W., Mathai, J., Eaton, J., Marshall, A.J., Semiadi, G., Rustam, R., Bernard, H., Alfred, R., Samejima, H., Duckworth, J.W., Breitenmoser-Wuersten, C., Belant, J.L., Hofer, H. & Wilting, A., 2013: The importance of correcting for sampling bias in MaxEnt species distribution models. *Diversity and Distributions*, 19(11), 1366–1379.

Kuhn, M. & Johnson, K., 2013: *Applied predictive modelling, Vol. 26.*, New York: Springer.

Landman, W.A., Mason, S.J., Tyson, P.D. & Tennant, W.J., 2001: Retro-active skill of multi- tiered forecasts of summer rainfall over southern Africa. *International Journal of Climatology*, 21(1), 1–19.

Launiainen, S., Rinne, J., Pumpanen, J., Kulmala, L., Kolari, P., Keronen, P., Siivola, E., Pohja, T., Hari, P. & Vesala, T., 2005: Eddy covariance measurements of CO2 and sensible and latent heat fluxes during a full year in a boreal pine forest trunk-space. *Boreal Environment Research*, 10(6), 569–588.

Liou, Y. & Kar, S.K. 2014: Evapotranspiration estimation with remote sensing and various surface energy balance algorithms—A review. *Energies*, 7, 2821–2849.

Li, W., Guo, Q. & Elkan, C., 2011: Can we model the probability of presence of species without absence data? *Ecography*, 34(6), 1096–1105.

Liu, C., Sun, P.-S. & Liu, S.R., 2016: A review of plant spectral reflectance response to water physiological changes. *Chinese Journal of Plant Ecology*, 40(1), 80–91.

Liu, Y., Mo, X., Hu, S., Chen, X. & Liu, S., 2020: Attribution analyses of evapotranspiration and gross primary productivity changes in Ziya-Daqing basins, China during 2001–2015. *Theoretical and Applied Climatology*, *139*(3–4), 1175–1189.

Loggerenberg, J. van., 2016: *Spatial and temporal variability of rainfall intensity over the Mooi River catchment*. Unpublished MSc Dissertation, North-West University, Potchefstroom.

Lu, H., Xia, Z., Fu, Y., Wang, Q., Xue, J. & Chu, J., 2020: Response of soil temperature, moisture, and spring maize (Zea mays L.) root/shoot growth to different mulching materials in semi-arid areas of northwest China. *Agronomy*, *10*(4), #10040453.

Luo, Y., Zhang, Z., Chen, Y., Li, Z. & Tao, F., 2020: ChinaCropPhen1km: a high-resolution crop phenological dataset for three staple crops in China during 2000-2015 based on leaf area index (LAI) products. *Earth System Science Data*, 12(1), 197–214.

Lynch, S.D., Zulu, J.T., King, K.N. & Knoesen, D.M., 2001: The analysis of 74 years of rainfall recorded by the Irwins on two farms south of Potchefstroom. *WaterSA*, 27(4), 559-564.

Majozi, N.P., Mannaerts, C.M., Ramoelo, A., Mathieu, R., Mudau, A.E. & Verhoef, W., 2017: An intercomparison of satellite-based daily evapotranspiration estimates under different eco-climatic regions in South Africa. *Remote Sensing*, 9(4), 1–21.

Mardikis, M.G., Kalivas, D.P. & Kollias, V.J., 2005: Comparison of interpolation methods for the prediction of reference evapotranspiration - An application in Greece. *Water Resources Management*, 19(3), 251–278.

Martens, B., Cabus, P., Jongh, I. & Verhoest, N.E.C., 2013: Merging weather radar observations with ground-based measurements of rainfall using an adaptive multiquadric surface fitting algorithm. *Journal of Hydrology*, 500, 84–96.

Mateos, L., González-Dugo, M.P., Testi, L., & Villalobos, F.J., 2013: Monitoring evapotranspiration of irrigated crops using crop coefficients derived from time series of satellite images. I. Method validation. *Agricultural Water Management*, 125, 81–91.

McMaster, G.S., Wilhelm, W.W., 1997: Growing degree-days: one equation, two interpretations, *Agricultural and Forest Meteorology*, 87(4), 291–300.

Merow, C., Smith, M.J. & Silander, J.A., 2013: A practical guide to MaxEnt for modeling species' distributions: What it does, and why inputs and settings matter. *Ecography,* 36(10), 1058-1069.

Milani, M., Marzo, A., Toscano, A., Consoli, S., Cirelli, G.L., Ventura, D. & Barbagallo, S., 2019: Evapotranspiration from horizontal subsurface flow constructed wetlands planted with different perennial plant species. *Water (Switzerland),* 11(10), #11102159.

Moeletsi, M.E., 2017: Mapping of maize growing period over the Free State Province of South Africa: Heat units approach. *Advances in Meteorology*, 2017, #7164068.

Mokhtari, A., Noory, H., Vazifedoust, M. & Bahrami, M., 2018: Estimating net irrigation requirement of winter wheat using model- and satellite-based single and basal crop coefficients. *Agricultural Water Management*, 208, 95–106.

Motulsky, H. & Christopoulos, A., 2004: *Fitting Models to Biological Data Using Linear and Nonlinear Regression: A practical guide to curve fitting*. Oxford: Oxford University Press.

Musick, J.T. & Dusek, D.A., 1980: Irrigated corn yield response to water. *Transactions of the American Society of Agricultural Engineers,* 23(1), 92–98.

Naimi, B. & Araújo, M. B., 2016: sdm: a reproducible and extensible R platform for species distribution modelling. *Ecography,* 39(4), 368-375.

Nagler, P.L., Cleverly, J., Glenn, E., Lampkin, D., Huete, A. & Wan, Z. 2005: Predicting riparian evapotranspiration from MODIS vegetation indices and meteorological data. *Remote Sensing of Environment*, 94(1), 17–30.

Neale, C. M. U., Bausch, W. C. & Heerman, D. F., 1989: Development of reflectance-based crop coefficients for corn. *Transactions of the ASAE*, 32(6), 1891–1900.

Pandži, M., Ljubii, N., Mimić, G., Pandži, J., Pejak, B. & Crnojević, V., 2020: A case study of monitoring maize dynamics in serbia by utilizing Sentinel-1 data and growing degree days. *ISPRS Annals of the Photogrammetry, Remote Sensing and Spatial Information Sciences*, 5(3), 117–124.

Parmar, H.V., & Gontia, N.K., 2016: Remote sensing based vegetation indices and crop coefficient relationship for estimation of crop evapotranspiration in Ozat-II canal command. *Journal of Agrometeorology*, 18(1), 137–139.

Pearlmutter, 2001: Ocean circulation: Thermohaline circulation. *Encyclopaedia of Atmospheric Science*, 4, 1549- 1555.

Peng, L.P., Cheng, F.Y., Hu, X.G., Mao, J.F., Xu, X.X., Zhong, Y., Li, S.Y. & Xian, H.L. 2019. Modelling environmentally suitable areas for the potential introduction and cultivation of the emerging oil crop Paeonia ostii in China. *Scientific Reports*, 9(1), 1–10.

Phillips, S.J., Anderson, R.P. & Schapire, R.E., 2006: Maximum entropy modeling of species geographic distributions. *Ecological Modeling*, 190(3–4), 231–259.

Pereira, L.S., Allen, R.G., Smith, M., & Raes, D., 2015: Crop evapotranspiration estimation with FAO56: Past and future. *Agricultural Water Management*, 147, 4–20.

Pereira, L.S., Paredes, P., Hunsaker, D.J., López-Urrea, R. & Mohammadi Shad, Z., 2021: Standard single and basal crop coefficients for field crops. Updates and advances to the FAO56 crop water requirements method. *Agricultural Water Management*, 243, #106466.

Pôças, I., Calera, A., Campos, I. & Cunha, M., 2020: Remote sensing for estimating and mapping single and basal crop coefficientes: A review on spectral vegetation indices approaches. *Agricultural Water Management*, 233, #106081.

Ramoelo, A., Majozi, N., Mathieu, R., Jovanovic, N., Nickless, A. & Dzikiti, S. 2014: Validation of global evapotranspiration product (MOD16) using flux tower data in the African savanna, South Africa. *Remote Sensing*, 6(8), 7406–7423.

Reason, C.J., Hachigonta, S. & Phaladi, R.F., 2005: Interannual variability in rainy season characteristics over the Limpopo Region of southern Africa. *International Journal of Climatology*, 25(14), 1835-1853.

Reyes-Gonzalez, A., Hay, C., Kjaersgaard, J., & Neale, C. 2015. Use of remote sensing to generate crop coefficient and estimate actual crop evapotranspiration. *American Society of Agricultural and Biological Engineers Annual International Meeting 2015*, *6*(November 2016), 4374–4385.

Reyes-González, A., Kjaersgaard, J., Trooien, T., Hay, C. & Ahiablame, L. 2018: Estimation of crop evapotranspiration using satellite remote sensing-based vegetation index. *Advances in Metereology,* Volume 2018, #4525021.

Rockström, J., Karlberg, L., Wani, S. P., Barron, J., Hatibu, N., Oweis, T., Bruggeman, A., Farahani, J. & Qiang, Z., 2010: Managing water in rainfed agriculture - The need for a paradigm shift. *Agricultural Water Management*, *97*(4), 543–550.

Rondinini, C., Wilson, K.A., Boitani, L., Grantham, H. & Possingham, H.P., 2006: Trade-offs of different types of species occurrence data for use in systematic conservation planning. *Ecology Letters*, 9, 1136-1145.

Rouault, M., 2014: Impact of ENSO on South African Water Management Areas. In Modelling and observing the atmosphere. Potchefstroom, 2014. *South African Society for Atmospheric Science Conference Proceedings*, 70-73.

Santos, C., Lorite, I.J., Tasumi, M., Allen, R.G. & Fereres, E., 2008: Integrating satellite-based evapotranspiration with simulation models for irrigation management at the scheme level. *Irrigation Science*, 26(3), 277–288.

Schulze, R.E., 1997: South African Atlas of Agrohydrology and Climatology. Water Research Commission, Pretoria, Report TT82/96.

Sello, L., 2019: *Spatiotemporal variability of evapotranspiration in Sutherland*, Unpublished MSc Dissertation, North-West University, South Africa.

Shearman, R.C., 1986: Kentucky bluegrass cultivar evapotranspiration rates. *HortScience*, 21(3):455-457.

Shen Z., Chen, L., Liao, Q., Liu, R. & Hong, Q. 2012: Impact of spatial rainfall variability on hydrology and nonpoint source pollution modelling. *Journal of Hydrology,* 472-473, 205–215.

Shoko, C., Dube, T., Sibanda, M., & Adelabu, S., 2014: Applying the Surface Energy Balance System (SEBS) remote sensing model to estimate spatial variations in evapotranspiration in Southern Zimbabwe. *Transactions of the Royal Soc*iety of *South Africa* 70, 47–55.

Sishodia, R.P., Ray, R.L. & Singh, S.K. 2020: Applications of remote sensing in precision agriculture: A review. *Remote Sensing*, 12(19), 1–31.

Stewart, B. A. & Peterson, G. A., 2015: Managing green water in dryland agriculture. *Agronomy Journal*, 107(4), 1544–1553.

Suyker, A.E. & Verma, S.B. 2009: Evapotranspiration of irrigated and rainfed maize-soybean cropping systems. *Agricultural and Forest Meteorology*, 149(3–4), 443–452.

Tchamba, J., 2018: *Modelling the potential distribution of Golden Eagle based on maximum entropy: The experimental cases of Sweden and Norway*. Unpublished BSc Report, University of Gävle, Sweden.

Todd, R., Evett, S.R. & Howell, T.A., 2000: The Bowen ratio-energy balance method for estimating latent heat flux of irrigated aflalfa. *Agricultural and Forest Meteorology*, 103(4), 335–348.

Ünlü, M., Kanber, R. & Kapur, B., 2010: Comparison of soybean evapotranspirations measured by weighing lysimeter and Bowen ratio-energy balance methods. *African Journal of Biotechnology*, 9(30), 4700–4713.

Veloz, S.D., 2009: Spatially autocorrelated sampling falsely inflates measures of accuracy for presence-only niche models. *Journal of Biogeography*, 36(12), 2290–2299.

Wang, C., Li, J., Liu, Q., Zhong, B., Wu, S. & Xia, C., 2017: Analysis of differences in phenology extracted from the enhanced vegetation index and the leaf area index. *Sensors (Switzerland)*, *17*(9), #17091982.

Wani, S.P., Sreedevi, T.K., Rockström, J. & Ramakrishna, Y.S., 2009: Rainfed agriculture - past trends and future prospects. *Rainfed Agriculture: Unlocking the Potential*, 1–35.

Xue, J. & Su, B., 2017: Significant remote sensing vegetation indices: A review of developments and applications. *Journal of Sensors*, Volume 2017, #1353691.

Yackulic, C.B., Chandler, R., Zipkin, E.F., Royle, J.A., Nichols, J.D., Campbell Grant, E.H. & Veran, S. 2013. Presence-only modelling using MAXENT: When can we trust the inferences? *Methods in Ecology and Evolution*, *4*(3), 236–243.

Yao, Y., Liang, S., Cheng, J., Liu, S., Fisher, J.B., Zhang, X., Jia, K., Zhao, X., Qin, Q., Zhao, B., Han, S., Zhou, G., Zhou, G., Li, Y. & Zhao, S., 2013: MODIS-driven estimation of terrestrial latent heat flux in China based on a modified Priestley-Taylor algorithm. *Agricultural and Forest Meteorology*, 171-172, 187–202.

Zeri, M., Hussain, M.Z., Anderson-Teixeira, K.J., Delucia, E. & Bernacchi, C.J., 2013: Water use efficiency of perennial and annual bioenergy crops in central Illinois. *Journal of Geophysical Research: Biogeosciences*, 118(2), 581–589.

Zhang, C. & Kovacs, J.M. 2012: The application of small unmanned aerial systems for precision agriculture: A review. *Precision Agriculture*, 13(6), 693–712.

Zhang, K., Kimball, J.S. & Running, S.W. 2016: A review of remote sensing based actual evapotranspiration estimation. *Wiley Interdisciplinary Reviews: Water*, 3(6), 834–853.

Appendix A

Appendix A shows corresponding ET_o values of each grid cell and satellite overpass date.

		Grid Cells																					
Overpass date		1868	1867	1820	1818	1724	1723	1721	1720	1719	1676	1675	1674	1671	1670	1669	1626	1625	1623	1621	1968	1917	1869
2021/11/30	ETo	4,7	4,7	4,9	4,1	4,4	4,5	4,5	4,2	4,7	4,6	4,2	4,6	4,6	4,7	4,7	4,8	4,5	4,5	4,2	4,8	4,3	4,4
2021/12/10	ETo	6,1	6	6,1	5,9	6,3	6	6,1	6,2	6,3	5,9	5,9	6	6,1	6,1	5,9	6,2	6,3	6	6	5,8	6,1	6,2
2021/12/25	ETo	6,3	6,2	6,3	5,9	6,1	6,1	6,1	6,3	6,4	6,5	6	6,2	6,2	6,1	6,3	6,4	6,2	6,1	6,3	6,3	6	6,2
2021/12/30	Eto	7	7	7,5	7,2	7,7	7,7	7,4	7,4	7	7,7	7,7	7,7	7,4	7	7	7,8	7,8	7,6	7,1	7,1	7	7,3
2022/01/24	Eto	5,4	5,4	5,4	5,2	5,3	5,3	5,2	5,2	5,2	5,6	5,6	5,3	5,2	5,2	5,2	5,3	5,3	5,2	5,1	5,7	5,4	5,6
2022/02/03	ETo	6,7	6,7	6,9	6,8	7	7	6,9	6,9	6,6	7,1	7,1	7	6,9	6,6	6,6	7,2	7,2	7,1	6,8	6,8	6,7	6,8
2022/02/13	Eto	6	6	5,8	5,8	6,1	6,1	6,1	6,1	6	5,9	5,9	6,1	6,1	6	6	6,3	6,3	6,3	6,1	6	6	6
2022/02/28	ETo	4,7	4,7	4,4	4,7	4,5	4,5	4,7	4,7	4,8	4,3	4,3	4,5	4,7	4,8	4,8	4,4	4,4	4,7	5	4,4	4,7	4,3
2022/03/26	ETo	3,4	3,4	3,7	3,6	3,8	3,8	3,5	3,5	3,6	4,1	4,1	3,8	3,5	3,6	3,6	3,9	3,9	3,6	3,6	3,5	3,4	3,5
		Field																					
		20	18	25	17	76	42	14	8	6	83	58	30	7	4	1	52	28	10	2	87	22	26
		21	19			77	43	15	9		84	59	31		5		53	29	11	3		23	27
						78	44	16			85	60	32				54		12			24	
						79	45				86	61	33				55		13				
						80	46					62	34				56						
						81	47					63	35				57						
						82	48					64	36										
							49					65	37										
							50					66	38										
							51					67	39										
												68	40										
												69	41										
												70											
												71											
												72											
												73											
												74											
												75											

Appendix B

Appendix B shows growth stage lengths and their associated cumulative growing degree days (CGGD) as deducted from literature compared to those calculated from temperature data obtained from the Zuurbekom weather station.

Date	DAP (days after planting)	Literature CGGD (cumulative GDD from Haarhoff, 2020)	Literature Growth Stage (deducted from Haarhoff, 2020) GDD)	Mooi River Catchment CGGD (calculated from Zuurbekom AWS temp. data)	Mooi River Catchment Growth Stage (calculated from GDD)
2021/11/11	1	14,1	Initial stage	11,15	Initial stage
2021/11/12	2	26,15	Initial stage	23,4	Initial stage
2021/11/13	3	35,3	Initial stage	33,45	Initial stage
2021/11/14	4	44,45	Initial stage	44,65	Initial stage
2021/11/15	5	53,6	Initial stage	57,25	Initial stage
2021/11/16	6	62,75	Initial stage	69,85	Initial stage
2021/11/17	7	71,9	Initial stage	83,65	Initial stage
2021/11/18	8	81,05	Initial Stage	96,4	Initial stage
2021/11/19	9	90,2	Initial stage	107,6	Initial stage
2021/11/20	10	99,35	Initial stage	118,1	Initial stage
2021/11/21	11	108,5	Initial stage	125,55	Initial stage
2021/11/22	12	117,65	Initial stage	135,05	Initial stage
2021/11/23	13	126,8	Initial stage	143,55	Initial stage
2021/11/24	14	135,95	Initial stage	152	Initial stage
2021/11/25	15	145,1	Initial stage	158,55	Initial stage
2021/11/26	16	154,25	Initial stage	164,35	Initial stage
2021/11/27	17	163,4	Initial stage	168,35	Initial stage
2021/11/28	18	172,55	Initial stage	177,3	Initial stage
2021/11/29	19	181,7	Initial stage	187,35	Initial stage
2021/11/30	20	190,85	Initial stage	199,55	Initial stage
2021/12/01	21	200	Initial stage	211,6	Initial stage
2021/12/02	22	210	Initial stage	221,2	Initial stage
2021/12/03	23	220	Initial stage	233,85	Initial stage
2021/12/04	24	230	Initial stage	244,3	Initial stage
2021/12/05	25	240	Initial stage	250,85	Initial stage
2021/12/06	26	250	Initial stage	261,65	Initial stage
2021/12/07	27	260	Initial stage	272,95	Initial stage
2021/12/08	28	270	Initial stage	282,65	Initial stage
2021/12/09	29	280	Initial stage	293,55	Development stage
2021/12/10	30	290	Development stage	305,55	Development stage

2021/12/11	31	300	Development stage	317,95	Development stage
2021/12/12	32	310	Development stage	327	Development stage
2021/12/13	33	320	Development stage	332,65	Development stage
2021/12/14	34	330	Development stage	342,85	Development stage
2021/12/15	35	340	Development stage	353,5	Development stage
2021/12/16	36	350	Development stage	362,3	Development stage
2021/12/17	37	360	Development stage	369,1	Development stage
2021/12/18	38	370	Development stage	373,2	Development stage
2021/12/19	39	380	Development stage	377	Development stage
2021/12/20	40	390	Development stage	384,2	Development stage
2021/12/21	41	400	Development stage	393,25	Development stage
2021/12/22	42	420	Development stage	402,6	Development stage
2021/12/23	43	440	Development stage	411,2	Development stage
2021/12/24	44	460	Development stage	420,4	Development stage
2021/12/25	45	480	Development stage	429,65	Development stage
2021/12/26	46	500	Development stage	440,15	Development stage
2021/12/27	47	520	Development stage	448,35	Development stage
2021/12/28	48	540	Development stage	456,95	Development stage
2021/12/29	49	560	Development stage	466,75	Development stage
2021/12/30	50	580	Development stage	479,05	Development stage
2021/12/31	51	600	Development stage	492,2	Development stage
2022/01/01	52	610	Development stage	503,35	Development stage
2022/01/02	53	620	Development stage	515,1	Development stage
2022/01/03	54	630	Development stage	526,75	Development stage
2022/01/04	55	640	Development stage	537,6	Development stage
2022/01/05	56	650	Development stage	548,7	Development stage
2022/01/06	57	660	Development stage	557,95	Development stage
2022/01/07	58	670	Development stage	569,6	Development stage
2022/01/08	59	680	Development stage	580,4	Development stage
2022/01/09	60	690	Development stage	590,2	Development stage
2022/01/10	61	700	Development stage	600,65	Development stage
2022/01/11	62	710	Development stage	611,65	Development stage
2022/01/12	63	720	Development stage	623,5	Development stage
2022/01/13	64	730	Development stage	634,2	Development stage
2022/01/14	65	740	Development stage	645,35	Development stage
2022/01/15	66	750	Development stage	656,85	Development stage
2022/01/16	67	760	Development stage	667,3	Development stage
2022/01/17	68	770	Development stage	678,75	Development stage
2022/01/18	69	780	Development stage	690,15	Development stage
2022/01/19	70	790	Development stage	700,8	Development stage

2022/01/20	71	800	Development stage	711,25	Development stage
2022/01/21	72	810	Development stage	721	Development stage
2022/01/22	73	820	Development stage	729,25	Development stage
2022/01/23	74	830	Development stage	736,65	Development stage
2022/01/24	75	840	Development stage	745,8	Development stage
2022/01/25	76	850	Development stage	757,5	Development stage
2022/01/26	77	860	Development stage	769,35	Development stage
2022/01/27	78	870	Mid-Season stage	780,9	Development stage
2022/01/28	79	880	Mid-Season stage	792,1	Development stage
2022/01/29	80	890	Mid-Season stage	801,05	Development stage
2022/01/30	81	900	Mid-Season stage	810,1	Development stage
2022/01/31	82	920	Mid-Season stage	821,05	Development stage
2022/02/01	83	940	Mid-Season stage	832	Development stage
2022/02/02	84	960	Mid-Season stage	843,35	Development stage
2022/02/03	85	980	Mid-Season stage	856,25	Development stage
2022/02/04	86	1000	Mid-Season stage	868,55	Mid-Season stage
2022/02/05	87	1020	Mid-Season stage	877,65	Mid-Season stage
2022/02/06	88	1040	Mid-Season stage	887,7	Mid-Season stage
2022/02/07	89	1060	Mid-Season stage	897,8	Mid-Season stage
2022/02/08	90	1080	Mid-Season stage	907,8	Mid-Season stage
2022/02/09	91	1100	Mid-Season stage	918,6	Mid-Season stage
2022/02/10	92	1105	Mid-Season stage	930,1	Mid-Season stage
2022/02/11	93	1110	Mid-Season stage	942,05	Mid-Season stage
2022/02/12	94	1115	Mid-Season stage	952,35	Mid-Season stage
2022/02/13	95	1120	Mid-Season stage	963,35	Mid-Season stage
2022/02/14	96	1125	Mid-Season stage	975,05	Mid-Season stage
2022/02/15	97	1130	Mid-Season stage	986,25	Mid-Season stage
2022/02/16	98	1135	Mid-Season stage	998,35	Mid-Season stage
2022/02/17	99	1140	Mid-Season stage	1008,85	Mid-Season stage
2022/02/18	100	1145	Mid-Season stage	1018,5	Mid-Season stage
2022/02/19	101	1150	Mid-Season stage	1029,15	Mid-Season stage
2022/02/20	102	1160	Mid-Season stage	1040,3	Mid-Season stage
2022/02/21	103	1170	Mid-Season stage	1051,7	Mid-Season stage
2022/02/22	104	1180	Mid-Season stage	1062,8	Mid-Season stage
2022/02/23	105	1190	Mid-Season stage	1074,45	Mid-Season stage
2022/02/24	106	1200	Mid-Season stage	1085,05	Mid-Season stage
2022/02/25	107	1210	Mid-Season stage	1096,25	Mid-Season stage
2022/02/26	108	1220	Mid-Season stage	1106,5	Mid-Season stage
2022/02/27	109	1230	Mid-Season stage	1118,35	Mid-Season stage
2022/02/28	110	1240	Mid-Season stage	1129,35	Mid-Season stage

2022/03/01	111	1250	Mid-Season stage	1139,85	Mid-Season stage
2022/03/02	112	1255	Mid-Season stage	1149,55	Mid-Season stage
2022/03/03	113	1260	Mid-Season stage	1160,6	Mid-Season stage
2022/03/04	114	1265	Late-season stage	1172,25	Mid-Season stage
2022/03/05	115	1270	Late-season stage	1181,75	Mid-Season stage
2022/03/06	116	1275	Late-season stage	1191,55	Mid-Season stage
2022/03/07	117	1280	Late-season stage	1202,6	Mid-Season stage
2022/03/08	118	1285	Late-season stage	1212,5	Mid-Season stage
2022/03/09	119	1290	Late-season stage	1218,7	Mid-Season stage
2022/03/10	120	1295	Late-season stage	1229,4	Mid-Season stage
2022/03/11	121	1300	Late-season stage	1240,85	Mid-Season stage
2022/03/12	122	1310	Late-season stage	1251,7	Mid-Season stage
2022/03/13	123	1320	Late-season stage	1262,4	Mid-Season stage
2022/03/14	124	1330	Late-season stage	1272,45	Late-season stage
2022/03/15	125	1340	Late-season stage	1281,7	Late-season stage
2022/03/16	126	1350	Late-season stage	1289,7	Late-season stage
2022/03/17	127	1360	Late-season stage	1296,1	Late-season stage
2022/03/18	128	1370	Late-season stage	1304,2	Late-season stage
2022/03/19	129	1380	Late-season stage	1313,6	Late-season stage
2022/03/20	130	1390	Late-season stage	1322,95	Late-season stage
2022/03/21	131	1400	Late-season stage	1327,9	Late-season stage
2022/03/22	132		Late-season stage	1335,15	Late-season stage
2022/03/23	133		Late-season stage	1343,75	Late-season stage
2022/03/24	134		Late-season stage	1352	Late-season stage
2022/03/25	135		Late-season stage	1361,2	Late-season stage
2022/03/26	136		Late-season stage	1369,55	Late-season stage
2022/03/27	137		Late-season stage	1377,7	Late-season stage
2022/03/28	138		Late-season stage	1385,85	Late-season stage
2022/03/29	139		Late-season stage	1394,2	Late-season stage
2022/03/30	140		Late-season stage	1403	Late-season stage